



Published in final edited form as:

J Med Chem. 2019 October 24; 62(20): 9078–9102. doi:10.1021/acs.jmedchem.9b00623.

Dual-Acting Cholinesterase-Human Cannabinoid Receptor 2 Ligands Show Pronounced Neuroprotection in Vitro and Overadditive and Disease-Modifying Neuroprotective Effects in Vivo

Matthias Scheiner[†], Dominik Dolles[†], Sandra Gunesch[†], Matthias Hoffmann[†], Massimo Nabissi[‡], Oliviero Marinelli[‡], Marina Naldi[§], Manuela Bartolini[§], Sabrina Petralla^{||}, Eleonora Poeta^{||}, Barbara Monti^{||}, Christina Falkeis[⊥], Michael Vieth[⊥], Harald Hübner[#], Peter Gmeiner[#], Rangan Maitra[∇], Tangui Maurice[○], Michael Decker^{*.†}

[†]Pharmaceutical and Medicinal Chemistry, Institute of Pharmacy and Food Chemistry, Julius Maximilian University of Würzburg, Am Hubland, 97074 Würzburg, Germany

[‡]School of Pharmacy, University of Camerino, Via Madonna delle Carceri 9, 62032 Camerino, Italy

[§]Department of Pharmacy and Biotechnology, University of Bologna, Via Belmeloro 6, 40126 Bologna, Italy

^{||}Department of Pharmacy and Biotechnology, University of Bologna, Via Selmi 3, 40126 Bologna, Italy

[⊥]Pathology, Clinical Center Bayreuth, Preuschwitzer Straße 101, 95445 Bayreuth, Germany

[#]Medicinal Chemistry, Department of Chemistry and Pharmacy, Friedrich-Alexander University Erlangen-Nürnberg, Schuhstraße 19, 91052 Erlangen, Germany

[∇]Center for Drug Discovery, Research Triangle Institute, Research Triangle Park, North Carolina 27709, United States

[○]MMDN, University of Montpellier, INSERM, EPHE, UMR-S1198, 34095 Montpellier, France

Abstract

*Corresponding Author: michael.decker@uni-wuerzburg.de. Tel.: +49-931-31-89676.

Author Contributions

Synthesis of the target compounds was performed by M.S. and D.D. Inhibitory, kinetic studies on hAChE and A β aggregation were performed by M.O., M.N., and M.B. Inhibitory potency on hBChE and hAChE was performed by S.G. and M.H., radioligand binding studies on CBRs by M.S., and CB₂R efficacy by cAMP-regulated gene expression by M.N. The calcium mobilization assay on CBRs was performed by R.M. and neuroprotection and neurotoxicity experiments by S.G. and M.S. Microglia effects were investigated by S.P., E.P., and B.M., and in vivo experiments were performed by M.S. and T.M. and liver histology by C.F. and M.V. Finally, MOR binding studies were performed by H.H. and P.G. All authors contributed to writing the manuscript and read and approved the final version.

Supporting Information

The Supporting Information is available free of charge on the [ACS Publications website](https://pubs.acs.org) at DOI: 10.1021/acs.jmedchem.9b00623.

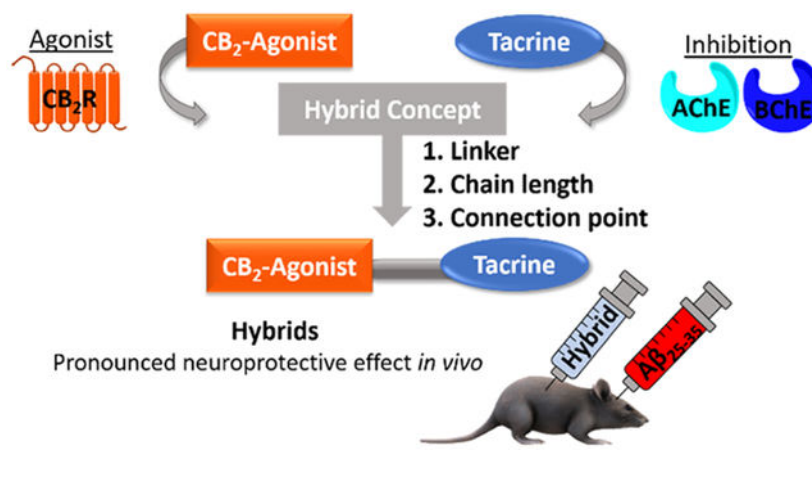
RP-HPLC chromatograms of the lead compounds (PDF)

Molecular formula strings (CSV)

The authors declare no competing financial interest.

We have designed and synthesized a series of 14 hybrid molecules out of the cholinesterase (ChE) inhibitor tacrine and a benzimidazole-based human cannabinoid receptor subtype 2 (hCB₂R) agonist and investigated them *in vitro* and *in vivo*. The compounds are potent ChE inhibitors, and for the most promising hybrids, the mechanism of human acetylcholinesterase (hAChE) inhibition as well as their ability to interfere with AChE-induced aggregation of β -amyloid ($A\beta$), and $A\beta$ self-aggregation was assessed. All hybrids were evaluated for affinity and selectivity for hCB₁R and hCB₂R. To ensure that the hybrids retained their agonist character, the expression of cAMP-regulated genes was quantified, and potency and efficacy were determined. Additionally, the effects of the hybrids on microglia activation and neuroprotection on HT-22 cells were investigated. The most promising *in vitro* hybrids showed pronounced neuroprotection in an Alzheimer's mouse model at low dosage (0.1 mg/kg, *i.p.*), lacking hepatotoxicity even at high dose (3 mg/kg, *i.p.*).

Graphical Abstract



INTRODUCTION

About 50 million people worldwide had to live with dementia in 2018.¹ In about 30 years, an increase of cases up to 152 million is expected. The most common form of dementia is Alzheimer's disease (AD). People aged 65 and over are considered at risk and are most likely to be affected.¹ Unfortunately, pharmacotherapy is very limited. Currently, only four drugs are approved for the treatment of AD. Three of them (donepezil, rivastigmine, and galantamine) are cholinesterase (ChE) inhibitors, while the fourth (memantine) is an *N*-methyl-D-aspartate (NMDA) receptor noncompetitive antagonist. All approved drugs are only symptomatically effective in the moderate stages of the disease and reduce but do not stop the progression and do not affect the cause of the disease.² The exact molecular mechanisms, as well as the causes for an AD outbreak still remain unknown. However, a variety of biochemical changes during the pathological process take place. AD hallmarks are the formation of amyloid-beta ($A\beta$) plaques in the extracellular brain parenchyma,³ the abnormal hyperphosphorylation of the microtubule-associated tau protein, and the formation of neurofibrillary tangles (NFTs) within neurons.⁴ Both the $A\beta$ aggregates and the NFTs lead to a progressive loss of cholinergic neurons in the brain, memory deficits, and cognitive

dysfunction.⁵⁻⁷ $A\beta$ itself has been shown to exert cytotoxic effects on cultured neurons,⁸ induce oxidative stress, and modify ionic homeostasis.^{9,10} Furthermore, in the post-mortem analysis of AD brain, an increased expression of inflammatory mediators has been observed.^{11,12} The increase seems to be partly triggered by microglia activation. Microglia cells are activated by various stimuli, including misfolded $A\beta$, its precursor protein (APP), and misfolded tau.^{13,14} In the early stage of AD, stimulation leads to a neuroprotective M2 microglia phenotype and can, therefore, promote $A\beta$ clearance via microglia's scavenger receptors (SRs), which hinder AD progression.^{15,16} However, it has been shown that there is a switch from the neuroprotective M2 to a more classically activated M1 phenotype at the later stage of AD. The M1 phenotype generally mediates defense from pathogens and tumor cells, and it is characterized by the production of proinflammatory cytokines, such as TNF- α , LL1 β , or reactive oxygen species (ROS), which are associated with the loss of neurons. Therefore, this switch can lead to an increased $A\beta$ production, a decreased $A\beta$ clearance, and, ultimately, to neuronal damage and progression of AD.¹⁶

The human endocannabinoid system has been intensively investigated, and two cannabinoid receptor (hCBR) subtypes have been discovered. The hCBR subtype 1 (hCB₁R) is the most abundant metabotropic receptor in the brain, and it is involved in a variety of physiological processes.¹⁷⁻¹⁹ The psychoactive effect of tetrahydrocannabinol (THC), the main psychoactive constituent of cannabis, is due to hCB₁R agonism.²⁰ The hCB₂R is mainly expressed in peripheral immune cells and has been originally described as the peripheral CBR,²¹ but later, it was found also in the central nervous system (CNS) where it is expressed on microglia and astrocytes.^{22,23} While the expression of the hCB₁R remains unchanged, the hCB₂R is abundantly and selectively expressed in neuritic plaque-associated astrocytes and microglia.^{24,25} In several in vitro and in vivo models of acute and chronic neurodegenerative disorders, the activation of the hCB₂R was shown to exert beneficial effects.²⁶ hCB₂R agonists can suppress microglia activation and the production of neurotoxic factors such as ROS, nitric oxide (NO), and proinflammatory mediators (TNF- α and cytokines).²⁷⁻²⁹ Administration of an hCB₂R agonist to rats, previously and intracerebrally treated with $A\beta_{40}$, the forty-amino acid long isoform of $A\beta$, promoted $A\beta$ clearance, decreased secretion of proinflammatory mediators, and, ultimately, led to an increased synaptic plasticity, cognition, and memory.³⁰ Furthermore, in vivo studies with transgenic Tg2576 mice overexpressing hAPP_{Swe} showed a lower $A\beta$ production, reduced reactive microglia cells, and improved cognition performance upon treatment with an hCB₂R agonist.³¹ Additionally, an hCB₂R knockout experiment with APP transgenic mice supports the potential of cannabinoid therapies targeting hCB₂R to reduce $A\beta$, as the knockout results in an increased $A\beta$ pathology and an alternation in tau processing.³²

Acetylcholinesterase (AChE)-inhibiting drugs for symptomatic cognition improvement in AD patients are related to the oldest theory of AD pathophysiology, the cholinergic hypothesis.² The theory describes the loss of cholinergic neurons and reduction of the neurotransmitter acetylcholine (ACh).³³ Inhibition of the metabolizing enzyme AChE raises ACh levels, leading to an improved cognitive performance. However, since AChE level decreases with the progression of AD,³⁴⁻³⁶ AChE inhibition seems to be only effective at early stages of disease. On the other hand, the levels of the less specific butyrylcholinesterase (BChE) remain unaltered or increase with AD progression.³⁵⁻³⁸ BChE

can hydrolyze ACh and, thereby, compensate the reduction of AChE activity. An experiment with AChE knockout mice supported this hypothesis. Indeed, no cholinergic hyperactivation in the absence of AChE was observed since BChE can take over the hydrolysis of ACh.³⁹ Results from further studies were in accordance with the role of the BChE in AD brains and showed a positive correlation between selective BChE inhibition and improved cognitive performance and memory.^{40–44}

There is even more diversity in the pathological processes and reasons for AD beyond the ones herein described. Because of this multifactorial and sporadic nature of AD, the classical approach “one target-one disease” reaches its limits or even makes it ineffective to develop an effective drug.⁴⁵ Conversely, a more promising approach seems to be the development of a multitarget drug capable of simultaneously acting at different targets.⁴⁶ To obtain such multitarget drugs, there are two common strategies: the hybrid and the “merged ligand”.⁴⁷ In the merged ligand strategy, two pharmacophores are fused into a single small molecule. The hybrid strategy foresees the combination of two molecules with two different pharmacologically active moieties by using a linker to form a larger molecule.^{45,47} Through the merged ligand strategy, we have recently achieved low-molecular-weight hCB₂R ligands endowed with hBChE inhibitory activity, which proved to exert neuroprotection even in vivo.⁴⁸ The design and improvement of such multi-target directed ligands (MTDLs) are challenging since minor chemical alternations can improve affinity at one target and diminish activity at the second one. Here, we describe hybrids out of similar benzimidazole units with the established tacrine unit to yield higher affinity at both targets.

Design.

Since AChE is a well-established target for the treatment of AD at the early and moderate stages, while BChE is a promising target for the moderate-to-advanced forms of AD, an inhibitor that is able to tackle both ChEs should be effective for a longer time span along AD progression. Such dual inhibitors have been described in the literature, among which tacrine **1**.⁴⁹ Tacrine was the first approved drug for the treatment of AD but was withdrawn from the market because of its dose-dependent hepatotoxicity.^{50,51} Due to its low molecular weight and excellent ChE inhibitory activity, tacrine **1** is an ideal starting point for the development of multitarget drugs (for recent review articles, see refs 52 and 53).

In developing tacrine hybrids, it is important to keep the potential hepatotoxic effect in mind. Linking or coupling with hepatoprotective compounds can reduce or even eliminate such a side effect.^{54–56}

In addition to the inhibition of the ChEs, the activation of the hCB₂R, as previously mentioned, represents a promising strategy in the treatment of AD. An example of a selective hCB₂R agonist is the benzimidazole-based derivative **2** described by AstraZeneca (see Figure 1)⁵⁷ and further investigated by us.^{48,50–60}

RESULTS AND DISCUSSION

Following the hybrid concept, coupling of structures **1** and **2** into a single molecule through a linker should yield a molecule with inhibitory properties toward ChEs and affinity for the

hCB₂R. Defining a suitable connecting position for the linker chain is a crucial task because an unsuitable connection between the two pharmacophore units can easily lead to a complete loss of activity or can reverse the behavior of the drug at the target, especially with regard to the hCB₂R (e.g., turn an agonist into an antagonist).⁶⁰ Linkage at the primary amine moiety at the position 9 of **1** is chemically easy to access, and substituted derivatives still show pronounced inhibitory properties toward ChEs.⁶¹

Taking advantage of the previous work on the structure-activity relationships (SARs) of the hCB₂R ligand **2**, two possible attachment positions for a linker were identified, that is, the amide moiety and the N¹ of the imidazole.⁵⁸ Connection of structures **1** and **2** through these two connection points lead to two sets of hybrid compounds: **3a–e** and **4a–e** (see Figure 2).

Modification of the tertiary amide group of the parent molecule **2** into a secondary amide group in derivatives **4a–e** might affect affinity and activity at the target. Hence, to investigate a possible effect of the number of substituents at this position, we designed a tertiary amide hybrid (hybrid **5**). After optimizing the spacer length, we designed hybrids with a functionalized linker. Therefore, we introduced a 2-poly-(ethylene glycol) (PEG) linker for higher rigidity and polarity (hybrids **6** and **7**). In addition, cystamine was introduced as a linker at the amide position to archive neuroprotective and putative hepatoprotective properties (**8**, see Figure 3).⁶²

Synthesis.

Based on these design strategies, tacrine-amine derivatives **12a–g** and **14** were synthesized and coupled to the benzimidazole core. Anthranilic acid **9** and cyclohexanone **10** were heated up with an excess of phosphoroxylchloride to yield the tetrahydroacridine derivative **11**.⁶³ By substitution with the corresponding diamine in excess, the tacrine-amine derivatives **12a–g** were obtained (Scheme 1).

For the synthesis of derivative **14**, the primary amine of tacrine-amine derivative **12c** was acetylated to form amide **13** in quantitative yield. In the next step, the amide was reduced to the secondary amine **14** in the presence of lithium aluminum hydride (Scheme 1).

Synthesis of derivatives **3a–e** and **6** started with 4-fluoro-3-nitrobenzoic acid **15**. To form the diethylamide **16**, oxalyl chloride and a catalytic amount of DMF were used, and then diethylamine was added. In the next step, the fluorine atom was substituted with the respective amine derivatives **12a–f** to form compounds **17a–f**, the reaction gave good to quantitative yield.

The nitro moiety was then reduced with tin(II) chloride dihydrate to obtain the anilinic amines **18a–f**, which were directly used for the next step. 2-(4-Ethoxyphenyl)acetic acid was activated with HBTU and added to amines **18a–f**. In the last step, the amides **19a–f** were cyclized in acetic acid to yield compounds **3a–e** and **6** (Scheme 2).

4-Fluoro-3-nitrobenzoic acid **15** served as the starting material for derivatives **4a–e**, **5**, **7**, and **8**. In the first step, the ethyl ester was formed as a protection group, and the fluorine atom was substituted with 3-methylbutan-1-amine to yield substituted ester **20** in a good yield. In

the next step, the nitro moiety was reduced with hydrogen over Pd/C to yield amine **21**, which was then directly reacted with HBTU-activated 2-(4-ethoxyphenyl)acetic acid to form amide **22**. Benzimidazole **23** was formed by stirring **22** in acetic acid under reflux. The ester was hydrolyzed under basic conditions. In the last step, acid **24** was activated with HBTU and reacted with the respective amines **12a–g** and **14** to yield hybrids **4a–e**, **5,7**, and **8** (Scheme 3).

PHARMACOLOGICAL PROFILE

Inhibition of Cholinesterases.

All synthesized compounds were assayed for their ability to inhibit human butyrylcholinesterase (hBChE) and human acetylcholinesterase (hAChE) using the colorimetric Ellman's assay (Table 1).⁶⁴ Tacrine **1** was selected as the reference compound and showed an $\text{pIC}_{50}(\text{hBChE}) = 7.9$ and $\text{pIC}_{50}(\text{hAChE}) = 6.8$. Previous studies showed no significant ChE inhibitory activity of the hCB₂R agonist **2** at 10 μM .⁵⁸ According to our expectations, all synthesized hybrids acted as ChE inhibitors. Compared to **1**, hybrids **3a**, **3b**, **3e**, and **4b** showed an increased inhibitory potency toward hBChE, while **3a** and **4b**, in addition, also showed a higher inhibitory activity toward hAChE. The higher inhibitory potency might be due to interaction with the PAS of the AChE (see Inhibition and Mode of Action toward hAChE), which was consequently followed up (cf. Figure 5). For a better overview of the selectivity, we correlated pIC_{50} values of hAChE and hBChE in Figure 4.

Inhibition Constants and Mode of Action toward hAChE.

To get further insights into the inhibition of hAChE, the mechanism of inhibition was investigated for one hybrid of each set with a pronounced inhibition of AChE. Specifically, hybrid **3e** of set 1 and **4b** of set 2 were selected. Additionally, cystamine hybrid **8** was investigated.

For the three selected compounds, the mechanism of inhibition was investigated by monitoring the catalytic rate at several substrate and inhibitor concentrations (see Experimental Section for details). Lineweaver-Burk reciprocal plots showed increasing slope (decreasing V_{max}) and increasing x intercept (increasing K_{m} values) at increasing inhibitor concentration (see Figure 5). This trend indicates a mixed-type inhibition, and thus, the inhibitor could bind simultaneously with the CAS and the PAS of hAChE. The inhibitor inhibition constant K_i and the inhibition constant for the enzyme-substrate-inhibitor complex (K_i') were estimated for each hybrid and are reported in Figure 5.

Inhibition of A β Aggregation.

Compounds able to bind the AChE's PAS may interfere with the AChE-induced A β oligomerization and fibrillization.^{65,66} Hence, given the ability of **3e**, **4b**, and **8** to contact AChE's PAS, the inhibitory activity on AChE-induced A β_{40} aggregation was investigated by a thioflavin T (ThT)-based fluorometric assay⁶⁵ and compared with that of the anti-AD drug **1** (see Figure 6). Results showed that compounds **3e** and **4b** were able to significantly reduce the proaggregating action of hAChE, while **1** was inactive, in agreement with a previous study.⁶⁵ Interestingly, percent inhibition values archived for **3e** and **4b** are close to activity

values previously obtained for the well-known multifunctional compound bis(7)tacrine (68.0% inhibition in the same assay conditions).⁶⁷ In the same experimental conditions, the cystamine derivate **8** was not able to significantly inhibit the AChE-induced A β ₄₀ aggregation.

Although **1** is not able to inhibit amyloid self-aggregation at a significant extent, several studies have shown that tacrine homo- and heterodimers may be endowed with such a beneficial property.⁵² Hence, the three selected hybrids were also assayed for their ability to inhibit A β ₄₂ self-aggregation by a similar ThT fluorescence assay.⁶⁸ Quite interestingly, compounds **3e** and **8** strongly inhibited A β ₄₂ aggregation when assayed at a 1:1 ratio with A β ₄₂, while, in the same conditions, inhibition by **4b** was quite weak (see Figure 6) since each compound is representative of a different subset of hybrids, SARs cannot be derived. However, it is clear that the spatial arrangement of pharmacophore fragments and the nature of the spacer chain strongly affect the inhibitory ability toward the spontaneous aggregation of the 42-amino acid isoform of A β .

The three hybrids showed different inhibition profiles toward the two aggregation phenomena. While hybrid **8** was able to significantly interfere with A β self-aggregation but not with the chaperonic action of hAChE toward A β , hybrid **4b** was able to significantly interfere with the chaperonic action of hAChE toward A β but only weakly with A β self-aggregation, and, finally, hybrid **3e** able to significantly inhibit both aggregation phenomena. Because of the strong inhibitory potency toward A β self-aggregation exerted by **3e**, it cannot be excluded that this activity can also synergistically contribute to the good inhibitory potency recorded in the AChE-induced amyloid aggregation assay. This might also explain the high inhibition value recorded in this assay, notwithstanding a K_i value in the submicromolar range.

Radioligand Binding Assays at hCB₁R and hCB₂R.

All synthesized compounds were tested for affinity to hCB₁R and hCB₂R using radioligand binding assays. Briefly, hCBRs were isolated from cell lines stably expressing receptors (CHO cells for hCB₁R or HEK cells in the case of hCB₂R). [³H]CP 55,940 was used as radioligand. As a positive control, the hCB₂R selective ligand **2** was used. In our tests, we measured a K_i (hCB₂R) = 37 nM and selectivity over hCB₁R [24% replacement (hCB₁R) of radioligand at 10 μ M]. All compounds showed affinity to hCB₂R within single- to two-digit micromolar range. In the case of compounds **3a–e**, the affinity toward hCB₂R increased with the length of the spacer, from K_i = 38.5 μ M (**3a**) to K_i = 4.5 μ M (**3e**). Part of this effect might be due to an increasing lipophilicity, which is a favorable feature for high-affinity hCB₂R ligands.⁷¹ Compounds **4a–e** all show a single-digit micromolar affinity toward hCB₂R. Experimental data did not support the correlation between affinity and chain length. The tertiary amide derivative **5**, which is the equivalent of derivative **4c**, showed the same affinity toward hCB₂R but a higher affinity toward hCB₁R, resulting in low selectivity. Hence, the number of substituents at the amide group influences selectivity. Hybrids **6** and **7** with a 2-PEG-linker, which confers a higher hydrophilicity and rigidity, showed a weaker affinity toward hCB₂R compared to the compounds with the longest alkylene linkers (**3e** and **4e**). The disulfide bond in hybrid **8** has no significant effect on affinity toward hCB₂R as the

equivalent derivative **4e** showed almost the same affinity (Table 1). Overall, the linkage of the two molecules has been associated with a loss of affinity at the hCB₂R compared to the parent molecule **2**, but the ligands still retain moderate affinity and good selectivity at hCB₂R. Since parent molecule **2** shares a high structural similarity with the known μ -opioid receptor (MOR) ligand etonitazene,⁴⁸ we investigated potential affinity and found a significant affinity of hybrids **3a**, **4a**, and **4e** (see Supplementary Table 1). In our previous work, we were able to show that an MOR “design out” approach is possible, if this is required with regard to the side effect profile.⁴⁸

Efficacy at hCB₂R.

The hCB₂R is coupled through G_{i/o} protein, so adenylate cyclase is inhibited in the case of activation. This results in a lower level of intracellular cAMP in the case of agonist binding or to an increased cAMP level in the case of an inverse agonist binding.⁷² The cAMP increase by forskolin (FSK) is further enhanced by an antagonist/reverse agonist binding, while the binding of an agonist reverts the effect.⁷³ This makes the intracellular detection of cAMP levels by immuno-assays a common method for the characterization of the efficacy of hCB₂R ligands. Going down the signaling pathway mediated by a conformational change of the receptor, the resulting difference in the cellular cAMP level changes the expression of cAMP-regulated genes (the reporter). The transcription of these genes is regulated by the transcription factor cAMP response element-binding protein (CREB). Binding of CREB to the cAMP responding element (CRE) is upstreaming gene expression.⁷⁴ A high cAMP level, induced by an antagonist binding, leads to a high expression of cAMP-regulated genes, while an agonist leads to the opposite effect. By quantifying the expression of these genes, it is possible to investigate the behavior of the ligand at the receptor. An example of a cAMP-regulated gene is the macrophage migration inhibitory factor (MIF) with a CRE in the proximal promoter region.⁷⁵ A further example is the signal transducer and activator of transcription (STAT-3) gene, which expression is also under CRE promoter control.⁷⁶ Both genes are highly expressed in multiple myeloma cells.^{77,78} Compounds **3e** and **4c** were evaluated, as previously described, at a concentration of 50 μ M.⁴⁸ In general, before examining the efficacy of the compounds, an MTT assay was carried out on U266 myeloma cells to evaluate a nontoxic concentration of the compounds (see Supplementary Figure 1). The efficacy of the compounds was investigated by the quantification of the cAMP-regulated MIF and STAT-3 genes by a qRT-PCR methodology. AM630 was measured as a reference antagonist/reverse agonist. Cells were treated with compound **2** as a reference agonist, **3e** and **4c** alone, and in combination with AM630. Compared to the vehicle, compounds **2**, **3e**, and **4c** show a decreased expression of both genes. Also, in combination experiments, all three compounds show a decreased level of both genes compared to the levels of only the AM630-treated cells (see Figure 7 and Supplementary Figure 2).

Furthermore, compounds **3e** and **4c** were characterized using a functional fluorescent hCB₂-activated G_{aq16}-coupled intracellular calcium mobilization assay in CHO-K1 cells overexpressing the receptor.^{79,80} Briefly, CHO-K1 cells were engineered to stably co-express hCB₁ or hCB₂ and G_{aq16}. Activation of hCB₁/CB₂ by an agonist then leads to generation of inositol phosphatase 3 (IP3) and activation of IP3 receptors, which, in turn, mobilizes intracellular calcium. Compounds **3e** and **4c** were identified as agonists of hCB₂R

with an EC_{50} of 911 ± 42 nM for compound **4c** and an $E_{max} = 39\%$. Compound **3e** shows an EC_{50} of 3.05 ± 0.2 μ M and an $E_{max} = 51\%$. Therefore, both compounds are partial agonists at hCB₂R. Both compounds were devoid of activity at hCB₁R. (see Figure 8).

Compounds **3e** and **4c** are therefore partial agonists at the hCB₂R as confirmed in two different assays. Since in our previous work, we also found agonist behavior for structurally related derivatives and because of the high structural similarity of all the hybrids described, we assume that all hybrids are agonists.⁴⁸

Effects on Microglia Activation.

To test a possible immunomodulatory effect, that is, the shift from the M1 neurotoxic to the M2 neuroprotective phenotype, of compounds **2**, **3e**, and **4a**, the murine microglial cell line N9 was exposed to 100 ng/mL lipopolysaccharide (LPS), which induces an M1 activation state, in the presence or absence of increasing concentrations (1, 2.5, and 5 μ M) of the test compounds. After 24 h of treatment, microglial conditioned media were collected, partly used for nitrite measurement, and partly concentrated for Western blot analysis. In parallel, microglial cells were collected, and the protein content was determined. Accumulation of nitrite in microglial conditioned media was measured by a colorimetric assay based on the Griess reaction, while the release of IL1 β and the expression of iNOS, TREM2, and TGF β 2 were tested through Western blot analysis.

Nitrite production due to iNOS induction and IL1 β release is the marker of M1, neurotoxic activated microglia, and induced by the LPS treatment, while the phagocytic proteins TREM2 and TGF β 2 are both makers of M2, neuroprotective microglia. As shown in Figure 9, compound **3e** strongly reduces in a dose-dependent way IL1 β release and nitrite accumulation, as well as iNOS expression induced by LPS-mediated activation of microglial cells, with no parallel change in TREM2 and TGF β 2 expression, thus indicating an immunomodulatory effect of the compound, which is similar to compounds **2** and **4a**.

Neuroprotective Properties on HT-22 Cells.

For the biological evaluation of compound **8** regarding its effects on murine hippocampal neurons (HT-22), we performed a glutamate assay as previously described.^{81,82} This neuronal cell line is derived from murine hippocampal tissue and is glutamate sensitive.⁸³ HT-22 cells lack ionotropic glutamate receptors. The addition of extracellular glutamate at high concentrations can be used to introduce intracellular ROS accumulation by blocking the cystine/glutamate antiporter, resulting in glutathione depletion. This neuronal oxidative stress results in cell injuries and eventually cell death.^{84–86} Before performing the neuroprotectivity assays, potential neurotoxicity of both compounds **4e** and **8** were evaluated in an MTT assay (see Figure 10A). Compound **8** showed concentration-dependent neuroprotectivity starting at 1 μ M (see Figure 10C). Treatment with 5 μ M compound **8** leads to neuroprotection comparable to the positive control quercetin at 25 μ M. Compound **4e** shows a similar neuroprotective behavior but decreases viability at 10 μ M due to the neurotoxic effect at this dose (see Figure 10B). The use of cystamine as a linker yielded a hybrid with lower neurotoxicity compared to the sulfur-free analogue **4e** with a neuroprotective behavior at a comparable low concentration. Furthermore, compounds **3a**,

3d, **3e**, **4a**, and **4b** were also investigated toward their neurotoxicity and neuroprotective behavior. In summary, compounds **3a**, **3d**, and **3e** show no neurotoxicity at the doses tested (max. 10 μM), while **4a** is toxic above 5 μM , and **4b** shows first toxicity effects at 5 μM . Compounds **4b** and **4a** show neuroprotective behavior only at 5 μM , while other compounds tested showed low neuroprotective behavior (**3e**) or none (**3a** and **3d**) (see Supplementary Figure 3).

In Vivo Studies.

The most promising compounds were tested regarding their procognitive effects in an in vivo AD mouse model. To induce AD such as neuroinflammation and cognitive deficits, oligomerized $\text{A}\beta_{25-35}$ peptide was intracerebroventricularly injected into the mouse brain.^{44,87,88} Since the addressed targets are located in the brain, hybrids must be able to penetrate the BBB. We first tested compounds, with the shortest spacer lengths, **3a** and **4a** with a low molecular weight. After the first positive results, we also tested compounds with a more pronounced in vitro profile.

Compounds were injected once daily (o.d.) and intraperitoneally (i.p.) from day 1, 20 min after the peptide injection, until day 7. Compounds were solubilized in pure DMSO at a concentration of 2 mg/mL and then diluted in water. Final DMSO concentration in the vehicle solution remained, however, high (60%), and innocuity was controlled by a daily observation on the mice behavior and weight gain control. None of the treatment affected significantly the weight gain during the week of treatment. Animals lost up to 1 g after the peptide injection but then regained regularly between 0.2 and 0.4 g daily (see Supplementary Figure 4).

Behavioral examination was performed between day 8 and 10 according to the procedure schematized in Supplementary Figure 5. All animals were sacrificed on day 11 (see Supplementary Figure 5).

Spontaneous alternation performance, which is an index of spatial working memory, was tested on day 8 in the Y-maze test. Long-term memory response was measured on day 10, in a step-through type passive avoidance task, with retention assessed for 24 h after training. Results confirmed that $\text{A}\beta_{25-35}$ induced significant learning impairments in the behavioral tests. Moreover, all compounds tested showed significant attenuations of $\text{A}\beta_{25-35}$ -induced learning impairments in both the short-term and the long-term memory responses (see Figure 11). Effective doses were slightly lower in the spontaneous alternation test (see Figure 11, upper panels) than in the passive avoidance test (see Figure 11, lower panels) and appeared often bell-shaped (see Figure 11d,f,i,j). Compound **3a** significantly prevented $\text{A}\beta_{25-35}$ -induced learning impairments at doses of 1 mg/kg and higher (see Figure 11b, 1). All other compounds, namely, **3d**, **3e**, **4a**, and **8**, significantly prevented the learning deficits at the lower dose of 0.3 mg/kg (see Figure 11c-j). Notably, compounds **3e**, **4a**, and **8** completely prevented $\text{A}\beta_{25-35}$ impairments in both tests at the most effective doses (resp., 0.3, 1, and 0.3 mg/kg), outlining the high efficiency of the compounds. It should be noted, at this point, that the hybrids show a significantly higher efficacy compared to the parent molecules **1** and **2**, which were also investigated in vivo in our previous work.^{48,87} It is possible that MOR activity of the compounds may marginally contribute to the

neuroprotective effect observed here. However, the only indirect measure we get from our experiments was that no significant change in pain sensitivity to footshock was measured, even at the highest drug dose during the passive avoidance training session. Shock sensitivity was 1.1 ± 0.3 for the group treated with compound **3a**, 3 mg/kg, and 0.9 ± 0.3 for compound **4a**, 1 mg/kg, versus 1.4 ± 0.3 for Veh-treated animals, suggesting that pain response was not affected by the compound treatments. Nevertheless, MORs have been shown to be involved in memory formation, particularly, in the context of memory formation associated with opiate drug abuse, by regulating GABAergic inputs and facilitating neuronal excitatory activity through the hippocampal CA1 area.⁸⁹ Therefore, the agonist (or antagonist) activity of the compounds at MORs and synergy of MOR and CB₂R activities on memory and neuroprotection is—at least in principle—possible. Indeed, the compounds tested exhibit a remarkably high in vivo efficacy, with sub-mg/kg active doses as compared with their low micromolar affinities in vitro on CB₂R or MORs. Their precise PK/PD profiles and any possible synergy between pharmacological targets should be examined to confirm that the compounds exhibit a very unique and interesting pharmacological activity.

Liver Histology.

Livers of mice treated with the high dose (3 mg/kg) were dissected out on day 12, after the behavioral experiments, post-fixed in buffered formalin 4%, and cut into 2 mm slices. At least two-thirds of the parenchyma was embedded, including all macroscopically visible abnormalities. The material underwent standardized dehydration and paraffin embedding as well as hematoxylin-eosin staining after well-established routine protocols. All slides were assessed by the same pathologist, completely blinded to the treatment protocols. The assessment included all typical liver changes seen with drug toxicity: Necrosis was reported focal, segmental, diffuse, or zonal in percentages and divided between fresh and long-standing necrosis. Steatosis was reported as macro- or microvesicular, given in percentages, as diffuse or zonal (lobular zones I–III). Fibrosis was assessed according to stages I to IV after Batts and Ludwig.⁹⁰ Inflammation is reported semiquantitatively in a four-tiered system 0–3 and divided into portal and/or lobular. Cholestasis was also reported in a four-tiered system 0–3 specified to intrahepatocytic or canalicular. Cell ballooning was also stated in percentage. After the assessment, the findings were realigned with the treating groups. Microvesicular steatosis was present in all groups, including controls (6/10) showing the highest ratio in group **3d** (6/6) and the lowest in group **4a** (2/9). Necrosis was differentiated into fresh necrosis and older necrosis. The fresh necrosis in these specimen was completed without reaction, only hours old. It was seen in all groups, including controls. The highest ratio was observed in the A β /V group (11/12) and group **3d** (5/6) with nearly all specimen affected. Older necrosis was reported in two specimen only, both in group A β /V. Other findings, such as discrete lobular inflammation, were seen only in a single specimen, not related to treatment groups. The results suggest drug-independent reasons for steatosis and fresh necrosis because they were also found in the control groups in a high percentage. One possible cause of the observed liver damage could be the high level of DMSO used for compound injection.⁹¹ No hepatotoxic relation to compound treatment could be established. Further experiments for long-time toxicity must be performed.

CONCLUSIONS

In the current study, sets of hybrid compounds combining tacrine **1** as ChE inhibitor and the hCB₂R agonist **2** were designed and synthesized using different molecular attachment points in the benzimidazole core, different spacer lengths, and structures. The newly synthesized compounds were first evaluated in a series of experiments to confirm activity on AD-relevant targets, namely, AChE, BChE, and hCB₂R. The hybrid compounds showed higher inhibition of ChEs compared to **1**. To follow this up, a kinetic study was performed. The study showed a mixed-type inhibition by compounds tested and suggests binding to a second site in ChE leading to higher inhibition. While **1** has no effect on A β aggregation when assayed at 1/1 ratio, all hybrids tested had an effect. Above all, **3e** showed a pronounced inhibition of self- and AChE-induced A β aggregation. Radioligand binding studies on hCB₂R showed a lower affinity from the nanomolar range of **2** to the single-digit micromolar range for the hybrids. Hybrids **3e** and **4c**, representative for the two different sets, were investigated by a cAMP-regulated gene expression experiment, which showed they maintained their agonist behavior at the hCB₂R. To investigate the effectiveness, microglial activity was investigated. Therefore, different M1 and M2 markers were quantified. Despite the significantly lower affinity for the hCB₂R compared to **2**, the compounds showed an immunomodulatory effect similar to the parent molecule **2**. The concept of incorporating a disulfide into the linker to introduce neuroprotection was investigated in a HT22 cell assay. Both tested compounds, **8** and the sulfur-free analogue **3e**, showed neuroprotection against glutamate-induced oxidative stress. Due to the promising in vitro profile, several compounds were tested in vivo and showed pronounced effects on short- and long-term memory, proving their ability to cross the BBB. Keeping the hepatotoxicity of **1** in mind, liver histology of high dose-treated animals (3 mg/kg) was carried out (Table 2). In first-line experiments, the tested hybrids showed no hepatotoxicity effect, but this must be further investigated. The high in vivo efficacy of the compounds should be emphasized, which is significantly higher in particular for the compounds **3e** and **8** (0.1 mg/kg), than for the parent molecules **1** and **2**, which were investigated in our previous work.^{48,87} Due to the significantly lower dosage compared to **1**, a lower liver-damaging side effect of the novel hybrids in a potential clinical application might be assumed. We consider these data also of interest for other drug discovery efforts with regard to tacrine-containing experimental therapeutics as well as hybrid molecules with higher molar mass aiming at CNS activity.

EXPERIMENTAL SECTION

Chemistry.

General Information. Reagents and Solvents.—All reagents were used without further purification and bought from common commercial suppliers. For anhydrous reaction conditions, THF was dried prior to use by refluxing over sodium slices with benzophenone as an indicator under an argon atmosphere.

Thin-Layer Chromatography (TLC).—To monitor reaction progress, thin-layer chromatography (precoated plates with silica gel, from Machery-Nagel: ALUGRAM Xtra

SIL G/UV₂₅₄) was carried out. The spots were visualized by UV light (254 and 366 nm), by staining in the iodine chamber, or by using spray reagents (Ehrlich's reagent: primary amines turn red). The eluent systems are indicated in volume (v) ratios of the respective solvents (v/v).

Preparative Thin-Layer Chromatography.—Silica gel (Merck KGaA: Silica gel 60 GF₂₅₄) was mixed with water. Glass plates were coated evenly with the mixture and dried at room temperature. The compound was dissolved in CH₂Cl₂ and applied to the starting line in small drops. The plate was then transferred to a preparative TLC chamber with the mobile phase. After successful separation, the plate was dried, and the product was detected under UV light (254 and 366 nm), scraped off, and then extracted with MeOH.

Column Chromatography.—Silica gel (particle size, 0.063–0.2 mm; Merck) was used for column chromatography. The eluent systems are indicated in volume (v) ratios of the respective solvents (v/v). Column chromatography was also performed using an Interchim Puri Flash 430 (Ultra Performance Flash Purification) instrument (Montluçon, France) connected to an Interchim Flash ELSD. Used columns were Silica 25 g (30 μ m) (Interchim, Montluçon, France).

Nuclear Magnetic Resonance Spectroscopy (NMR).—Measurements of NMR spectra were performed on a Bruker Advance 400 (¹H NMR: 400 MHz; ¹³C NMR: 101 MHz). ¹H and ¹³C NMR spectra were calibrated with the hydrogen signal of the respective solvent as the internal standard. In this work, CDCl₃, CD₃OD, and D₂O were used as solvents (¹H: CDCl₃, 7.26 ppm; ¹H: CD₃OD, 3.31 ppm; ¹H: D₂O, 4.79 ppm; ¹³C: CDCl₃, 77.16 ppm; ¹³C: CD₃OD, 49.0 ppm). *J* is the coupling constant in hertz (s⁻¹). The abbreviations of the indicated signal diversities were s = singlet, d = doublet, t = triplet, q = quartet, and m = multiplet.

Liquid Chromatography/Mass Spectrometry (LC/MS).—Measurements for verification and purity of the compounds were performed by LC/MS (from Shimadzu), comprising a DGU-20A3R controller, pump LC-20AB, degasser DGU-20A, and SPD-20A UV/Vis detector. ESI ionization was accomplished by an LCMS-2020 single quadrupole mass spectrometer. As a stationary phase, for analytical purpose, a Synergi 4U fusion-RP 80 Å (150 × 4.6 mm) column and for preparative purpose, a Synergi 4U fusion-RP 80 Å (250 × 10.0 mm) were used. As a mobile phase, a gradient of MeOH/water (both containing 0.1% formic acid) (phase A/phase B) was used. The compounds were dissolved in MeOH and filtered through syringe filters.

The parameters for the methods are given as follows: flow rate, 1.0 mL/min; UV detection, 254 nm; scan range, 100–800 *m/z*; gradient: A, H₂O (0.1% CF₃COOH) and B, MeOH (0.1% CF₃COOH); 0–8 min 5% → 90% B, 8–13 min 90% B, 13–14 min 90% → 10% B, and 14–18 min 10% → 5% B.

Compounds were only used for biological evaluation if the purity was ≥ 95%.

General Procedures. General Procedure I for Nucleophilic Substitution of Aryl Chloride by a Diamine (for Compounds 12a–g).—The chloride compound **11** was dissolved in hexanol, and the corresponding diamine was added. The mixture was stirred for 24 h under reflux conditions under an argon atmosphere. The solvent was evaporated under high vacuum using an evaporator. The residue was dissolved in CH₂Cl₂ and extracted with water. The organic layer was dried over anhydrous MgSO₄, and the solvent was removed in vacuo.

General Procedure II for Aromatic Substitution of Fluoride by Amines (for Compounds 17a–f and 20).—The respective fluoride compound and the respective amine were dissolved in THF, and then NEt₃ was added. The mixture was stirred at room temperature overnight. The solvent was then removed in vacuo, and the residue was dissolved in CH₂Cl₂ and washed with water. The organic layers were combined and dried over anhydrous MgSO₄, and the solvent was removed in vacuo.

General Procedure III for Reduction of an Aromatic Nitro Moiety with Stannous Chloride Dihydrate (for Compounds 18a–f).—The respective nitro compound was dissolved in ethanol, and SnCl₂·2H₂O was added. The mixture was stirred under reflux conditions under an argon atmosphere for 5 h. Then, the mixture was basified with NH_{3(aq)} (25%), and the precipitate was filtered off by suction. The filtrate was concentrated in vacuo. The residue was dissolved in CH₂Cl₂ and washed with 1M NaOH. The organic layers were combined and dried over anhydrous MgSO₄, and the solvent was removed in vacuo. The product was directly used in the next reaction, without further purification, and just characterized by mass spectrometry.

General Procedure IV for Amide Formation with HBTU-Activated Ester (for Compounds 19a–f and 22).—The respective acid was dissolved in DMF then NEt₃, and HBTU was added. This mixture was added to a solution of the respective amine in DMF. The mixture was stirred overnight at room temperature, and the solvent was then removed in vacuo. The residue was dissolved in CH₂Cl₂ and washed with a saturated NaHCO₃ solution. The organic layers were combined and dried over anhydrous MgSO₄, and the solvent was removed in vacuo.

General Procedure V for Ring Closure to Benzimidazole (for Compounds 3a–e, 6, and 23).—The respective amide was dissolved in glacial acetic acid. The mixture was stirred depending on the reaction progress for 2–6 h under reflux conditions and was then concentrated in vacuo. The residue was basified with NH_{3(aq)} (25%) and extracted with CH₂Cl₂. The organic layers were combined, dried over anhydrous MgSO₄, and concentrated in vacuo.

Synthesis. 2-(4-Ethoxybenzyl)-N,N-diethyl-1-(2-((1,2,3,4-tetrahydroacridin-9-yl)amino)ethyl)-1H-benzo[d]imidazole-5-carboxamide (3a).—The reaction was carried out according to general procedure V using 3-(2-(4-ethoxyphenyl)acetamido)-N,N-diethyl-4-((2-((1,2,3,4-tetrahydroacridin-9-yl)amino)ethyl)amino)benzamide **19a** (258 mg, 0.43 mmol). The crude product was purified by column chromatography (20:1:0.1 CH₂Cl₂/MeOH/NH_{3(aq)} (25%)), and product **3a** (210 mg, 0.36 mmol, 84%) was obtained as a yellow

oil. ^1H NMR (400 MHz, CDCl_3): δ 7.86 (d, J = 8.2 Hz, 1H), 7.70 (s, 1H), 7.57 (d, J = 8.3 Hz, 1H), 7.51–7.45 (m, 1H), 7.24–7.15 (m, 2H), 7.11 (d, J = 8.3 Hz, 1H), 6.90 (d, J = 8.6 Hz, 2H), 6.66–6.61 (m, 2H), 4.13 (t, J = 6.6 Hz, 2H), 4.04 (s, 2H), 3.88 (s, 1H), 3.82 (q, J = 7.0 Hz, 2H), 3.56–3.23 (m, 6H), 2.96 (t, J = 6.4 Hz, 2H), 2.31 (t, J = 6.3 Hz, 2H), 1.83–1.75 (m, 2H), 1.74–1.66 (m, 2H), 1.27 (t, J = 7.0 Hz, 3H), 1.15 (s, 6H) ppm. ^{13}C NMR (101 MHz, CDCl_3): δ 171.7, 158.8, 158.2, 154.9, 149.2, 147.2, 142.2, 135.9, 131.6, 129.4, 128.9, 128.7, 127.7, 124.6, 122.0, 121.7, 120.6, 118.0, 117.9, 114.9, 109.5, 63.5, 47.3, 44.5, 34.0, 33.8, 24.8, 22.9, 22.7, 14.9, 14.2 ppm. ESI: m/z calcd for $\text{C}_{36}\text{H}_{42}\text{N}_5\text{O}_2$ [$\text{M} + \text{H}$] $^+$, 576.33; found, 576.25; retention time, 7.90 min; HPLC purity, 97%.

2-(4-Ethoxybenzyl)-N,N-diethyl-1-(3-((1,2,3,4-tetrahydroacridin-9-yl)amino)propyl)-1H-benzo[d]imidazole-5-carboxamide (3b).—The reaction was carried out according to general procedure V using 3-(2-(4-ethoxyphenyl)acetamido)-*N,N*-diethyl-4-((3-((1,2,3,4-tetrahydroacridin-9-yl)amino)propyl)amino)benzamide **19b** (104 mg, 0.17 mmol). The crude product was purified by preparative thin-layer chromatography (10:1:0.1 $\text{CH}_2\text{Cl}_2/\text{MeOH}/\text{NH}_3(\text{aq})$ (25%)), and product **3b** (23 mg, 39.0 μmol , 23%) was obtained as a yellow oil. ^1H NMR (400 MHz, CDCl_3): δ 8.16 (d, J = 7.8 Hz, 1H), 8.06 (d, J = 8.0 Hz, 1H), 7.74 (s, 1H), 7.56–7.49 (m, 2H), 7.27–7.22 (m, 2H), 7.15 (d, J = 7.9 Hz, 2H), 6.62 (d, J = 8.3 Hz, 2H), 4.43 (s, 2H), 4.00–3.92 (m, 2H), 3.77 (q, J = 6.9 Hz, 2H), 3.57–3.48 (m, 2H), 3.40–3.13 (m, 4H), 3.08–3.03 (m, 2H), 2.59–2.51 (m, 2H), 2.20–2.12 (m, 2H), 1.75–1.71 (m, 4H), 1.29–1.17 (m, 8H) ppm. ^{13}C NMR (101 MHz, CDCl_3): δ 171.0, 158.4, 156.7, 154.2, 151.0, 145.9, 142.3, 134.2, 132.2, 129.8, 128.4, 128.1, 127.5, 124.5, 122.4, 121.8, 119.7, 117.7, 115.9, 115.0, 111.7, 63.5, 46.0, 42.8, 33.9, 32.0, 29.8, 24.8, 22.4, 22.1, 14.9, 14.2 ppm. ESI: m/z calcd for $\text{C}_{37}\text{H}_{45}\text{N}_5\text{O}_2$ [$\text{M} + 2\text{H}$] $^{2+}$, 295.68; found, 295.60; retention time, 7.82 min; HPLC purity, 98%.

2-(4-Ethoxybenzyl)-N,N-diethyl-1-(4-((1,2,3,4-tetrahydroacridin-9-yl)amino)butyl)-1H-benzo[d]imidazole-5-carboxamide (3c).—The reaction was carried out according to general procedure V using 3-(2-(4-ethoxyphenyl)acetamido)-*N,N*-diethyl-4-((4-((1,2,3,4-tetrahydroacridin-9-yl)amino)butyl)amino)benzamide **19c** (166 mg, 0.27 mmol). The crude product was purified by column chromatography (10:1:0.1 $\text{CH}_2\text{Cl}_2/\text{MeOH}/\text{NH}_3(\text{aq})$ (25%)), and product **3c** (46 mg, 76.2 μmol , 28%) was obtained as a yellow oil. ^1H NMR (400 MHz, CDCl_3): δ 7.90 (d, J = 8.3 Hz, 1H), 7.82 (d, J = 8.3 Hz, 1H), 7.75 (s, 1H), 7.55 (t, J = 11.1, 4.0 Hz, 1H), 7.34 (t, J = 7.3 Hz, 1H), 7.29–7.26 (m, 1H), 7.18 (d, J = 8.3 Hz, 1H), 7.09 (d, J = 8.6 Hz, 2H), 6.76 (d, J = 8.6 Hz, 2H), 4.20 (s, 2H), 3.97 (t, J = 7.1 Hz, 2H), 3.87 (q, J = 7.0 Hz, 2H), 3.64–3.36 (m, 4H), 3.30 (t, J = 6.7 Hz, 2H), 3.05 (t, J = 5.8 Hz, 2H), 2.62 (t, J = 5.7 Hz, 2H), 1.9–1.83 (m, 4H), 1.61–1.49 (m, 4H), 1.30 (t, J = 7.0 Hz, 3H), 1.26–1.19 (m, 6H) ppm. ^{13}C NMR (101 MHz, CDCl_3): δ 171.8, 158.7, 157.2, 154.5, 150.3, 147.5, 142.2, 135.9, 131.3, 129.5, 128.9, 128.5, 127.9, 124.1, 122.5, 121.5, 120.6, 117.8, 116.9, 115.9, 109.5, 63.5, 48.7, 43.9, 33.9, 29.8, 28.9, 27.0, 25.0, 23.1, 22.9, 14.8, 14.2 ppm. ESI: m/z calcd for $\text{C}_{38}\text{H}_{47}\text{N}_5\text{O}_2$ [$\text{M} + 2\text{H}$] $^{2+}$, 302.69; found, 302.65; retention time, 7.92 min; HPLC purity, 98%.

2-(4-Ethoxybenzyl)-N,N-diethyl-1-(5-((1,2,3,4-tetrahydroacridin-9-yl)amino)pentyl)-1H-benzo[d]imidazole-5-carboxamide (3d).—The reaction was

carried out according to general procedure V using 3-(2-(4-ethoxyphenyl)acetamido)-*N,N*-diethyl-4-((5-((1,2,3,4-tetrahydroacridin-9-yl)amino)pentyl)amino)benzamide **19d** (346 mg, 0.47 mmol). The crude product was purified by column chromatography (10:1:0.1 CH₂Cl₂/MeOH/NH₃(aq) (25%)), and product **3d** (22 mg, 35.6 μmol, 51%) was obtained as a yellow oil. ¹H NMR (400 MHz, CDCl₃): δ 8.05–7.98 (m, 2H), 7.72 (s, 1H), 7.56 (t, *J* = 7.6 Hz, 1H), 7.33 (t, *J* = 7.7 Hz, 1H), 7.25–7.19 (m, 2H), 7.11 (d, *J* = 8.5 Hz, 2H), 6.78 (d, *J* = 8.5 Hz, 2H), 4.22 (s, 2H), 3.98 (t, *J* = 7.2 Hz, 2H), 3.92 (q, *J* = 7.0 Hz, 2H), 3.61 (t, *J* = 7.1 Hz, 2H), 3.56–3.32 (m, 4H), 3.06–3.01 (m, 2H), 2.55–2.49 (m, 2H), 1.83–1.75 (m, 4H), 1.67–1.52 (m, 4H), 1.32 (t, *J* = 7.0 Hz, 3H), 1.28–1.13 (m, 8H) ppm. ¹³C NMR (101 MHz, CDCl₃): δ 172.0, 158.2, 154.7, 154.7, 153.4, 142.1, 141.1, 135.9, 131.1, 131.1, 129.6, 128.0, 124.7, 123.9, 122.7, 121.4, 117.6, 117.3, 115.0, 112.4, 109.7, 63.6, 48.1, 44.0, 33.8, 31.1, 26.7, 29.2, 24.5, 24.2, 22.3, 21.3, 14.8, 14.1 ppm. ESI: *m/z* calcd for C₃₉H₄₉N₅O₂ [M + 2H]²⁺, 309.70; found, 309.65; retention time, 8.07 min; HPLC purity, 99%.

2-(4-Ethoxybenzyl)-*N,N*-diethyl-1-(6-((1,2,3,4-tetrahydroacridin-9-yl)amino)hexyl)-1H-benzo[d]imidazole-5-carboxamide (3e).—The reaction was carried out according to general procedure V using 3-(2-(4-ethoxyphenyl)acetamido)-*N,N*-diethyl-4-((6-((1,2,3,4-tetrahydroacridin-9-yl)amino)hexyl)amino)benzamide **19e** (142 mg, 0.22 mmol). The crude product was purified by preparative thin-layer chromatography (10:1:0.1 CH₂Cl₂/MeOH/NH₃(aq) (25%)), and product **3e** (70 mg, 0.11 mmol, 50%) was obtained as a yellow oil. ¹H NMR (400 MHz, CDCl₃): δ 7.96–7.90 (m, 2H), 7.75 (s, 1H), 7.55 (t, *J* = 8.1 Hz, 1H), 7.33 (t, *J* = 9.2 Hz, 1H), 7.30–7.27 (m, 1H), 7.25–7.22 (m, 1H), 7.11 (d, *J* = 8.6 Hz, 2H), 6.79 (d, *J* = 8.6 Hz, 2H), 4.23 (s, 2H), 3.98–3.90 (m, 4H), 3.61–3.33 (m, 6H), 3.09–3.03 (m, 2H), 2.70–2.64 (m, 2H), 1.92–1.86 (m, 4H), 1.59–1.47 (m, 4H), 1.33 (t, *J* = 7.0 Hz, 3H), 1.30–1.13 (m, 10H) ppm. ¹³C NMR (101 MHz, CDCl₃): δ 171.9, 158.2, 154.5, 151.1, 146.9, 142.19, 136.0, 131.2, 129.6, 128.7, 128.3, 128.1, 125.4, 123.9, 122.9, 121.5, 120.1, 117.7, 155.8, 115.0, 109.6, 63.6, 49.3, 44.1, 33.9, 33.7, 31.6, 29.5, 26.8, 26.7, 24.9, 23.1, 22.7, 14.9, 14.3 ppm. ESI: *m/z* calcd for C₄₀H₅₁N₅O₂ [M + 2H]²⁺, 316.70; found, 316.90; retention time, 8.27 min; HPLC purity, 95%.

2-(4-Ethoxybenzyl)-1-isopentyl-*N*-(2-((1,2,3,4-tetrahydroacridin-9-yl)amino)ethyl)-1H-benzo[d]imidazole-5-carboxamide (4a).—The reaction was carried out according to general procedure V using 2-(4-ethoxybenzyl)-1-isopentyl-1*H*-benzo[d]imidazole-5-carboxylic acid **24** (271 mg, 0.74 mmol), *N*¹-(1,2,3,4-tetrahydroacridin-9-yl)ethane-1,2-diamine **12a** (179 mg, 0.74 mmol), HBTU (281 mg, 0.74 mmol), and NEt₃ (145 μL, 1.05 mmol). The crude product was purified by preparative thin-layer chromatography (10:1:0.1 CH₂Cl₂/MeOH/NH₃(aq) (25%)), and product **4a** (35.0 mg, 59.3 μmol, 8%) was obtained as a yellow oil. ¹H NMR (400 MHz, CDCl₃): δ 8.24 (s, 1H), 8.13 (d, *J* = 8.7 Hz, 1H), 7.84 (d, *J* = 8.5 Hz, 1H), 7.62 (d, *J* = 8.6 Hz, 1H), 7.44 (t, *J* = 7.7 Hz, 1H), 7.34 (d, *J* = 8.5 Hz, 1H), 7.30–7.24 (m, 2H), 7.06 (d, *J* = 8.4 Hz, 2H), 6.70 (d, *J* = 8.4 Hz, 2H), 4.21 (s, 2H), 4.04–3.99 (m, 4H), 3.92–3.83 (m, 4H), 2.83–2.79 (m, 2H), 2.69–2.62 (m, 2H), 1.85–1.71 (m, *J* = 25.6, 5.6 Hz, 4H), 1.63–1.52 (m, 1H), 1.44–1.39 (m, 2H), 1.34 (t, *J* = 7.0 Hz, 3H), 0.90 (d, *J* = 6.6 Hz, 6H) ppm. ¹³C NMR (101 MHz, CDCl₃): δ 168.8, 158.2, 155.3, 155.0, 152.3, 147.8, 142.1, 138.0, 130.6, 129.7, 128.5, 127.5, 125.5, 124.7, 122.1, 120.0, 118.7, 117.1, 115.1, 114.9, 109.8, 63.6, 44.7, 42.5, 40.6, 38.3, 33.7,

31.5, 29.8, 26.3, 24.2, 22.5, 21.3, 14.9 ppm. ESI: m/z calcd for $C_{37}H_{45}N_5O_2$ $[M + 2H]^{2+}$: 295.68; found: 295.75; retention time: 8.96 min; HPLC purity, 96%.

2-(4-Ethoxybenzyl)-1-isopentyl-N-(3-((1,2,3,4-tetrahydroacridin-9-yl)amino)propyl)-1H-benzo[d]imidazole-5-carboxamide (4b).—The reaction was carried out according to general procedure V using 2-(4-ethoxybenzyl)-1-isopentyl-1H-benzo[d]imidazole-5-carboxylic acid **24** (370 mg, 1.01 mmol), N^1 -(1,2,3,4-tetrahydroacridin-9-yl)propane-1,3-diamine **12b** (200 mg, 0.78 mmol), HBTU (326 mg, 1.33 mmol), and NEt_3 (184 μL , 1.33 mmol). The crude product was purified by column chromatography (20:1:0.1 $CH_2Cl_2/MeOH/NH_3(aq)$ (25%)), and product **4b** (67.0 mg, 0.11 mmol, 14%) was obtained as a yellow oil. 1H NMR (400 MHz, $CDCl_3$): δ 8.37 (s, 1H), 8.24 (d, $J = 8.7$ Hz, 1H), 8.20 (d, $J = 8.4$ Hz, 1H), 7.97 (d, $J = 8.5$ Hz, 1H), 7.54 (t, $J = 7.7$ Hz, 1H), 7.35 (t, $J = 7.8$ Hz, 1H), 7.25 (d, $J = 10.0$ Hz, 1H), 7.08 (d, $J = 8.4$ Hz, 2H), 6.76 (d, $J = 8.4$ Hz, 2H), 4.19 (s, 2H), 3.97–3.88 (m, 6H), 3.71–3.65 (m, 2H), 3.–3.09 (m, 2H), 2.75 (t, $J = 5.8$ Hz, 2H), 2.07–2.00 (m, 2H), 1.85–1.74 (m, 4H), 1.57–1.48 (m, 1H), 1.35 (t, $J = 7.0$ Hz, 3H), 1.33–1.24 (m, 2H), 0.87 (d, $J = 6.6$ Hz, 6H) ppm. ^{13}C NMR (101 MHz, $CDCl_3$): δ 169.4, 158.2, 155.5, 155.0, 152.0, 148.3, 142.3, 137.7, 131.6, 129.6, 128.1, 127.8, 125.0, 124.2, 122.2, 119.1, 117.8, 116.6, 115.6, 114.9, 109.4, 63.6, 44.3, 42.8, 38.2, 36.2, 36.7, 33.8, 31.2, 29.3, 26.2, 24.6, 22.5, 21.1, 14.9 ppm. ESI: m/z calcd for $C_{38}H_{47}N_5O_2$ $[M + 2H]^{2+}$, 302.69; found, 302.75; retention time, 8.82 min; HPLC purity, 98%.

2-(4-Ethoxybenzyl)-1-isopentyl-N-(4-((1,2,3,4-tetrahydroacridin-9-yl)amino)butyl)-1H-benzo[d]imidazole-5-carboxamide (4c).—The reaction was carried out according to general procedure V using 2-(4-ethoxybenzyl)-1-isopentyl-1H-benzo[d]imidazole-5-carboxylic acid **24** (286 mg, 0.78 mmol), N^1 -(1,2,3,4-tetrahydroacridin-9-yl)butane-1,4-diamine **12c** (161 mg, 0.60 mmol), HBTU (250 mg, 0.66 mmol), and NEt_3 (141 μL , 1.02 mmol). The crude product was purified by preparative thin-layer chromatography (10:1:0.1 $CH_2Cl_2/MeOH/NH_3(aq)$ (25%)), and product **4c** (38.0 mg, 0.62 mmol, 10%) was obtained as a yellow oil. 1H NMR (400 MHz, $CDCl_3$): δ 8.26 (s, 1H), 8.18 (d, $J = 8.7$ Hz, 1H), 8.07 (d, $J = 8.4$ Hz, 1H), 7.86 (d, $J = 8.5$ Hz, 1H), 7.51 (t, $J = 7.6$ Hz, 1H), 7.32 (t, $J = 7.6$ Hz, 1H), 7.23 (d, $J = 8.5$ Hz, 1H), 7.06 (d, $J = 8.6$ Hz, 2H), 6.72 (d, $J = 8.4$ Hz, 2H), 4.18 (s, 2H), 3.96–3.88 (m, 6H), 3.56–3.49 (m, 2H), 3.03 (t, $J = 5.9$ Hz, 2H), 2.60 (t, $J = 5.7$ Hz, 2H), 1.96–1.88 (m, 2H), 1.81–1.70 (m, 6H), 1.56–1.48 (m, 1H), 1.34 (t, $J = 7.0$ Hz, 3H), 1.31–1.23 (m, 2H), 0.86 (d, $J = 6.6$ Hz, 6H) ppm. ^{13}C NMR (101 MHz, $CDCl_3$): δ 168.4, 158.2, 155.8, 154.9, 153.2, 142.9, 142.1, 137.5, 132.2, 129.6, 128.6, 127.7, 125.1, 124.7, 122.1, 120.5, 118.6, 116.5, 116.0, 114.9, 109.4, 63.6, 47.9, 42.8, 39.3, 38.3, 33.7, 29.8, 28.6, 28.1, 26.8, 26.2, 23.9, 22.4, 20.8, 14.9 ppm. ESI: m/z calcd for $C_{39}H_{49}N_5O_2$ $[M + 2H]^{2+}$, 309.70; found, 309.70; retention time, 8.77 min; HPLC purity, 98%.

2-(4-Ethoxybenzyl)-1-isopentyl-N-(5-((1,2,3,4-tetrahydroacridin-9-yl)amino)pentyl)-1H-benzo[d]imidazole-5-carboxamide (4d).—The reaction was carried out according to general procedure V using 2-(4-ethoxybenzyl)-1-isopentyl-1H-benzo[d]imidazole-5-carboxylic acid **24** (286 mg, 0.78 mmol), N^1 -(1,2,3,4-tetrahydroacridin-9-yl)pentane-1,5-diamine **12d** (170 mg, 0.60 mmol), HBTU (250 mg, 0.66

mmol), and NEt_3 (141 μL , 1.02 mmol). The crude product was purified by column chromatography (20:1:0.1 $\text{CH}_2\text{Cl}_2/\text{MeOH}/\text{NH}_3(\text{aq})$ (25%)), and product **4d** (57.0 mg, 0.32 mmol, 15%) was obtained as a yellow oil. ^1H NMR (400 MHz, CDCl_3): δ 8.15 (d, $J = 8.7$ Hz, 1H), 8.04 (s, 1H), 7.85 (d, $J = 8.5$, 1H), 7.82–7.77 (m, 1H), 7.60 (t, $J = 7.3$ Hz, 1H), 7.40–7.34 (m, 2H), 7.08 (d, $J = 8.1$ Hz, 2H), 6.67 (d, $J = 7.0$ Hz, 2H), 4.28 (s, 2H), 4.10–4.04 (m, 2H), 3.91–3.84 (m, 4H), 3.49–3.45 (m, 2H), 2.89–2.85 (m, 2H), 2.43–2.38 (m, 2H), 1.90–1.85 (m, 2H), 1.65–1.58 (m, 2H), 1.60–1.56 (m, 4H), 1.46–1.43 (m, 1H), 1.32 (t, $J = 7.0$ Hz, 4H), 1.26–1.25 (m, 5H), 0.94 (d, $J = 6.8$ Hz, 6H) ppm. ^{13}C NMR (101 MHz, CDCl_3): δ 169.5, 158.2, 155.5, 154.2, 153.6, 143.3, 142.3, 137.4, 130.7, 129.8, 128.5, 127.4, 125.2, 124.2, 122.5, 119.7, 118.0, 117.3, 115.8, 114.9, 109.9, 63.6, 47.5, 43.0, 39.2, 38.3, 33.1, 29.8, 29.0, 28.2, 27.9, 26.8, 26.3, 23.6, 22.5, 20.4, 14.9 ppm. ESI: m/z calcd for $\text{C}_{40}\text{H}_{51}\text{N}_5\text{O}_2$ $[\text{M} + 2\text{H}]^{2+}$, 316.70; found, 316.75; retention time, 8.82 min; HPLC purity, 98%.

2-(4-Ethoxybenzyl)-1-isopentyl-N-(6-((1,2,3,4-tetrahydroacridin-9-yl)amino)hexyl)-1H-benzo[d]imidazole-5-carboxamide (4e).—The reaction was carried out according to general procedure V using 2-(4-ethoxybenzyl)-1-isopentyl-1H-benzo[d]imidazole-5-carboxylic acid **24** (114 mg, 0.31 mmol), N^1 -(1,2,3,4-tetrahydroacridin-9-yl)hexane-1,6-diamine **12e** (92.2 mg, 0.31 mmol), HBTU (118 mg, 0.31 mmol), and NEt_3 (65.1 μL , 0.47 mmol). The crude product was purified by column chromatography (20:1:0.1 $\text{CH}_2\text{Cl}_2/\text{MeOH}/\text{NH}_3(\text{aq})$ (25%)), and product **4e** (40.0 mg, 61.9 μmol , 20%) was obtained as a yellow oil. ^1H NMR (400 MHz, CDCl_3): δ 8.11 (s, 1H), 8.05 (d, $J = 8.2$ Hz, 1H), 7.78–7.75 (m, 2H), 7.55–7.50 (m, 1H), 7.37–7.32 (m, 1H), 7.29–7.26 (m, 1H), 7.08 (d, $J = 8.8$ Hz, 2H), 6.74 (d, $J = 8.8$ Hz, 2H), 4.21 (s, 2H), 4.02–3.86 (m, 6H), 3.64 (t, $J = 6.6$ Hz, 2H), 3.47–3.40 (m, 2H), 2.62 (t, $J = 5.7$ Hz, 2H), 1.87–1.80 (m, 4H), 1.75–1.68 (m, 2H), 1.65–1.59 (m, 2H), 1.56–1.51 (m, 1H), 1.42–1.32 (m, 9H), 0.88 (d, $J = 6.6$ Hz, 6H) ppm. ^{13}C NMR (101 MHz, CDCl_3): δ 168.3, 158.2, 155.2, 154.7, 153.4, 143.3, 142.2, 137.5, 130.5, 129.6, 128.9, 127.7, 124.4, 124.0, 122.0, 118.1, 118.0, 117.0, 115.1, 114.9, 109.6, 63.6, 48.9, 42.8, 42.5, 39.9, 38.2, 36.6, 33.8, 31.3, 31.1, 29.5, 26.4, 26.2, 24.1, 22.4, 21.8, 14.9 ppm. ESI: m/z calcd for $\text{C}_{41}\text{H}_{53}\text{N}_5\text{O}_2$ $[\text{M} + 2\text{H}]^{2+}$, 323.71; found, 323.80; retention time, 8.94 min; HPLC purity, 95%.

2-(4-Ethoxybenzyl)-N-ethyl-1-isopentyl-N-(4-((1,2,3,4-tetrahydroacridin-9-yl)amino)butyl)-1H-benzo[d]imidazole-5-carboxamide (5).—The reaction was carried out according to general procedure V using 2-(4-ethoxybenzyl)-1-isopentyl-1H-benzo[d]imidazole-5-carboxylic acid **24** (23.7 mg, 64.6 μmol), N^1 -ethyl- N^4 -(1,2,3,4-tetrahydroacridin-9-yl)butane-1,4-diamine **14** (16.0 mg, 53.8 μmol), HBTU (24.5 mg, 64.6 μmol), and NEt_3 (14.9 μL , 0.11 mmol). The solvent was removed in vacuo, and the residue was dissolved in CH_2Cl_2 and washed with $\text{NaHCO}_3(\text{aq})$. The crude product was purified by preparative TLC (20:1:0.1 $\text{CH}_2\text{Cl}_2/\text{MeOH}/\text{NH}_3(\text{aq})$ (25%)). The product **5** (21 mg, 32.5 μmol , 60%) was obtained as a brown oil. ^1H NMR (400 MHz, CDCl_3): δ 7.89 (d, $J = 8.1$ Hz, 1H), 7.75–7.73 (s, 1H), 7.56–7.51 (m, 1H), 7.36–7.30 (m, 1H), 7.27–7.23 (m, 3H), 7.14 (d, $J = 8.6$ Hz, 2H), 6.82 (d, $J = 8.6$ Hz, 2H), 4.24 (s, 2H), 4.02–3.95 (m, 4H), 3.58–3.42 (m, 4H), 3.08–3.03 (m, 2H), 2.77–2.69 (m, 2H), 1.94–1.88 (m, 4H), 1.83–1.65 (m, 6H), 1.59–1.51 (m, 1H), 1.41–1.35 (m, 6H), 1.29–1.23 (m, 2H), 0.90 (d, $J = 6.6$ Hz, 6H) ppm. ^{13}C NMR

(101 MHz, CDCl₃): δ 168.4, 158.2, 155.4, 154.8, 153.7, 142.2, 142.2, 137.5, 130.5, 129.6, 128.9, 127.9, 125.0, 124.0, 121.3, 119.9, 117.8, 116.9, 115.2, 115.0, 109.7, 63.6, 52.4, 48.0, 44.1, 42.8, 41.1, 38.3, 33.9, 30.5, 28.3, 26.3, 24.2, 22.5, 22.3, 21.2, 14.9, 14.2. ppm. ESI: m/z calcd for C₄₁H₃₂N₅O₂ [M + 1H]¹⁺, 646.41; found, 646.25; retention time 8.94 min; HPLC purity, 99%.

2-(4-Ethoxybenzyl)-N,N-diethyl-1-(2-(2-(2-((1,2,3,4-tetrahydroacridin-9-yl)amino)ethoxy)ethoxy)ethyl)-1H-benzo[d]imidazole-5-carboxamide (6).—

The reaction was carried out according to general procedure V using 3-(2-(4-ethoxyphenyl)acetamido)-*N,N*-diethyl-4-((2-(2-(2-((1,2,3,4-tetrahydroacridin-9-yl)amino)ethoxy)ethoxy)-ethyl)amino)benzamide **19f** (398 mg, 0.58 mmol). The crude product was purified by column chromatography (CH₂Cl₂/MeOH/NH₃(aq) (25%) 16:1:0.1), and product **6** (220 mg, 33.1 mmol, 57%) was obtained as a brown oil. ¹H NMR (400 MHz, CDCl₃): δ 7.95–7.89 (m, 2H), 7.68 (s, 1H), 7.50 (t, J =6.9 Hz, 1H), 7.31–7.27 (m, 1H), 7.22 (d, J =8.3, 1H), 7.07 (d, J =8.4 Hz, 2H), 6.73 (d, J =8.4 Hz, 2H), 4.25 (s, 2H), 4.13 (t, J =5.4 Hz, 2H), 3.90 (q, J =7.0 Hz, 2H), 3.58 (t, J =5.1 Hz, 2H), 3.51 (t, J =5.4 Hz, 2H), 3.46–3.41 (m, 4H), 3.54–3.32 (m, 4H), 3.39–3.35 (m, 2H), 3.02 (t, J =6.0 Hz, 2H), 2.62 (t, J =5.9 Hz, 2H), 1.86–1.75 (m, 4H), 1.31 (t, J =7.0 Hz, 3H), 1.21–1.06 (m, 6H) ppm. ¹³C NMR (101 MHz, CDCl₃): δ 171.7, 158.0, 157.1, 155.3, 151.6, 145.5, 142.0, 135.1, 131.1, 129.5, 129.1, 127.9, 126.9, 124.1, 123.0, 122.2, 119.7, 117.4, 116.4, 114.8, 109.8, 70.8, 70.3, 69.4, 63.4, 48.2, 14.1 ppm. ESI: m/z calcd for C₄₀H₅₁N₅O₄ [M + 2H]²⁺, 332.70; found, 332.70; retention time, 7.89 min; HPLC purity, 99%.

2-(4-Ethoxybenzyl)-1-isopentyl-N-(2-(2-(2-((1,2,3,4-tetrahydroacridin-9-yl)amino)ethoxy)ethoxy)ethyl)-1H-benzo[d]imidazole-5-carboxamide (7).—

The reaction was carried out according to general procedure V using 2-(4-ethoxybenzyl)-1-isopentyl-1*H*-benzo[*d*]-imidazole-5-carboxylic acid **24** (40 mg, 0.11 mmol), *N*-(2-(2-(2-aminoethoxy)ethoxy)ethyl)-1,2,3,4-tetrahydroacridin-9-amine **12f** (36.2 mg, 0.11 mmol), HBTU (41.7 mg, 0.11 mmol), and NEt₃ (23.6 μ L, 0.17 mmol). The crude product was purified by column chromatography (16:1:0.1 CH₂Cl₂/MeOH/NH₃(aq) (25%)), and product **7** (33.0 mg 48.7 μ mol, 44%) was obtained as a brown oil. ¹H NMR (400 MHz, CDCl₃): δ 8.08 (s, 1H), 8.00 (d, J =8.1 Hz, 1H), 7.94 (d, J =8.4 Hz, 1H), 7.72 (d, J =8.5, 1H), 7.56–7.52 (m, 1H), 7.32 (t, J =8.0, 1H), 7.15 (d, J =8.5 Hz, 1H), 7.08 (d, J =8.6 Hz, 2H), 6.76 (d, J =8.7 Hz, 2H), 4.17 (s, 2H), 3.95–3.90 (m, 4H), 3.85–3.81 (m, 2H), 3.72–3.67 (m, 10H), 3.02–2.98 (m, 2H), 2.58 (t, J =7.8 Hz, 2H), 1.85–1.78 (m, 4H), 1.56–1.49 (m, 1H), 1.35 (t, J =7.0 Hz, 3H), 1.30–1.27 (m, 2H), 0.86 (d, J =6.6 Hz, 6H) ppm. ¹³C NMR (101 MHz, CDCl₃): δ 168.0, 158.2, 155.2, 154.95, 153.3, 143.0, 142.1, 137.5, 130.5, 129.7, 128.5, 127.7, 124.6, 123.7, 122.1, 118.4, 117.9, 117.0, 114.7, 114.9, 109.5, 70.4, 70.3, 70.0, 69.9, 63.6, 48.1, 42.8, 39.8, 38.2, 33.8, 31.2, 29.8, 26.2, 23.9, 22.4, 21.8, 14.9 ppm. ESI: m/z calcd for C₄₁H₅₃N₅O₄ [M + 2H]²⁺, 339.80; found, 339.70; retention time, 8.75 min; HPLC purity, 98%.

2-(4-Ethoxybenzyl)-1-isopentyl-N-(2-((2-((1,2,3,4-tetrahydroacridin-9-yl)amino)ethyl)disulfaneyl)ethyl)-1H-benzo[d]imidazole-5-carboxamide (8).—

The reaction was carried out according to general procedure V using 2-(4-ethoxybenzyl)-1-

isopentyl-1*H*-benzo[*d*]-imidazole-5-carboxylic acid **24** (48 mg, 0.13 mmol), *N*-(2-((2-aminoethyl)disulfanyl)ethyl)-1,2,3,4-tetrahydroacridin-9-amine (35 mg, 0.11 mmol), HBTU (49 mg, 0.13 mmol), and NEt₃ (26 μL, 0.19 mmol). The crude product was purified by preparative thin-layer chromatography (18:1:0.1 CH₂Cl₂/MeOH/NH₃(aq) (25%)), and product **8** (35 mg, 51.4 μmol, 47%) was obtained as a yellow oil. ¹H NMR (400 MHz, CDCl₃): δ = 8.15 (d, *J* = 1.3 Hz, 1H), 8.00–7.96 (m, 1H), 7.84 (dd, *J* = 8.5, 0.8 Hz, 1H), 7.77 (dd, *J* = 8.5, 1.6 Hz, 1H), 7.53–7.50 (m, 1H), 7.35–7.32 (m, 1H), 7.29–7.25 (m, 1H), 7.13–7.08 (m, 2H), 6.86 (t, *J* = 5.8 Hz, 1H), 6.80–6.76 (m, 2H), 4.23 (s, 2H), 4.01–3.92 (m, 4H), 3.89–3.82 (m, 2H), 3.75 (q, *J* = 6.3 Hz, 2H), 3.04–2.96 (m, 2H), 2.95–2.86 (m, 4H), 2.71 (s, 2H), 1.86 (t, *J* = 2.8 Hz, 4H), 1.62–1.50 (m, 1H), 1.42–1.33 (m, 5H), 0.88 (d, *J* = 5.3 Hz, 6H) ppm. ¹³C NMR (101 MHz, CDCl₃): δ 168.3, 158.2, 157.4, 155.3, 151.2, 145.8, 142.3, 137.7, 129.6, 129.4, 128.4, 127.7, 127.1, 124.4, 123.1, 122.1, 119.9, 118.2, 116.6, 115.0, 109.6, 63.6, 46.9, 42.9, 39.0, 38.9, 38.2, 37.9, 33.8, 33.0, 26.3, 24.8, 22.8, 22.5, 14.9 ppm. ESI: *m/z* calcd for C₃₉H₄₉N₅O₂S₂ [M + 2H]²⁺, 341.66; found, 341.70; retention time, 9.38 min; HPLC purity, 96%.

9-Chloro-1,2,3,4-tetrahydroacridine (11).—2-Aminobenzoic acid **9** (1.00 g, 7.29 mmol) and cyclohexanone **10** (883 μL, 8.53 mmol) were combined in a flask and cooled down to 0 °C. Then, POCl₃ (8.00 mL) was slowly added. Afterward, the mixture was stirred for 3 h under reflux conditions and then concentrated to a slurry in vacuo. The slurry was dissolved in ethyl acetate and neutralized with aqueous sodium hydroxide. The mixture was extracted with ethyl acetate. The organic layers were combined and dried over anhydrous MgSO₄, and the solvent was removed in vacuo. The crude product was purified by recrystallization from acetone. The product **11** (988 mg, 4.54 mmol, 62%) was obtained as a brown solid. mp = 66 °C. ¹H NMR (400 MHz, CDCl₃): δ 8.17 (d, *J* = 8.4, 1H), 7.98 (d, *J* = 8.5 Hz, 1H), 7.69–7.63 (m, 1H), 7.56–7.50 (m, 1H), 3.13 (t, *J* = 5.6 Hz, 2H), 3.03 (t, *J* = 6.4 Hz, 2H), 1.97–1.93 (m, 4H) ppm. ¹³C NMR (101 MHz, CDCl₃): δ 159.4, 146.2, 141.8, 129.4, 128.9, 128.3, 126.6, 125.4, 123.7, 33.9, 27.5, 22.6, 21.5 ppm. ESI: *m/z* calcd for C₁₃H₁₃ClN [M + H]⁺, 218.07; found, 218.00; retention time, 9.97 min.

N¹-(1,2,3,4-Tetrahydroacridin-9-yl)ethane-1,2-diamine (12a).—The reaction was carried out according to general procedure I using 9-chloro-1,2,3,4-tetrahydroacridine **11** (800 mg, 3.67 mmol) and ethane-1,2-diamine (1.23 mL, 18.35 mmol). The product **12a** (557 mg, 2.31 mmol, 63%) was obtained as a brown oil. ¹H NMR (400 MHz, CDCl₃): δ 7.94 (d, *J* = 8.4 Hz, 1H), 7.85 (d, *J* = 8.5 Hz, 1H), 7.48 (t, *J* = 10.0, 5.1 Hz, 1H), 7.26 (t, 1H), 4.75 (s, 1H), 3.43–3.36 (m, 2H), 3.03–2.97 (m, 2H), 2.89–2.81 (m, 2H), 2.72–2.65 (m, 2H), 1.86–1.80 (m, 4H) ppm. ¹³C NMR (101 MHz, CDCl₃): δ 157.5, 149.9, 146.4, 127.7, 127.2, 122.6, 121.8, 119.5, 115.5, 50.0, 41.4, 33.0, 23.8, 22.0, 21.8 ppm. ESI: *m/z* calcd for C₁₅H₂₀N₃ [M + H]⁺, 242.17; found, 242.10; retention time, 4.09 min.

N¹-(1,2,3,4-Tetrahydroacridin-9-yl)propane-1,3-diamine (12b).—The reaction was carried out according to general procedure I using 9-chloro-1,2,3,4-tetrahydroacridine **11** (600 mg, 2.76 mmol) and propane-1,3-diamine (1.15 mL, 13.8 mmol). The product **12b** (530 mg, 1.97 mmol, 80%) was obtained as a brown oil (417 mg, 1.63 mmol, 59%). ¹H NMR (400 MHz, CDCl₃): δ 7.87 (m, 1H), 7.83–7.79 (m, 1H), 7.46–7.39 (m, 1H), 7.24–7.19

(1 H), 3.48 (t, $J = 6.7$ Hz, 2H), 3.01 (t, $J = 6.1$ Hz, 2H), 2.89 (t, $J = 6.2$ Hz, 2H), 2.60 (t, $J = 5.9$ Hz, 2H), 1.85–1.76 (m, 4H), 1.85–1.76 (m, 2H) ppm. ^{13}C NMR (101 MHz, CDCl_3): δ 157.3, 149.9, 146.3, 127.6, 127.2, 122.6, 121.9, 119.1, 114.8, 47.0, 39.4, 33.1, 26.4, 24.1, 22.1, 21.8 ppm. ESI: m/z calcd for $\text{C}_{16}\text{H}_{22}\text{N}_3$ $[\text{M} + \text{H}]^+$, 256.18; found, 256.10; retention time, 4.26 min.

N^1 -(1,2,3,4-Tetrahydroacridin-9-yl)butane-1,4-diamine (12c).—The reaction was carried out according to general procedure I using 9-chloro-1,2,3,4-tetrahydroacridine **11** (535 mg, 2.45 mmol) and butane-1,4-diamine (1.08 g, 12.3 mmol). The product **12c** (530 mg, 1.97 mmol, 80%) was obtained as a brown oil. ^1H NMR (400 MHz, CDCl_3): δ 7.99–7.92 (m, 2H), 7.57–7.52 (m, 1H), 7.36–7.31 (m, 1H), 3.53 (t, $J = 7.1$ Hz, 2H), 3.07 (t, $J = 6.3$ Hz, 2H), 2.76 (t, $J = 6.9$ Hz, 2H), 2.71 (t, $J = 6.2$ Hz, 2H), 1.93–1.88 (m, 4H), 1.76–1.68 (m, 2H), 1.61–1.52 (m, 2H) ppm. ^{13}C NMR (101 MHz, CDCl_3): δ 157.9, 151.1, 146.7, 128.6, 128.1, 123.7, 122.9, 119.9, 115.6, 49.29, 41.72, 33.56, 30.76, 29.06, 24.82, 22.98, 22.61 ppm. ESI: m/z calcd for $\text{C}_{17}\text{H}_{24}\text{N}_3$ $[\text{M} + \text{H}]^+$, 270.20; found, 270.10; retention time, 4.26 min.

N^1 -(1,2,3,4-Tetrahydroacridin-9-yl)pentane-1,5-diamine (12d).—The reaction was carried out according to general procedure I using 9-chloro-1,2,3,4-tetrahydroacridine **11** (600 mg, 2.76 mmol) and pentane-1,5-diamine (1.62 mL, 13.8 mmol). The product **12d** (427 mg, 1.51 mmol, 55%) was obtained as a brown oil. ^1H NMR (400 MHz, CDCl_3): δ 8.09 (d, $J = 8.4$ Hz, 1H), 7.91–7.86 (m, 1H), 7.62–7.56 (m, 1H), 7.30–7.24 (m, 1H), 3.41 (t, $J = 7.0$ Hz, 2H), 3.07–3.03 (m, 2H), 3.02–2.98 (m, 2H), 2.96–2.89 (m, 2H), 2.66–2.60 (m, 4H), 1.62–1.39 (m, 6H) ppm. ^{13}C NMR (101 MHz, CDCl_3): δ 158.5, 150.6, 146.6, 128.6, 128.2, 123.5, 122.7, 120.3, 115.9, 49.3, 41.9, 33.2, 32.8, 31.7, 27.4, 24.8, 23.0, 22.6, ppm. ESI: m/z calcd for $\text{C}_{18}\text{H}_{26}\text{N}_3$ $[\text{M} + \text{H}]^+$, 284.21; found, 284.15; retention time, 4.66 min.

N^1 -(1,2,3,4-Tetrahydroacridin-9-yl)hexane-1,6-diamine (12e).—The reaction was carried out according to general procedure I using 9-chloro-1,2,3,4-tetrahydroacridine **11** (500 mg, 2.30 mmol) and hexane-1,6-diamine (1.50 mL, 11.5 mmol). The product **12e** was obtained as a brown oil (343 mg, 1.15 mmol, 50%). ^1H NMR (400 MHz, CDCl_3): δ 7.94 (d, $J = 8.4$ Hz, 1H), 7.89 (d, $J = 8.4$ Hz, 1H), 7.53 (t, $J = 6.8$ Hz, 1H), 7.32 (t, $J = 6.8$ Hz, 1H), 3.47 (t, $J = 7.2$ Hz, 2H), 3.04 (t, $J = 6.5$ Hz, 2H), 2.72–2.65 (m, 4H), 1.92–1.88 (m, 4H), 1.69–1.60 (m, 2H), 1.46–1.35 (m, 6H) ppm. ^{13}C NMR (101 MHz, CDCl_3): δ 158.8, 151.0, 147.74, 129.0, 128.8, 124.1, 123.3, 120.6, 116.2, 49.9, 42.5, 34.4, 32.2, 27.3, 27.1, 25.2, 23.4, 23.2 ppm. ESI: m/z calcd for $\text{C}_{19}\text{H}_{28}\text{N}_3$ $[\text{M} + 2\text{H}]^{2+}$, 149.62; found, 149.65; retention time, 5.38 min.

N -(2-(2-(2-Aminoethoxy)ethoxy)ethyl)-1,2,3,4-tetrahydroacridin-9-amine (12f).—The reaction was carried out according to general procedure I using 9-chloro-1,2,3,4-tetrahydroacridine **11** (600 mg, 2.76 mmol) and 2,2'-(ethane-1,2-diylbis(oxy))bis(ethan-1-amine) (2.00 mL, 13.8 mmol). The product **12f** (864 mg, 2.62 mmol, 95%) was obtained as a brown oil. ^1H NMR (400 MHz, CDCl_3): δ = 7.95 (d, $J = 8.5$ Hz, 1H), 7.89 (d, $J = 8.5$ Hz, 1H), 7.58–7.59 (m, 1H), 7.37–7.30 (m, 1H), 3.67–3.56 (m, 8H), 3.50 (t, $J = 5.2$ Hz, 2H), 3.05 (t, $J = 6.0$ Hz, 2H), 2.88–2.84 (m, 2H), 2.76 (t, $J = 5.7$ Hz, 2H), 1.94–1.86 (m, 4H) ppm.

^{13}C NMR (101 MHz, CDCl_3): δ 158.7, 150.4, 147.5, 128.8, 128.2, 123.8, 122.7, 120.8, 117.5, 73.6, 70.5, 70.3, 70.3, 48.6, 41.8, 24.7, 23.1, 22.9, 22.6 ppm. ESI: m/z calcd for $\text{C}_{19}\text{H}_{28}\text{N}_3\text{O}_2$ $[\text{M} + \text{H}]^+$, 330.22; found, 330.05; retention time, 4.60 min.

N-(2-((2-Aminoethyl)disulfaneyl)ethyl)-1,2,3,4-tetrahydroacridin-9-amine (12g).

—2,2'-Dithiobis(ethylamine)dihydrochloride (608 mg, 2.70 mmol) was suspended in hexanol, and NEt_3 (1.49 mL, 10.8 mmol) was added. The reaction vessel was closed and stirred for 30 min at 160 °C. Then, 9-chloro-1,2,3,4-tetrahydroacridine **11** (117 mg, 0.54 mg) was added, and the mixture was stirred for further 12 h at 160 °C. The solvent was removed under high vacuum at 60 °C. The crude product was purified using RP flash chromatography to yield **12g** (80 mg, 0.33 mmol, 44%) as a pale yellow oil. ^1H NMR (400 MHz, MeOD): δ 8.44 (d, $J=8.7$ Hz, 1H), 7.88–7.86 (m, 2H), 7.65–7.61 (m, 1H), 4.33 (t, $J=6.6$ Hz, 2H), 3.34–3.29 (m, 2H), 3.24 (t, $J=6.6$ Hz, 2H), 3.08 (t, $J=5.3$ Hz, 2H), 3.03 (t, $J=6.9$ Hz, 2H), 2.79 (t, $J=5.7$ Hz, 2H), 2.02–1.94 (m, 4H) ppm. ^{13}C NMR (101 MHz, MeOD): $\delta=156.8, 151.0, 138.2, 132.8, 125.3, 124.9, 118.9, 115.9, 112.3, 46.29, 38.0, 36.7, 33.7, 28.1, 23.9, 21.6, 20.4$ ppm. ESI: m/z calcd for $\text{C}_{17}\text{H}_{24}\text{N}_3\text{S}_2$ $[\text{M} + \text{H}]^+$, 334.14; found, 334.00; retention time, 5.31 min.

N-(4-((1,2,3,4-Tetrahydroacridin-9-yl)amino)butyl)acetamide (13).— N^1 -(1,2,3,4-

Tetrahydroacridin-9-yl)butane-1,4-diamine **12c** (51.0 mg, 0.19 mmol) was dissolved in CH_2Cl_2 , and acetic acid anhydride (359 μL , 3.80 mmol) was added at room temperature. After stirring for 5 min, the mixture was basified by washing with a saturated NaHCO_3 solution. The organic layer was dried over anhydrous MgSO_4 and concentrated in vacuo. The product **13** (59.2 mg, 0.19 mmol, quant.) was obtained as a pale yellow oil. ^1H NMR (400 MHz, CDCl_3): δ 8.13–8.10 (m, 1H), 7.95–7.91 (m, 1H), 7.53–7.48 (m, 1H), 7.34–7.30 (m, 1H), 3.79 (t, $J=7.1$ Hz, 2H), 3.26 (q, $J=6.5$ Hz, 2H), 2.99 (t, $J=6.0$ Hz, 2H), 2.55 (t, $J=5.7$ Hz, 2H), 1.84–1.75 (m, 6H), 1.66–1.59 (m, 2H), 1.23 (s, 3H) ppm. ^{13}C NMR (101 MHz, CDCl_3): δ 171.2, 155.11, 151.7, 139.3, 131.6, 124.7, 124.3, 120.8, 116.2, 111.3, 47.8, 38.7, 28.5, 28.1, 26.5, 24.1, 23.1, 22.0, 20.8 ppm. ESI: m/z calcd for $\text{C}_{19}\text{H}_{26}\text{N}_3\text{O}$ $[\text{M} + \text{H}]^+$, 312.21; found, 312.05; retention time, 6.58 min.

N^1 -Ethyl- N^4 -(1,2,3,4-tetrahydroacridin-9-yl)butane-1,4-diamine (14).—

N^1 -(4-((1,2,3,4-Tetrahydroacridin-9-yl)amino)butyl)acetamide **13** (218 mg, 0.70 mmol) was dissolved in dry THF. LiAlH_4 (133 mg, 3.50 mmol) was added, the mixture was stirred for 48 h under reflux conditions, and then $\text{NH}_3(\text{aq})$ (25%) was carefully added to the mixture on ice. The mixture was concentrated in vacuo, dissolved in ethyl acetate, and washed with a mixture of water/ $\text{NH}_3(\text{aq})$ (25%) (1:1). The combined organic layers were dried over anhydrous MgSO_4 and concentrated in vacuo. The crude product was purified by column chromatography (4:1:0.1 $\text{CH}_2\text{Cl}_2/\text{MeOH}/\text{NH}_3(\text{aq})$ (25%)). The product **14** (144 mg, 0.48 mmol, 69%) was obtained as a yellow oil. ^1H NMR (400 MHz, CDCl_3): δ 7.98–7.90 (m, 2H), 7.56–7.51 (m, 1H), 7.35–7.29 (m, 1H), 3.52 (t, $J=6.8$ Hz, 2H), 3.07–3.03 (m, 2H), 2.72–2.65 (m, 6H), 1.92–1.86 (m, 4H), 1.76–1.61 (m, 4H), 1.14 (t, $J=$ Hz, 3H) ppm. ^{13}C NMR (101 MHz, CDCl_3): $\delta=157.8, 151.2, 146.6, 128.7, 127.9, 123.8, 123.0, 119.9, 115.6, 49.2, 49.0, 44.0, 33.5, 29.3, 27.1, 24.8, 23.0, 22.6, 14.7$ ppm. ESI: m/z calcd for $\text{C}_{19}\text{H}_{28}\text{N}_3$ $[\text{M} + 2\text{H}]^{2+}$, 149.62; found, 149.65; retention time, 4.77 min.

N,N-Diethyl-4-fluoro-3-nitrobenzamide (16).—4-Fluoro-3-nitrobenzoic acid **15** (1.00 g, 5.4 mmol) was dissolved in CH₂O₂ and cooled down to 0 °C. A catalytic amount of *N,N*-dimethylformamide was added, and oxalylchloride (2.31 mL, 27.01 mmol) was added dropwise. The mixture was stirred for 10 min at 0 °C, allowed to come to room temperature, and then stirred again for 1 h. The mixture was then evaporated, and the residue was dissolved in CH₂Cl₂ and cooled down to 0 °C. Then, a mixture of HNEt₂ (621 μL, 1.1 mmol) and NEt₃ (2.24 mL, 16.2 mmol) in CH₂Cl₂ was slowly added to the cold mixture. After stirring for 3 h at room temperature, the mixture was washed with water. The combined organic layers were dried over anhydrous MgSO₄ and concentrated in vacuo. The product **16** (918 mg, 3.82 mmol, 71%) was obtained as a yellow oil. ¹H NMR (400 MHz, CDCl₃): δ 8.11 (d, *J* = 7.0 Hz, 1H), 7.66–7.70 (m, 1 H), 7.35 (d, *J* = 10.4 Hz, 1H), 3.65–3.18 (m, 4H), 1.30–1.11 (m, 6H) ppm. ¹³C NMR (101 MHz, CDCl₃): δ 167.5, 156.8, 154.1, 136.9, 133.8, 124.4, 118.8, 43.4, 14.0 ppm. ESI: *m/z* calcd for C₁₁H₁₄FN₂O₃ [M + H]⁺, 241.10; found, 241.10.

N,N-Diethyl-3-nitro-4-((2-((1,2,3,4-tetrahydroacridin-9-yl)-amino)ethyl)amino)benzamide (17a).—The reaction was carried out according to general procedure II using *N,N*-diethyl-4-fluoro-3-nitrobenzamide **16** (351 mg, 1.46 mmol), **12a** (388 mg, 1.61 mmol), and NEt₃ (304 μL, 2.19 mmol). The crude product was purified by column chromatography (20:1:0.1 CH₂Cl₂/MeOH/NH₃) (25%). The product **17a** (475 mg, 1.03 mmol, 71%) was obtained as a yellow oil. ¹H NMR (400 MHz, CDCl₃): δ 8.27 (t, *J* = 5.2 Hz, 1H), 8.24 (d, *J* = 1.8 Hz, 1H), 7.91 (t, *J* = 8.5 Hz, 2H), 7.53 (t, *J* = 7.6 Hz, 1H), 7.46 (d, *J* = 8.8 Hz, 1H), 7.33 (t, *J* = 7.6 Hz, 1H), 6.76 (d, *J* = 8.8 Hz, 1H), 4.27 (s, 1H), 3.77–3.70 (m, 2H), 3.55–3.48 (m, 2H), 3.46–3.32 (m, 4H), 3.04 (t, *J* = 6.0 Hz, 2H), 2.71 (t, *J* = 5.8 Hz, 2H), 1.91–1.81 (m, 4H), 1.18 (t, *J* = 7.0 Hz, 6H) ppm. ¹³C NMR (101 MHz, CDCl₃): δ 169.2, 158.9, 149.5, 147.3, 145.5, 135.1, 131.3, 128.9, 128.6, 125.7, 124.5, 124.4, 122.2, 120.8, 118.2, 113.8, 47.4, 43.6, 34.0, 25.0, 22.9, 22.7 ppm. ESI: *m/z* calcd for C₂₆H₃₃N₅O₃ [M + H]⁺, 462.57; found, 462.15; retention time, 7.718 min.

N,N-Diethyl-3-nitro-4-((3-((1,2,3,4-tetrahydroacridin-9-yl)-amino)propyl)amino)benzamide (17b).—The reaction was carried out according to general procedure II using *N,N*-diethyl-4-fluoro-3-nitrobenzamide **16** (173 mg, 0.72 mmol), **12b** (165 mg, 0.65 mmol), and NEt₃ (136 μL, 0.98 mmol). The crude product was purified by flash chromatography (gradient CH₂Cl₂, MeOH), and the product **17b** (110 mg, 0.23 mmol, 36%) was obtained as a brown oil. ¹H NMR (400 MHz, CDCl₃): δ 8.23 (d, *J* = 2.0 Hz, 1H), 8.16 (t, *J* = 5.1 Hz, 1H), 7.89 (d, *J* = 8.4, 2H), 7.54–7.50 (m, 1H), 7.49–7.45 (m, 1H), 7.33–7.27 (m, 1H), 6.74 (d, *J* = 8.9 Hz, 1H), 3.60 (t, *J* = 6.9 Hz, 2H), 3.49–3.30 (m, 6H), 3.03 (t, *J* = 5.3 Hz, 2H), 2.68 (t, *J* = 5.5 Hz, 2H), 2.09–1.98 (m, 2H), 1.90–1.81 (m, 4H), 1.18 (t, *J* = 7.1 Hz, 6H) ppm. ¹³C NMR (101 MHz, CDCl₃): δ = 169.9, 154.6, 151.6, 145.9, 143.1, 135.8, 130.3, 129.1, 128.6, 124.2, 124.8, 123.5, 122.6, 119.0, 115.5, 113.8, 52.9, 42.6, 41.6, 34.7, 26.9, 24.5, 22.4, 22.0, 13.3 ppm. ESI: *m/z* calcd for C₂₇H₃₄N₅O₃ [M + H]⁺, 476.26; found, 476.15; retention time, 7.83 min.

N,N-Diethyl-3-nitro-4-((4-((1,2,3,4-tetrahydroacridin-9-yl)-amino)butyl)amino)benzamide (17c).—The reaction was carried out according to

general procedure II using *N,N*-diethyl-4-fluoro-3-nitrobenzamide **16** (430 mg, 1.79 mmol), **12c** (439 mg, 1.63 mmol), and NEt_3 (340 μL , 2.45 mmol). The crude product was purified by flash chromatography (gradient CH_2Cl_2 /MeOH), and the product **17c** (212 mg, 0.43 mmol, 26%) was obtained as a brown oil. ^1H NMR (400 MHz, CDCl_3): δ 8.26 (d, $J = 2.0$ Hz, 1H), 8.16 (t, $J = 4.9$ Hz, 1H), 7.96–7.92 (m, 2H), 7.58–7.51 (m, 2H), 7.37–7.32 (m, 1H), 6.81 (d, $J = 8.9$ Hz, 1H), 3.57 (t, $J = 6.2$ Hz, 2H), 3.45–3.33 (m, 6H), 3.09–3.05 (m, 2H), 2.72–2.67 (m, 2H), 1.92–1.86 (m, 4H), 1.85–1.79 (m, 4H), 1.20 (t, $J = 7.1$ Hz, 6H) ppm. ^{13}C NMR (101 MHz, CDCl_3): δ 169.4, 154.4, 151.0, 146.6, 145.8, 135.4, 131.0, 128.9, 128.1, 125.8, 124.2, 124.1, 122.8, 120.0, 116.1, 113.9, 53.6, 48.9, 42.9, 33.5, 29.3, 26.5, 25.0, 23.0, 22.7, 13.8 ppm. ESI: m/z calcd for $\text{C}_{28}\text{H}_{36}\text{N}_5\text{O}_3$ $[\text{M} + \text{H}]^+$, 490.28; found, 490.15; retention time, 8.04 min.

***N,N*-Diethyl-3-nitro-4-((5-((1,2,3,4-tetrahydroacridin-9-yl)-amino)pentyl)amino)benzamide (17d).**—

The reaction was carried out according to general procedure II using *N,N*-diethyl-4-fluoro-3-nitrobenzamide **16** (221 mg, 0.92 mmol), **12d** (237 mg, 0.84 mmol), and NEt_3 (173 μL , 1.26 mmol). The crude product was purified by flash chromatography (gradient CH_2Cl_2 , MeOH), and the product **17d** (160 mg, 0.32 mmol, 38%) was obtained as a brown oil. ^1H NMR (400 MHz, CDCl_3): δ 8.21 (d, $J = 2.0$ Hz, 1H), 8.13–8.05 (m, 3H), 7.56–7.51 (m, 1H), 7.50–7.46 (m, 1H), 7.35–7.30 (m, 1H), 6.81 (d, $J = 8.9$ Hz, 1H), 3.72 (t, $J = 7.2$ Hz, 2H), 3.45–3.35 (m, 3H), 3.33–3.27 (m, 2H), 3.12–3.07 (m, 2H), 2.67–2.63 (m, 2H), 1.87–1.79 (m, 6H), 1.77–1.70 (m, 2H), 1.58–1.50 (m, 2H), 1.17 (t, $J = 7.1$ Hz, 6H) ppm. ^{13}C NMR (101 MHz, CDCl_3): δ 169.4, 154.6, 153.3, 145.8, 142.7, 135.2, 130.7, 130.4, 125.7, 124.5, 124.3, 123.8, 123.7, 118.0, 114.0, 113.5, 53.1, 48.5, 42.9, 31.1, 30.0, 28.6, 24.6, 24.3, 22.5, 21.7, 13.7 ppm. ESI: m/z calcd for $\text{C}_{29}\text{H}_{38}\text{N}_5\text{O}_3$ $[\text{M} + \text{H}]^+$, 504.30; found, 504.15; retention time, 8.36 min.

***N,N*-Diethyl-3-nitro-4-((6-((1,2,3,4-tetrahydroacridin-9-yl)-amino)hexyl)amino)benzamide (17e).**—

The reaction was carried out according to general procedure II using *N,N*-diethyl-4-fluoro-3-nitrobenzamide **16** (341 mg, 1.42 mmol), **12e** (458 mg, 1.56 mmol), and NEt_3 (297 μL , 2.13 mmol). The product **17e** (230 mg, 0.44 mmol, 31%) was obtained as a brown oil and used in the next reaction step without further purification. ^1H NMR (400 MHz, CDCl_3): δ 8.55 (d, $J = 8.4$ Hz, 1H), 8.26 (d, $J = 2.0$ Hz, 1H), 8.18–8.13 (m, 2H), 7.73–7.67 (m, 1H), 7.57–7.52 (m, 1H), 7.48–7.42 (m, 1H), 6.86 (d, $J = 8.9$ Hz, 1H), 3.94 (t, $J = 7.0$ Hz, 2H), 3.51–3.37 (m, 4H), 3.36–3.29 (m, 4H), 2.60 (t, $J = 6.2$ Hz, 2H), 1.91–1.83 (m, 4H), 1.69–1.58 (m, 4H), 1.57–1.53 (m, 4H), 1.21 (t, $J = 7.1$ Hz, 6H) ppm. ^{13}C NMR (101 MHz, CDCl_3): δ 168.5, 155.45, 152.0, 146.0, 142.04, 135.4, 129.52, 129.2, 125.4, 124.9, 123.7, 123.2, 121.6, 118.7, 114.0, 113.6, 53.1, 48.2, 43.0, 31.3, 31.2, 28.8, 26.8, 26.6, 26.3, 23.8, 20.8, 13.8 ppm. ESI: m/z calcd for $\text{C}_{30}\text{H}_{40}\text{N}_5\text{O}_3$ $[\text{M} + \text{H}]^+$, 518.31; found, 518.40; retention time, 8.55 min.

***N,N*-Diethyl-3-nitro-4-((2-(2-((1,2,3,4-tetrahydroacridin-9-yl)-amino)ethoxy)ethoxy)ethyl)amino)benzamide (17f).**—

The reaction was carried out according to general procedure II using *N,N*-diethyl-4-fluoro-3-nitrobenzamide **16** (475 mg, 1.98 mmol), **12f** (718 mg, 2.18 mmol), and NEt_3 (410 μL , 2.97 mmol). The crude product was purified by flash chromatography (gradient CH_2Cl_2 /MeOH), and product **17f** (575 mg,

1.05 mmol, 53%) was obtained as a brown oil and used in the next reaction step without further purification. ¹H NMR (400 MHz, CDCl₃): δ 8.41–8.35 (m, 2H), 8.22 (d, *J* = 2.0 Hz, 1H), 8.11–8.07 (m, 1H), 7.66–7.60 (m, 1H), 7.56–7.52 (m, 1H), 7.42–7.37 (m, 1H), 6.86 (d, *J* = 8.9 Hz, 1H), 4.01–3.95 (m, 2H), 3.83–3.73 (m, 4H), 3.75–3.70 (m, 4H), 3.52–3.48 (m, 2H), 3.47–3.35 (m, 4H), 3.27–3.22 (m, 2H), 2.68–2.63 (m, 2H), 1.90–1.83 (m, 4H), 1.20 (t, *J* = 7.1 Hz, 6H) ppm. ¹³C NMR (101 MHz, CDCl₃): δ 169.3, 154.30, 151.4, 145.8, 143.1, 135.4, 131.1, 125.7, 125.0, 124.3, 124.2, 123.6, 121.3, 117.6, 116.0, 114.1, 70.9, 70.5, 70.0, 69.0, 52.7, 48.1, 42.8, 30.1, 23.9, 22.4, 21.4, 13.7 ppm. ESI: *m/z* calcd for C₃₀H₄₀N₅O₅ [M + H]⁺, 550.30; found, 550.25; retention time, 8.05 min.

3-Amino-N,N-diethyl-4-((2-((1,2,3,4-tetrahydroacridin-9-yl)-amino)ethyl)amino)benzamide (18a).—

The reaction was carried out according to general procedure III using *N,N*-diethyl-3-nitro-4-((2-((1,2,3,4-tetrahydroacridin-9-yl)amino)ethyl)amino)benzamide **17a** (475 mg, 1.03 mmol) and SnCl₂·2H₂O (1.44 g, 6.39 mmol). The product **18a** (325 mg, 0.75 mmol, 73%) was obtained as a colorless oil and directly used for the next reaction without purification. ESI: *m/z* calcd for C₂₆H₃₅N₅O [M + H]⁺, 432.28; found, 432.30; retention time, 7.534 min.

3-Amino-N,N-diethyl-4-((3-((1,2,3,4-tetrahydroacridin-9-yl)-amino)propyl)amino)benzamide (18b).—

The reaction was carried out according to general procedure III using *N,N*-diethyl-3-nitro-4-((3-((1,2,3,4-tetrahydroacridin-9-yl)amino)propyl)amino)benzamide **17b** (110 mg, 0.23 mmol) and SnCl₂·2H₂O (323 mg, 1.43 mmol). The product **18b** (89.1 mg, 0.20 mmol, 87%) was obtained as a colorless oil and directly used for the next reaction without purification. ESI: *m/z* calcd for C₂₇H₃₆N₅O [M + H]⁺, 223.65; found, 223.65; retention time, 7.84 min.

3-Amino-N,N-diethyl-4-((4-((1,2,3,4-tetrahydroacridin-9-yl)-amino)butyl)amino)benzamide (18c).—

The reaction was carried out according to general procedure III using *N,N*-diethyl-3-nitro-4-((4-((1,2,3,4-tetrahydroacridin-9-yl)amino)butyl)amino)benzamide **17c** (212 mg, 0.43 mmol) and SnCl₂·2H₂O (602 mg, 2.67 mmol). The product **18c** (154 mg, 0.34 mmol, 79%) was obtained as a colorless oil and directly used for the next reaction without purification. ESI: *m/z* calcd for C₂₈H₃₈N₅O [M + 2H]²⁺, 230.66; found, 230.60; retention time, 7.17 min.

3-Amino-N,N-diethyl-4-((5-((1,2,3,4-tetrahydroacridin-9-yl)-amino)pentyl)amino)benzamide (18d).—

The reaction was carried out according to general procedure III using *N,N*-diethyl-3-nitro-4-((5-((1,2,3,4-tetrahydroacridin-9-yl)amino)pentyl)amino)benzamide **17d** (236 mg, 0.47 mmol) and SnCl₂·2H₂O (657 mg, 2.91 mmol). The product **18d** (222 mg, 0.47 mmol, quant.) was obtained as a colorless oil and directly used for the next reaction without purification. ESI: *m/z* calcd for C₂₉H₄₀N₅O [M + 2H]²⁺, 237.67; found, 237.65; retention time, 7.73 min.

3-Amino-N,N-diethyl-4-((6-((1,2,3,4-tetrahydroacridin-9-yl)-amino)hexyl)amino)benzamide (18e).—

The reaction was carried out according to general procedure III using *N,N*-diethyl-3-nitro-4-((6-((1,2,3,4-tetrahydroacridin-9-

yl)amino)hexyl)amino)benzamide **17e** (230 mg, 0.44 mmol) and SnCl₂·2H₂O (616 mg, 2.73 mmol). The product **18e** (140 mg, 0.29 mmol, 66%) was obtained as a colorless oil and directly used for the next reaction without purification. ESI: *m/z* calcd for C₃₀H₄₂N₅O [M + 2H]²⁺, 244.68; found, 244.65; retention time, 7.93 min.

3-Amino-N,N-diethyl-4-((2-(2-((1,2,3,4-tetrahydroacridin-9-yl)amino)ethoxy)ethoxy)ethyl)amino)benzamide (18f).—The reaction was carried out according to general procedure III using *N,N*-diethyl-3-nitro-4-((2-(2-((1,2,3,4-tetrahydroacridin-9-yl)amino)-ethoxy)ethoxy)ethyl)amino)benzamide **17f** (575 mg, 1.05 mmol) and SnCl₂·2H₂O (1.47 g, 8.51 mmol). The product **18f** (290 mg, 0.56 mmol, 53%) was obtained as a colorless oil and directly used for the next reaction without purification. ESI: *m/z* calcd for C₃₀H₄₂N₅O₃ [M + 2H]²⁺, 260.67; found, 260.60; retention time, 7.50 min.

3-(2-(4-Ethoxyphenyl)acetamido)-N,N-diethyl-4-((2-((1,2,3,4-tetrahydroacridin-9-yl)amino)ethyl)amino)benzamide (19a).—The reaction was carried out according to general procedure IV using 3-amino-*N,N*-diethyl-4-((2-((1,2,3,4-tetrahydroacridin-9-yl)amino)-ethyl)amino)benzamide **18a** (325 mg, 0.75 mmol), 2-(4-ethoxyphenyl)acetic acid (30 mg, 0.83 mmol), HBTU (313 mg, 0.83 mmol), and triethylamine (156 μL, 1.13 mmol). The product **19a** (258 mg, 0.43 mmol, 57%) was obtained as an orange/brown oil. ¹H NMR (400 MHz, CDCl₃): δ 8.72 (s, 1H), 7.97 (d, *J* = 8.5 Hz, 1H), 7.89 (d, *J* = Hz, 1H), 7.52 (t, *J* = 7.6 Hz, 1H), 7.32 (t, *J* = 7.6 Hz, 1H), 7.23 (d, *J* = 8.5 Hz, 2H), 7.15 (d, *J* = 1.4 Hz, 1H), 7.00 (dd, *J* = 8.3, 1.4 Hz, 1H), 6.74 (d, *J* = 8.5 Hz, 2H), 6.46 (d, *J* = 8.4 Hz, 1H), 4.73 (s, 1H), 4.64 (t, *J* = 5.3 Hz, 1H), 3.85 (q, *J* = 7.0 Hz, 2H), 3.66–3.59 (m, 4H), 3.39 (s, 4H), 3.26–3.18 (m, 2H), 3.01 (t, *J* = 6.1 Hz, 2H), 2.63 (t, *J* = 6.0 Hz, 2H), 1.89–1.75 (m, 4H), 1.32 (t, *J* = 7.0 Hz, 3H), 1.15 (s, 6H) ppm. ¹³C NMR (101 MHz, CDCl₃): δ 171.7, 171.1, 158.1, 157.9, 150.9, 146.5, 143.2, 130.2, 128.7, 127.8, 127.2, 125.3, 125.2, 124.7, 124.0, 123.8, 122.9, 120.2, 116.9, 114.7, 111.1, 63.4, 47.6, 44.3, 42.9, 33.5, 24.8, 22.9, 22.6, 14.8 ppm. ESI: *m/z* calcd for C₃₆H₄₅N₅O₃ [M + H]⁺, 594.78; found, 594.25; retention time, 8.101 min.

3-(2-(4-Ethoxyphenyl)acetamido)-N,N-diethyl-4-((3-((1,2,3,4-tetrahydroacridin-9-yl)amino)propyl)amino)benzamide (19b).—The reaction was carried out according to general procedure IV using 3-amino-*N,N*-diethyl-4-((3-((1,2,3,4-tetrahydroacridin-9-yl)amino)-propyl)amino)benzamide **18b** (154 mg, 0.34 mmol), 2-(4-ethoxyphenyl)acetic acid (136 mg, 0.37 mmol), HBTU (140 mg, 0.37 mmol), and triethylamine (70.6 μL, 0.51 mmol). The product **19b** (104 mg, 0.17 mmol, 50%) was obtained as an orange/brown oil. ¹H NMR (400 MHz, CDCl₃): δ 8.07 (s, 1H), 8.02 (d, *J* = 9.5 Hz, 1H), 7.59–7.55 (m, 1H), 7.47–7.44 (m, 1H), 7.29–7.28 (m, 1H), 7.24 (d, *J* = 8.4 Hz, 2H), 7.05–7.02 (m, 1H), 6.76–6.74 (m, 2H), 6.56–6.52 (m, 1H), 3.92–3.83 (m, 4H), 3.73 (s, 2H), 3.42–3.36 (m, 4H), 3.22–3.15 (m, 2H), 2.73–2.68 (m, 2H), 2.43–2.36 (m, 2H), 2.03–1.97 (m, 2H), 1.71–1.65 (m, 4H), 1.32 (t, *J* = 7.0 Hz, 3H), 1.20–1.09 (m, 6H) ppm. ¹³C NMR (101 MHz, CDCl₃): δ 172.1, 171.9, 162.7, 157.2, 151.9, 146.6, 143.5, 130.6, 129.4, 127.3, 126.7, 125.8, 124.7, 124.6, 123.0, 121.1, 119.5, 118.5, 115.5, 114.8, 111.0, 63.5,

46.1, 42.8, 42.5, 39.4, 29.8, 29.5, 24.8, 22.4, 22.1, 14.9, 13.7 ppm. ESI: m/z calcd for $C_{37}H_{47}N_5O_3$ $[M + 2H]^{2+}$, 304.69; found, 304.70; retention time, 8.23 min.

3-(2-(4-Ethoxyphenyl)acetamido)-N,N-diethyl-4-((4-((1,2,3,4-tetrahydroacridin-9-yl)amino)butyl)amino)benzamide (19c).—The reaction was carried out according to general procedure IV using 3-amino-*N,N*-diethyl-4-((4-((1,2,3,4-tetrahydroacridin-9-yl)amino)butyl)amino)benzamide **18c** (139 mg, 0.30 mmol), 2-(4-ethoxyphenyl)acetic acid (121 mg, 0.33 mmol), HBTU (125 mg, 0.33 mmol), and triethylamine (62.3 μ L, 0.45 mmol). The product **19c** (166 mg, 0.27 mmol, 90%) was obtained as a brown oil. 1H NMR (400 MHz, $CDCl_3$): δ 7.97 (s, 1H), 7.79–7.77 (m, 1H), 7.53–7.50 (m, 1H), 7.34–7.31 (m, 1H), 7.24 (d, J = 8.6 Hz, 2H), 7.17–7.14 (m, 1H), 7.06–7.02 (m, 1H), 6.81 (d, J = 8.6 Hz, 2H), 6.50–6.46 (m, 1H), 4.03–3.91 (m, 4H), 3.64 (s, 2H), 3.42–3.31 (m, 4H), 3.05–3.00 (m, 2H), 2.94–2.90 (m, 2H), 2.63–2.57 (m, 2H), 1.87–1.80 (m, 4H), 1.73–1.56 (m, 4H), 1.33 (t, J = 7.0 Hz, 3H), 1.19–1.11 (m, 6H) ppm. ^{13}C NMR (101 MHz, $CDCl_3$): δ 171.7, 171.4, 162.1, 158.4, 152.4, 144.7, 143.8, 130.5, 129.8, 127.2, 126.9, 125.9, 124.9, 124.3, 123.6, 121.9, 119.5, 118.9, 115.7, 115.1, 111.1, 63.6, 48.9, 47.2, 44.4, 43.1, 32.2, 28.7, 26.3, 24.7, 22.7, 22.2, 14.9, 13.6 ppm. ESI: m/z calcd for $C_{38}H_{49}N_5O_3$ $[M + 2H]^{2+}$, 311.69; found, 311.70; retention time, 8.39 min.

3-(2-(4-Ethoxyphenyl)acetamido)-N,N-diethyl-4-((5-((1,2,3,4-tetrahydroacridin-9-yl)amino)pentyl)amino)benzamide (19d).—The reaction was carried out according to general procedure IV using 3-amino-*N,N*-diethyl-4-((5-((1,2,3,4-tetrahydroacridin-9-yl)amino)pentyl)amino)benzamide **19d** (222 mg, 0.47 mmol), 2-(4-ethoxyphenyl)acetic acid (191 mg, 0.52 mmol), HBTU (197 mg, 0.52 mmol), and triethylamine (98.4 μ L, 0.71 mmol). The product **19d** (299 mg, 0.47 mmol, quant.) was obtained as a brown oil. 1H NMR (400 MHz, $CDCl_3$): δ 8.11 (d, J = 8.7 Hz, 1H), 7.59–7.56 (m, 2H), 7.43–7.36 (m, 2H), 7.27–7.25 (m, 2H), 6.92–6.87 (m, 1H), 6.79 (d, J = 8.6 Hz, 2H), 6.33 (d, J = 8.5 Hz, 1H), 3.95 (q, J = 14.0, 7.0 Hz, 2H), 3.86–3.82 (m, 2H), 3.69 (s, 2H), 3.46–3.37 (m, 4H), 3.00–2.95 (m, 2H), 2.69–2.64 (m, 2H), 2.50–2.45 (m, 2H), 1.80–1.72 (m, 6H), 1.69–1.63 (m, 2H), 1.37–1.33 (m, 5H), 1.30–1.21 (m, 6H) ppm. ^{13}C NMR (101 MHz, $CDCl_3$): δ 171.8, 171.2, 161.4, 157.6, 153.1, 146.7, 143.7, 130.5, 129.5, 127.3, 126.7, 125.8, 124.8, 124.5, 123.5, 122.2, 119.6, 118.8, 115.7, 114.9, 111.3, 63.6, 48.6, 47.4, 45.1, 43.2, 30.2, 29.9, 28.4, 28.2, 23.56, 22.2, 22.1, 14.9, 13.7 ppm. ESI: m/z calcd for $C_{39}H_{51}N_5O_3$ $[M + 2H]^{2+}$, 318.70; found, 318.65; retention time, 8.75 min.

3-(2-(4-Ethoxyphenyl)acetamido)-N,N-diethyl-4-((6-((1,2,3,4-tetrahydroacridin-9-yl)amino)hexyl)amino)benzamide (19e).—The reaction was carried out according to general procedure IV using 3-amino-*N,N*-diethyl-4-((6-((1,2,3,4-tetrahydroacridin-9-yl)amino)hexyl)amino)benzamide **18e** (140 mg, 0.29 mmol), 2-(4-ethoxyphenyl)acetic acid (52.3 mg, 0.29 mmol), HBTU (133 mg, 0.35 mmol), and triethylamine (61.0 μ L, 0.44 mmol). The product **19e** (142 mg, 0.22 mmol, 76%) was obtained as a brown oil. 1H NMR (400 MHz, $CDCl_3$): δ 8.56 (s, 1H), 8.15 (d, J = 8.7 Hz, 1H), 7.88 (d, J = 8.4 Hz, 1H), 7.53 (t, J = 7.2 Hz, 1H), 7.35 (t, J = 8.0 Hz, 1H), 7.25 (d, J = 8.6 Hz, 2H), 7.04–7.00 (m, 1H), 6.75 (d, J = 8.6 Hz, 2H), 6.48–6.44 (m, 1H), 3.92 (q, J = 7.0 Hz, 2H), 3.81 (m, 2H), 3.71 (s, 2H), 3.49–3.32 (m, 4H), 2.96–2.91 (m, 2H), 2.88–2.83 (m, 2H), 2.54–2.49 (m, 2H), 1.80–1.68

(m, 6H), 1.54–1.47 (m, 2H), 1.37–1.31 (m, 4H), 1.25 (t, $J=7.3$ Hz, 3H), 1.14–1.09 (m, 6H) ppm. ^{13}C NMR (101 MHz, CDCl_3): δ 172.0, 170.8, 162.7, 158.1, 156.0, 150.5, 144.07, 130.4, 129.4, 127.6, 127.0, 125.8, 125.1, 124.9, 123.8, 122.6, 119.9, 119.0, 115.7, 114.7, 111.3, 63.5, 48.1, 46.3, 45.2, 43.2, 31.5, 30.3, 28.6, 28.3, 26.2, 25.9, 21.8, 20.7, 14.9, 13.7 ppm. ESI: m/z calcd for $[\text{M} + 2\text{H}]^{2+}$, 325.70; found: 325.75; retention time: 8.76 min.

3-(2-(4-Ethoxyphenyl)acetamido)-N,N-diethyl-4-((2-(2-((1,2,3,4-tetrahydroacridin-9-yl)amino)ethoxy)ethoxy)ethyl)amino)benzamide (19f).—

The reaction was carried out according to general procedure IV using 3-amino-*N,N*-diethyl-4-((2-(2-((1,2,3,4-tetrahydroacridin-9-yl)amino)ethoxy)ethoxy)ethyl)amino)-benzamide **18f** (290 mg, 0.56 mmol), 2-(4-ethoxyphenyl)acetic acid (122 mg, 0.62 mmol), HBTU (235 mg, 0.62 mmol), and triethylamine (116 μL , 0.84 mmol). The product **19f** (398 mg, 0.58 mmol, quant.) was obtained as a brown oil. ^1H NMR (400 MHz, CDCl_3): δ 8.03–7.96 (m, 2H), 7.87 (d, $J=8.3$ Hz, 1H), 7.51 (t, $J=8.0$ Hz, 1H), 7.31 (t, $J=7.2$ Hz, 1H), 7.20 (d, $J=8.6$ Hz, 2H), 7.07–7.03 (m, $J=8.4$, 1.9 Hz, 1H), 6.81 (d, $J=8.6$ Hz, 2H), 6.56–6.52 (m, 1H), 3.99–3.92 (m, 2H), 3.71–3.67 (m, 2H), 3.63–3.56 (m, 10H), 3.42–3.31 (m, 4H), 3.17 (t, $J=5.3$ Hz, 2H), 2.99–2.94 (m, 2H), 2.67–2.62 (m, 2H), 1.84–1.76 (m, 4H), 1.36 (t, $J=7.2$ Hz, 3H), 1.14–1.09 (m, 6H) ppm. ^{13}C NMR (101 MHz, CDCl_3): δ 171.5, 170.9, 158.3, 156.6, 152.1, 144.9, 143.4, 130.5, 129.5, 127.0, 126.4, 125.7, 124.6, 124.3, 123.5, 123.3, 119.5, 118.7, 115.9, 115.0, 111.6, 70.4, 70.3, 70.2, 69.6, 63.5, 53.5, 48.3, 45.8, 43.5, 29.8, 24.4, 22.8, 22.3, 14.9, 13.7 ppm. ESI: m/z calcd for $\text{C}_{40}\text{H}_{51}\text{N}_5\text{O}_5$ $[\text{M} + 2\text{H}]^{2+}$, 341.70; found, 341.70; retention time, 8.34 min.

Ethyl 4-(isopentylamino)-3-nitrobenzoate (20).—4-Fluoro-3-nitro-benzoic acid (1.00 g, 5.40 mmol) was dissolved in ethanol, and a cat. amount (few drops) of H_2SO_4 (95–97%) was added. After stirring overnight under reflux conditions, the mixture was basified with triethylamine, and 3-methylbutan-1-amine (691 μL , 5.94 mmol) was added. After stirring under reflux conditions overnight, the mixture was concentrated in vacuo. The residue was dissolved in CH_2Cl_2 and washed with 1 M $\text{HCl}_{(\text{aq})}$ and NaHCO_3 solution. The organic layers were combined, dried over anhydrous MgSO_4 , and concentrated in vacuo. The product **20** (1.46 g, 5.22 mmol, 97%) was obtained as a yellow oil. ^1H NMR (400 MHz, CDCl_3): δ 8.88–8.85 (m, 1H), 8.31 (s, 1H), 8.07–8.03 (m, 1H), 6.88–6.83 (m, 1H), 4.35 (q, $J=7.1$ Hz, 2H), 3.39–3.33 (m, 2H), 1.83–1.72 (m, 1H), 1.65 (q, $J=7.1$ Hz, 2H), 1.38 (t, $J=7.1$ Hz, 3H), 0.99 (d, $J=6.7$ Hz, 6H) ppm. ^{13}C NMR (101 MHz, CDCl_3): δ 165.3, 147.9, 136.5, 131.3, 129.6, 117.5, 113.6, 61.1, 41.6, 37.8, 26.1, 22.6, 14.5 ppm. ESI: m/z calcd for $\text{C}_{14}\text{H}_{21}\text{N}_2\text{O}_4$ $[\text{M} + \text{H}]^+$, 281.15; found, 281.00; retention time, 11.85 min.

Ethyl 3-Amino-4-(isopentylamino)benzoate (21).—Ethyl 4-(iso-pentylamino)-3-nitrobenzoate **20** (1.46 g, 5.22 mmol) was dissolved in MeOH and a cat. amount of Pd/C (10%) was added. The mixture was stirred under a hydrogen atmosphere (8 bar) at room temperature for 3 h. The clear mixture was filtered off by suction over Celite. The combined organic layers were dried over anhydrous MgSO_4 and concentrated in vacuo, and product **36** (1.31 g, 5.22 mmol, quant.) was obtained as a colorless oil. The product was directly used for the next reaction step without further purification. ESI: m/z calcd for $\text{C}_{14}\text{H}_{23}\text{N}_2\text{O}_2$ $[\text{M} + \text{H}]^+$, 251.18; found, 251.05; retention time, 10.34 min.

Ethyl 3-(2-(4-Ethoxyphenyl)acetamido)-4-(isopentylamino)-benzoate (22).—The reaction was carried out according to general procedure V using 3 ethyl 3-amino-4-(isopentylamino)benzoate **21** (1.31 g, 5.22 mmol), 2-(4-ethoxyphenyl)acetic acid (1.03 g, 5.74 mmol), HBTU (2.18 g, 5.74 mmol), and NEt₃ (1.08 mL, 7.83 mmol). The product **22** (2.15 g, 5.22 mmol, quant.) was obtained as an orange/brown oil. ¹H NMR (400 MHz, CDCl₃): δ 7.86–7.82 (m, 1H), 7.73–7.71 (m, 1H), 7.32–7.29 (m, 2H), 6.97–6.94 (m, 2H), 6.65 (d, *J* = 8.7 Hz, 1H), 4.32 (q, *J* = 7.1 Hz, 2H), 4.17 (q, *J* = 7.1 Hz, 2H), 3.74 (s, 2H), 3.14–3.08 (m, 2H), 1.70–1.65 (m, 1H), 1.50–1.40 (m, 5H), 1.37 (t, *J* = 7.1 Hz, 3H), 0.96 (d, *J* = 6.6 Hz, 6H) ppm. ¹³C NMR (101 MHz, CDCl₃): δ 170.8, 158.6, 147.2, 130.5, 130.2, 130.1, 127.8, 126.5, 121.5, 118.4, 115.4, 114.6, 63.7, 60.5, 41.8, 38.8, 38.3, 26.1, 22.7, 14.9, 14.6 ppm. ESI: *m/z* calcd for C₂₄H₃₃N₂O₄ [M + H]⁺, 413.24; found, 413.10; retention time, 11.04 min.

Ethyl 2-(4-Ethoxybenzyl)-1-isopentyl-1H-benzo[d]imidazole-5-carboxylate (23).—The reaction was carried out according to general procedure V using ethyl 3-(2-(4-ethoxyphenyl)acetamido)-4-(isopentylamino)benzoate **22** (2.15 g, 5.22 mmol). The crude product was purified by column chromatography (20:1:0.1 CH₂Cl₂/MeOH/NH₃(aq) (25%)), and product **23** (1.67 g, 4.23 mmol, 81%) was obtained as a purple oil. ¹H NMR (400 MHz, CDCl₃): δ 8.44 (s, 1H), 7.95–7.91 (m, 1H), 7.21 (d, *J* = 8.4 Hz, 1H), 7.10 (d, *J* = 8.8 Hz, 2H), 6.78 (d, *J* = 8.8 Hz, 2H), 4.35 (q, *J* = 7.1 Hz, 2H), 4.20 (s, 2H), 3.96–3.89 (m, 4H), 1.56–1.46 (m, 1H), 1.39–1.28 (m, 8H), 0.85 (d, *J* = 6.8 Hz, 6H) ppm. ¹³C NMR (101 MHz, CDCl₃): δ 167.2, 158.1, 155.1, 142.2, 138.5, 129.5, 127.7, 124.4, 123.8, 121.7, 114.9, 108.9, 63.4, 60.7, 42.7, 38.0, 33.8, 26.1, 22.3, 14.7, 14.4 ppm. ESI: *m/z* calcd for C₂₄H₃₁N₂O₃ [M + H]⁺, 395.23; found, 395.15; retention time, 11.11 min.

2-(4-Ethoxybenzyl)-1-isopentyl-1H-benzo[d]imidazole-5-carboxylic Acid (24).—Ethyl 2-(4-ethoxybenzyl)-1-isopentyl-1H-benzo[d]imidazole-5-carboxylate **23** (250 mg, 0.63 mmol) was dissolved in THF, and lithium hydroxide (150 mg, 0.63 mmol) in water was added. After 48 h of harsh stirring under reflux conditions, the mixture was concentrated in vacuo, and the residue was acidified with 2 M HCl(aq). Then, CH₂Cl₂ was added, and the organic layer was washed with water. The organic layers were combined, dried over anhydrous MgSO₄, and concentrated in vacuo. Product **24** (231 mg, 0.63 mmol, quant.) was obtained as a purple oil. ¹H NMR (400 MHz, D₂O): δ 8.10–8.07 (m, 1H), 7.80–7.75 (m, *J* = 9.9 Hz, 1H), 7.29 (d, *J* = 8.5 Hz, 1H), 7.06 (d, *J* = 8.5 Hz, 2H), 6.78 (d, *J* = 8.3 Hz, 2H), 4.10 (s, 2H), 3.94–3.88 (m, 2H), 3.86–3.80 (m, 2H), 1.36–1.27 (m, 1H), 1.21 (t, *J* = 6.9 Hz, 3H), 1.08–1.01 (m, 2H), 0.66 (d, *J* = 6.6 Hz, 6H) ppm. ¹³C NMR (101 MHz, DMSO): δ 167.6, 166.2, 158.4, 135.7, 132.8, 130.6, 128.0, 126.5, 125.3, 125.2, 117.2, 115.5, 63.7, 43.8, 37.1, 31.1, 25.8, 22.2, 14.8 ppm. ESI: *m/z* calcd for C₂₂H₂₇N₂O₃ [M + H]⁺, 367.20; found, 367.15; retention time, 10.13 min.

Pharmacology.

Inhibition of hBChE.—BChE (E.C. 3.1.1.8, from humans) was kindly provided by Oksana Lockridge from the University of Nebraska Medical Center. 5,5'-Dithiobis(2-nitrobenzoic acid) and ATC iodide were obtained from Fluka Analytical, and tacrine hydrochloride was purchased from Sigma-Aldrich. Inhibitory activities were evaluated using

Ellman's method.⁶⁴ The stock solutions of the test compounds were prepared in ethanol (33.3 mM) and diluted to the desired concentrations. For the testing, 50 μL of 5,5'-dithiobis(2-nitrobenzoic acid) and 50 μL of enzyme were added to 1.5 mL of the buffer. After 50 μL of the test compound was added, the mixture was incubated for 4.5 min. Afterward, 10 μL of acetylthiocholine iodide was added, and the mixture was allowed to incubate for further 2.5 min. Enzyme activity was then observed via UV ($\lambda = 412 \text{ nm}$). IC_{50} values were determined graphically from inhibition curves using Pad Prism 5.0 software. Experiments were carried out three times independently.

Inhibition of hAChE and hBChE.—The hAChE inhibitory activity was evaluated spectrophotometrically at 37 °C by Ellman's method.⁶⁴ AChE stock solution was prepared by dissolving recombinant hAChE lyophilized powder (Sigma, Italy) in 0.1 M phosphate buffer (pH = 8.0) containing Triton X-100 0.1%. The stock solution of BChE from human serum (Sigma, Italy) was prepared by dissolving the lyophilized powder in an aqueous solution of gelatin 0.1%. Stock solutions of inhibitors (1 or 2 mM) were prepared in methanol. The assay solution consisted of a 0.1 M phosphate buffer at pH 8.0, with the addition of 340 μM 5,5'-dithiobis(2-nitrobenzoic acid), 0.02 unit/mL hAChE or hBChE, and 550 μM substrate (acetylthiocholine iodide or butyrylthiocholine iodide for AchE or BchE, respectively). Fifty microliter aliquots of increasing concentration of the tested compound were added to the assay solution and preincubated for 20 min at 37 °C with the enzyme. Upon addition of the substrate, the increase in absorbance at 412 nm was monitored for 3 min. Assays were carried out with a blank containing all components except the enzyme to account for the nonenzymatic reaction. The reaction rates were compared, and the percent inhibition was calculated. IC_{50} values were determined graphically from inhibition curves using GraphPad Prism 4.03 software. Experiments were carried out three times independently.

Investigation of Inhibitory Constants and Mode of Inhibition toward hAChE.—To assess the mechanism of action and inhibitory constant reciprocal plots of $1/V$ versus $1/[S]$ were constructed using relatively low concentrations of substrate (ACTh, 0.111–0.554 mM). The evaluation of the enzyme activity was carried out by Ellman's method.⁶⁴ The plots were assessed by a weighted least square analysis that assumed the variance of V to be a constant percentage of V for the entire data set. The mechanism of inhibition was assessed by comparing the overlaid Lineweaver-Burk plots with the theoretical trends for competitive, mixed-type, and noncompetitive inhibition. To determine the inhibition constant K_i , slopes of reciprocal plots were replotted against the concentration of the tested inhibitor (3e, range 0–100 nM; 4b, range 0–7.5 nM; 8, range 0–25.0 nM), and K_i was determined as the intersect on the negative x axis. The K_i' (dissociation constant for the enzyme-substrate-inhibitor complex) value was determined by plotting the apparent $1/V_{\text{max}}$ versus inhibitor concentration.⁹² Data analysis was performed using GraphPad Prism 4.03 software. Experiments were carried out three times independently.

Inhibition of AChE-Induced $\text{A}\beta_{40}$ Aggregation.⁶⁵— $\text{A}\beta_{40}$, supplied as trifluoroacetate salt, was purchased from Bachem AG (Switzerland). $\text{A}\beta_{40}$ (2 mg mL^{-1}) was dissolved in 1,1,1,3,3,3-hexafluoro-2-propanol (HFIP), lyophilized, and redissolved in DMSO to achieve

a 2.3 mM stock solution. Stock solutions of tested inhibitors were prepared in methanol (2.0 mM) and diluted in the assay buffer. Aliquots of A β ₄₀ peptide (2 μ L) were incubated for 24 h at room temperature in 0.215M sodium phosphate buffer (pH 8.0) at a final concentration of 230 μ M. For co-incubation experiment aliquots (16 μ L) of hAChE solution (final concentration, 2.30 μ M; A β /AChE molar ratio, 100:1) and hAChE in the presence of 2 μ L of the tested inhibitor (final inhibitor concentration, 100 μ M) in 0.215 M sodium phosphate buffer solution (pH 8.0) were added. Blanks containing A β ₄₀ alone, hAChE alone, and A β ₄₀ plus tested inhibitors in 0.215 M sodium phosphate buffer (pH 8.0) were also prepared. The final volume of each sample was 20 μ L. To quantify amyloid fibril formation, the thioflavin T fluorescence method was then applied.⁹³ The fluorescence intensities related to fibril formation were monitored for 300 s at $\lambda_{em} = 490$ nm ($\lambda_{exc} = 446$ nm). Fluorescence intensities of samples without and with an inhibitor were compared, and percent inhibition was calculated.⁶⁵ The experiment was carried out two times independently, and each was performed in duplicate.

Inhibition of A β ₄₂ Self-Aggregation.—As reported in a previously published protocol,⁶⁸ HFIP-pretreated A β ₄₂ samples (Bachem AG, Switzerland) were solubilized with a CH₃CN/0.3 mM Na₂CO₃/250 mM NaOH (48.4:48.4:3.2) mixture to obtain a 500 μ M stock solution. Experiments were performed by diluting (final A β concentration, 50 μ M) and incubating the peptide in 10 mM phosphate buffer (pH = 8.0) containing 10 mM NaCl, at 30 °C for 24 h with and without an inhibitor (50 μ M, A β /inhibitor = 1:1). Blanks containing the tested inhibitors were also prepared. Each assay was run in duplicate. To quantify amyloid fibril formation, the thioflavin T fluorescence method was used.⁹³ After incubation, samples were diluted to a final volume of 2.0 mL with 50 mM glycine-NaOH buffer (pH 8.5) containing 1.5 μ M thioflavin T. A 300 s time scan of the fluorescence intensity was carried out ($\lambda_{exc} = 446$ nm; $\lambda_{em} = 490$ nm, FP-6200 fluorometer, Jasco Europe), and values at the plateau were averaged after subtracting the background fluorescence of 1.5 μ M thioflavin T solution. The fluorescence intensities obtained in the absence and in the presence of tested inhibitors were compared, and the percent inhibition due to the presence of the inhibitor was calculated by the following formula: $100 - (IF_i/IF_o \times 100)$, where IF_i and IF_o are the fluorescence intensities obtained for A β ₄₂ in the presence and in the absence of inhibitor, respectively. The experiment was carried out two times independently, and each was performed in duplicate.

Radioligand Binding Studies on hCB₂R and hCB₁R and Efficacy. HEK hCB₂R Cell Line.—Human embryonic kidney cells (HEK) stably expressing the hCB₂R were grown in Dulbecco's modified Eagle's medium containing high glucose supplemented with 8% fetal calf serum and 25 μ g/mL zeocin in a 37 °C incubator in the presence of 5% CO₂. Cells were passaged twice a week.

CHO hCB₁R Cell Line.—Chinese hamster ovary cells (CHO) stably expressing the hCB₁R were grown in Ham's F-12 Nutrient Mix supplemented with 8% fetal calf serum and 400 μ g/mL geneticin in a 37 °C incubator in the presence of 5% CO₂. Cells were passaged twice a week.

U266 Cell Line.—The U266 cell line was purchased from ATCC (LGC Standards, Milan, IT). Cell authentication was performed by IST (Genova, Italy). Cells were cultured in an RPMI 1640 medium (Lonza, Milan, IT) supplemented with 10% fetal bovine serum (FBS), 2 mM L-glutamine, 100 IU/mL penicillin, 100 µg/mL ampicillin/streptomycin, 1 mM sodium pyruvate and grown at 37 °C with 5% CO₂ and 95% humidity.

Cell Thawing.—Cells were removed from liquid nitrogen stocks and warmed up in a 37 °C water bath. Then, the cells were resuspended in 10 mL of DMEM (high glucose) and 8–10% FCS. The suspension was centrifuged for 5 min at 1000 rpm, and the supernatant was discarded. The pellet was resuspended in 10 mL of DMEM (high glucose) with 2.5 µL (25 µg/mL) of zeocin and 8–10% FCS. The suspension was transferred into a tissue culture flask and then placed in an incubator (37 °C, 5% CO₂, humid). The medium was changed on the following day.

Cell Passaging.—The passaging rate was determined by examining the cells under the light microscope. The medium was discarded, and cells were washed gently by adding 5 mL of PBS. The PBS was discarded, and 3 mL of Trypsin/EDTA was added. The flask was placed in the incubator for 5 min. After incubation, 7 mL of DMEM (high glucose) with 8–10% FCS was added. The cells were washed down and transferred into a falcon tube. The tube was centrifuged for 5 min at 1000 rpm. The supernatant was discarded, and 5–10 mL of DMEM (high glucose) with zeocin (25 µg/mL) and 8–10% FCS was added. The cell suspension was divided into aliquots according to the passaging rate of the cells. Cells were passaged twice a week.

Binding Studies. Membrane Preparation.—The cells were passaged according to their passaging rate (1:8) and plated on petri dishes 3 days before preparation. The preparation itself was carried out on ice. The medium was dispensed, and the cells were washed with 5 mL of PBS. Then, 3.5 mL of preparation buffer (50mM Tris, 1 mM MgCl₂·6H₂O, 1 mM EDTA, pH 7.4) were added. The cells were scrubbed from the surface, and the cell suspensions were combined. The combined suspension was treated two times for 10 s with an ultraturrax. The cell lysate was then centrifuged for 10 min at 3200 rpm at 4 °C. The supernatant was transferred to ultracentrifugation tubes and centrifugated for 50 min at 37,000 rpm at 4 °C. The supernatant was discarded, and the pellet was resuspended in binding buffer (50 mM Tris, 5 mM MgCl₂·6 H₂O, 2.5 mM EDTA, pH 7.4). The protein concentration of the pellet was determined using the Bradford assay (according to vendor's description). The suspension was passaged, and the aliquots were shock-frosted in liquid nitrogen and stored at –80 °C until further use.

Radioligand Binding Assay.—SR-144,528 (inverse agonist for hCB₂R) was purchased from Santa Cruz Biotechnology Inc. Unlabeled CP 55,940 (agonist for hCB₂R and hCB₁R) was obtained from Sigma-Aldrich Life Science. Radioactive labeled [³H]CP 55,940 was acquired by Hartmann Analytic GmbH. Rimonabant (inverse agonist for hCB₁R) was obtained by an in-house synthesis. Saturation assays were carried out similar to Murkherjee et al.⁹⁴ to determine the K_d value of the membrane samples. Saturation assays were carried out using eight concentrations of [³H]CP 55,940, ranging from 0.088 to 4.4 nM. Reactions

were started by adding 8 μg membrane per well of a 96 well Multiscreen filter plate (Millipore) containing the radioligand in assay buffer (50 mM Tris-HCl, pH 7.4; 5 mM $\text{MgCl}_2 \cdot 6 \text{H}_2\text{O}$; 2.5 mM EDTA; 2 mg/mL BSA). After incubating for 3 h at RT, the reaction was stopped by vacuum filtration, and each well was washed four times with 100 μL of cold binding buffer (50 mM Tris-HCl, pH 7.4; 5 mM $\text{MgCl}_2 \cdot 6 \text{H}_2\text{O}$; 2.5 mM EDTA). The filter plate was dried at 40 $^\circ\text{C}$. The activity was measured in a Microbeta Trilux counter (Wallac) using an IRGA Safe plus-scintillation cocktail (PerkinElmer). Competition assays were performed with 5–11 concentrations of replacing ligands (0.1 nM–0.4 mM) and 0.44 nM [^3H]CP 55,940. Nonspecific binding was determined using 10 μM **2** for hCB_2R and 10 μM rimonabant for hCB_1R .

Statistical Analysis.—To determine the IC_{50} values, statistical evaluations and sigmoidal dose-response curve fittings were performed using GraphPad Prism 5 software applying nonlinear regression and one site fit $\log\text{IC}_{50}$ as curve fitting functions. K_i values were determined according to the Cheng-Prusoff equation when the displacement of [^3H]CP 55,940 was higher than 60% at 100 μM test compound concentration

$$K_i = \frac{\text{IC}_{50}}{1 + \frac{[\text{L}^*]}{K_D}}$$

with $[\text{L}^*]$ as radioligand concentration (0.44 nM), and the K_i value was calculated for at least two individual experiments. K_D values and standard errors were determined for hCB_2R K_D (hCB_2R) = 4.16 ± 3.04 and for CB_1R K_D (hCB_1R) = 2.24 ± 1.15 .

hCB_2R Efficacy. MTT Assay.—The U266 cell line (4×10^4 cells/mL) was plated on 96-well plates to a final volume of 100 μL /well. After incubating for 1 day, compounds or vehicles were added at different concentrations. Six replicates were used for each treatment. At the indicated time point, cell viability was assessed by adding 0.8 mg/mL 3-[4,5-dimethylthiazol-2-yl]-2,5-diphenyl tetrazolium bromide (MTT) (Sigma-Aldrich) to the medium. After 3 h, the plates were centrifuged, the supernatant was discarded, and the pellet was solubilized with 100 μL /well DMSO. The absorbance of the samples against a background control (medium alone) was measured at 570 nm using an ELISA reader microliter plate (BioTek Instruments, Winooski, VT, USA). For some experiments, 1 h of preincubation with Forskolin or AM630 was performed. Each sample was evaluated in six wells and in two independent experiments.

cAMP Assay.—U266 cells (1×10^6 /mL) were plated in 24-well plates and treated with the appropriate compounds for 2 h. After treatment, the cells were processed for the detection of cAMP levels, using the cAMP assay kit (Enzo Life Sciences, Farmingdale, NY, USA) in accordance to the manufacturer's protocol. U266 cells were treated with Forskolin (10 μM), AM630 (25 μM), or compound (50 μM) for 2 h. For combination treatments, U266 cells were preincubated with AM630 (25 μM) for 30 min before adding the compounds. The concentration of cAMP was calculated by measuring the absorbance at 450 nm with an ELISA reader. Each compound was evaluated in duplicate and in two independent assays. cAMP levels were stated as pmol/mg protein.

RNA Extraction and qRT-PCR.—Total RNA from treated and vehicle U266 cells was extracted using the RNeasy Mini Kit (Qiagen) at the appropriate time points, and cDNA was synthesized using the High-Capacity cDNA Archive Kit (Applied Biosystems, Foster City, PA) according to the manufacturer's instructions. Quantitative real-time polymerase chain reactions (qRT-PCR) for MIF, STAT-3, and GAPDH were performed using the iQ5 multicolor real-time PCR detection system (Bio-Rad, Hercules, CA). The PCR reaction was performed with SYBR Green qPCR mastermix (Qiagen) using 500 ng of cDNA for the reaction, following the amplification protocol indicated by the manufacturer's instruction. All samples were tested in triplicates in the same plate, GAPDH levels were used to normalize mRNA contents, and target gene levels were calculated by the 2^{-CT} method. cDNA from Forskolin-treated cells was used as CREB-induced MIF and STAT-3 as a positive control. cDNA from MD-48-treated cells was used for CB₂ agonist MIF and STAT-3 gene expression control. cDNA from AM630-treated cells was used for antagonist/inverse agonist CB₂ MIF and STAT-3 expression control. Each sample was evaluated in triplicate and in three different experiments.

Statistical Analysis.—The statistical significance for MTT and qRT-PCR assays was determined using the analysis of variance (ANOVA) test. The calculation of IC₅₀ was performed by a nonlinear fit of log-dose versus response, using GraphPad Prism 5.01 software. cAMP concentration was calculated utilizing a four-parameter logistic (4PL) curve fitting program.

Calcium Mobilization Assay.—Compounds were tested using a fluorescence-based assay. Briefly, CHO-K1 cells were engineered to either co-express hCB₁R and G_{αq16} or hCB₂R and G_{αq16}. Activation of the receptor therefore leads to mobilization of intracellular calcium. Cells were seeded out in 96-well plates and incubated overnight. The next day, cells were loaded with the fluorescent dye calcein-4 AM. Calcium flux was monitored using an automated plate reader (FlexStation, Molecular Devices). Statistical analysis was performed using GraphPad Prism 5 software.

Effects on Microglia.

Cell Cultures.—Mouse N9 microglial cells were cultured in Dulbecco's modified Eagle's medium (DMEM) supplemented with 10% heat-inactivated fetal bovine serum (FBS), 1% penicillin/streptomycin, and 2 mM glutamine (all cell cultures' reagents were from Aurogene Srl, Rome, Italy). At confluence, after a short wash with sterile PBS, microglia were trypsinized for 5 min at 37 ° C, and trypsin was inactivated with a complete DMEM medium. Detached cells were then collected, centrifuged for 5 min at 300g, and resuspended to be counted. For experiments, microglial cells were plated at the density of 2.5×10^5 in a 35 mm Ø dish and exposed to 100 ng/mL lipopolysaccharide (LPS), in the presence or absence of increasing concentrations of the compound to be tested. After 24 h of treatment, microglial conditioned media were collected and partly used for nitrite measurement, partly filtered through 0.22 μm filters, concentrated using Microcon YM-3 (Millipore, Billerica, MA), and resuspended in 12 μL of 4× loadingbuffer (0.2 M Tris-HCl, pH 6.8; 8% sodium dodecyl sulfate; 40% glycerol; 0.4% bromophenol blue, and 0.4 M dithiothreitol; Sigma-

Aldrich) for Western blot analysis. In parallel, microglial cells were collected in 2× loading buffer (LB; 50 μ L per dish) for Western blot analysis.

Western Blotting.—Concentrated microglial conditioned media and cell samples were briefly sonicated and loaded into 12% sodium dodecyl sulfate-polyacrylamide gel electrophoresis (SDS-PAGE; Bio-Rad). After electrophoresis and transfer onto nitrocellulose membranes (GE Healthcare, Milano, Italy), membranes were blocked for 1 h in blocking solution PBS-0.1% Tween-20 (Sigma-Aldrich), 4% nonfat dry milk (Bio-Rad) and incubated overnight at 4 °C with primary antibodies in PBS-0.1% Tween-20. Primary antibodies used were rabbit anti-iNOS, rabbit anti-IL1 β , rabbit anti-TREM2, and rabbit anti-TGF β 2, and mouse anti-GAPDH (all 1:1000 dilution except for anti-GAPDH used 1:20,000 dilution, all from Santa Cruz Biotechnology). Membranes were then incubated with specific secondary antibodies conjugated to horseradish peroxidase (goat anti-rabbit and goat anti-mouse, both at 1:2000 dilution and from Santa Cruz) for 90 min at room temperature in PBS-0.1% Tween-20. Labeled proteins were visualized by using the Clarity Western ECL substrate (Bio-Rad) and detected using Bio-Rad Image Lab software with a ChemiDoc MP imaging system (Bio-Rad).

Nitrite Assay.—Accumulation of nitrite in microglial conditioned media was measured by a colorimetric assay based on the Griess reaction. A nitrate standard curve was performed with NaNO₂ at known concentrations. Sulfanilamide (5 mM; Sigma-Aldrich) was added to the culture medium and the standard curve. Sulfanilamide reacts with nitrite under acidic conditions to form a diazonium cation, which subsequently couples to *N*-1-naphthyl-ethylenediamine dihydrochloride (NEDA, 40 mM; Sigma-Aldrich) to produce a colored azo dye. After 15 min of incubation at room temperature in the dark, absorbance was read at 540 nm with a multiplate spectrophotometric reader (Bio-Rad Laboratories Srl, Segrate, Milano, Italy).

Statistical Analysis.—All quantitative data are presented as means \pm SE from at least three independent experiments. Statistical significance between different treatments was calculated using GraphPad Prism 6 software applying one-way analysis of variance (ANOVA) followed by post hoc comparison through Bonferroni's test. A value of $p < 0.05$ was considered statistically significant.

Neuroprotection on HT-22 Cells.

Cell Culture.—HT-22 cells were grown in Dulbecco's modified Eagle's medium (DMEM, Sigma-Aldrich, Munich, Germany) supplemented with 10% (v/v) heat-inactivated fetal calf serum (FCS) and 1% (v/v) penicillin/streptomycin. Cells were passaged every 2 days and incubated at 37 °C with 5% CO₂ in a humidified incubator. Compounds were dissolved in DMSO, (Sigma-Aldrich, Munich, Germany) and diluted with medium. Generally, 80% confluent cells were seeded with 5000 cells per well into sterile 96-well plates and were incubated for 24 h.

Neurotoxicity.—For the neurotoxicity assay, the previous medium was discarded, and different concentrations of the compound were added to the wells. DMSO (0.5%) in DMEM

served as control. Cells were incubated for 24 h. After incubation, an MTT assay was performed.

Neuroprotection.—For neuroprotection, 5 mM glutamate (monosodium-L-glutamate, Sigma-Aldrich, Munich, Germany) was co-incubated with different concentrations of respective compounds for 24 h. Quercetin (25 μ M, Sigma-Aldrich, Munich, Germany) served as a positive control. After 24 h of incubation, an MTT assay was performed.

MTT Assay.—Cell viability was determined using the 3-(4,5-dimethylthiazol-2-yl)-2,5-diphenyl tetrazolium bromide (MTT, Sigma-Aldrich, Munich, Germany) assay. MTT solution (4 mg/mL in PBS) was diluted 1:10 with medium and added to the wells after removal of the previous medium. Cells were incubated for 3 h when the supernatant was removed and lysis buffer (10% SDS) was applied. The next day, absorbance at 560 nm was determined with a multiwell plate photometer (Tecan, SpectraMax 250).

Statistical Analysis.—Results are presented as percentage to untreated control cells. Data are expressed as means \pm SD of three different independent experiments, and each was performed in sextuplicate. Analysis was accomplished using GraphPad Prism 5 software applying one-way ANOVA followed by Dunnett's multiple comparison post-test. Levels of significance: * $p < 0.05$; ** $p < 0.01$; *** $p < 0.001$.

In Vivo Studies.

Aim of the Study.—To test five compounds **3a**, **3d**, **3e**, **4a**, and **6** as protectant drugs in the in vivo mouse model of Alzheimer's disease induced by intracerebroventricular (i.c.v.) injection of oligomerized A β 25–35 peptide. Each compound was injected intraperitoneally (i.p.) o.d. between day 1 and 7, as summarized in Supplementary Figure 4. The peptide was injected on day 1, and behavioral examination was performed between days 8 and 10. All animals were then sacrificed on day 11 and their brain stored at -80 °C awaiting further biochemical analyses. In addition, the livers of high dose-treated animals (3 mg/kg) were removed and fixed in form-aldehyde solution.

Animals.—Male Swiss mice, 6 weeks old and weighing 30–35 g, from Janvier (Saint-Berthevin, France), were kept for housing, and experiments took place within the animal facility building of the University of Montpellier (CECEMA, Office of Veterinary Services agreement #B-34-172-23). Animals were housed in groups with access to food and water ad libitum, except during behavioral experiments. They were kept in a temperature and humidity-controlled animal facility on a 12 h/12 h light/dark cycle (lights off at 07:00 p.m.). All animal procedures were conducted in strict adherence to the European Union directive of September 22, 2010 (2010/63/UE) and authorized (file #1485-15034) by the National Ethic Committee (Paris, France).

Drug Preparation.—Compounds were weighed and solubilized in pure DMSO, and a stock solution at 2 mg/mL was prepared in DMSO/ddH₂O. The percentage of DMSO in ddH₂O for 3 mg/kg dose was 30%. Stock solution in DMSO was stored for 1 week at +4 °C,

and the injection solutions were made fresh daily. Vehicle solutions used for control groups were DMSO 30% in H₂O.

Amyloid Peptide Preparation and Injection.—Mice were anesthetized with isoflurane 2.5% and were injected i.c.v. with A β _{25–35} peptide (9 nmol/mouse) or vehicle solution (distilled water), in a final volume of 3 μ L/mouse, according to the previously described method.^{87,95–99} Homogeneous oligomeric preparation of A β _{25–35} peptide was performed by incubation for 4 days at 37 °C according to Maurice et al.⁸⁷ Since it is well established that vehicle solution similar as a control scrambled A β _{25–35} peptide failed to induce toxicity and therefore affect learning abilities, vehicle-treated animals served as controls.^{87,95–100}

Spontaneous Alternation Performances.—On day 8, all animals were tested for spontaneous alternation performance in the Y maze, an index of spatial working memory. The Y maze is made of gray polyvinyl chloride. Each arm is 40 cm long, 13 cm high, 3 cm wide at the bottom, 10 cm wide at the top, and converging at an equal angle. Each mouse will be placed at the end of one arm and allowed to move freely through the maze during an 8 min session. The series of arm entries, including possible returns into the same arm, was checked visually. An alternation was defined as entries into all three arms on consecutive occasions. The number of maximum alternations is, therefore, the total number of arm entries minus two, and the percentage of alternation was calculated as (actual alternations/maximum alternations) \times 100. Parameters included the percentage of alternation (memory index) and the total number of arm entries (exploration index).^{87,95,96,98,99} Animals that shown an extreme behavior (alternation percentage of <20% or >90% or number of arm entries <10) were discarded from the calculation. In this study, 11 animals were discarded accordingly (3.2% attrition).

Passive Avoidance Test.—On days 9 and 10, a passive avoidance test was performed. The apparatus is a two-compartment (15 \times 20 \times 15 cm high) box with one compartment illuminated with white polyvinyl chloride walls and the other darkened with black polyvinyl chloride walls and a grid floor. A guillotine door separates each compartment. A 60 W lamp positioned 40 cm above the apparatus lights up the white compartment during the experiment. Scrambled foot shocks (0.3 mA for 3 s) were delivered to the grid floor using a shock generator scrambler (Lafayette Instruments, Lafayette, USA). The guillotine door was initially closed during the training session. During the training session, on day 9, each mouse was placed into the white compartment. After 5 s, the door was raised. When the mouse entered the darkened compartment and placed all its paws on the grid floor, the door was closed, and the foot shock was delivered for 3 s. The step-through latency, that is, the latency spent to enter the darkened compartment, and the number of vocalizations was recorded. The retention test was carried out 24 h after training, on day 10. Each mouse was placed again into the white compartment. After 5 s, the door was raised. The step-through and escape latencies (corresponding to the re-exit from the darkened compartment) were recorded up to 300 s. Animals that show all latencies during the training and retention session lower than 10 s are considered as failing to respond to the procedure and were discarded from the calculations. In this study, nine animals were discarded accordingly (2.6% attrition).

Sacrifice and Brain and Liver Sampling.—On day 11, all animals were sacrificed, their brains dissected out to isolate the hippocampus and cortex. Samples were frozen in liquid nitrogen and stored at -80°C awaiting further analysis. For treated with the high dose (3 mg/kg) of compounds, the livers were also dissected out, post-fixed in formalin, and kept at 4°C .

Statistical Analyses.—All values, except passive avoidance latencies, were expressed as means \pm SEM. Statistical analyses were performed on the different conditions using one-way ANOVA (F value), followed by Dunnett's post hoc multiple comparison test. Passive avoidance latencies do not follow a Gaussian distribution since upper cutoff times are set. They were therefore analyzed using a Kruskal-Wallis nonparametric ANOVA (H value), followed by Dunn's multiple comparison test. $p < 0.05$ was considered as statistically significant.

Supplementary Material

Refer to Web version on PubMed Central for supplementary material.

ACKNOWLEDGMENTS

We thank O. Lockridge (University of Nebraska Medical Center) for providing human BChE. We thank S. Kachler and Professor K.-N. Klotz (Institute of Pharmacology and Toxicology, University of Würzburg) for technical support and workspace for radioligand binding studies. Mrs. Nicola Arveda's technical assistance is acknowledged for the assays involving hAChE.

Funding

M.D. acknowledges the German Research Council (Deutsche Forschungsgemeinschaft (DFG) DFG DE 1546/6-3 and M.D. and T.M. also acknowledge support from Campus France (PHC Procope) and the German Academic Exchange Service (DAAD) with funds of the Federal Ministry of Education and Research (BMBF). The Italian Ministry of Education, Universities and Research (MIUR) is acknowledged for financial support. M.H. acknowledges the German Academic Scholarship Foundation ("Studienstiftung des deutschen Volkes") for a Ph.D. fellowship and the Elite Network of Bavaria (International Doctoral program "Receptor Dynamics") for support.

ABBREVIATIONS

Aβ	amyloid-beta
ACh	acetylcholine
AChE	acetylcholinesterase
ACth	acetylthiocholine
AD	Alzheimer's disease
ANOVA	analysis of variance
APP	amyloid precursor protein
BBB	blood-brain-barrier
BChE	butyrylcholinesterase

cAMP	cyclic adenosine monophosphate
CAS	catalytic active site
ChE	cholinesterase
CHO	Chinese hamster ovary
CNS	central nervous system
Cpd	compound
CRE	cAMP response element
CREB	cAMP response element-binding protein
DMSO	dimethyl sulfoxide
FSK	forskolin
GAPDH	glycerin-aldehyde-3-phosphat-dehydrogenase
GTPγS	guanosine 5' [γ -thio]triphosphate
HBTU	2-(1 <i>H</i> -benzotriazol-1-yl)-1,1,3,3-tetramethyluronium hexafluorophosphate
hCB$_{1/2}$R	human cannabinoid receptor 1/2
HEK	human embryonic kidney
i.c.v.	intracerebroventricular
IL1β	interleukin 1 beta
iNOS	inducible nitric oxide synthase
i.p.	intraperitoneal
LPS	lipopolysaccharide
MIF	macrophage migration inhibitory factor
MTT	3-(4,5-dimethylthiazol-2-yl)-2,5-diphenyltetrazolium bromide
NMDA	<i>N</i> -methyl-D-aspartate
MOR	μ -opioid receptor
PAS	peripheral anionic site
PEG	polyethylene glycol
ROS	reactive oxygen species
(q)RT/PCR	(quantitative) reverse transcription polymerase chain reaction

SAR	structure-activity relationship
SD	standard deviation
SR	scavenger receptor
STAT-3	signal transducer and activator of transcription
ST-PA	step-through passive avoidance
TGFβ2	transforming growth factor beta-2
THC	tetrahydrocannabinol
THF	tetrahydrofuran
TNF	tumor necrosis factor
TREM2	triggering receptor expressed on myeloid cells 2
V or VEI	vehicle
YMT	Y-maze test

REFERENCES

- (1). Patterson C World Alzheimer report 2018; ADI: London, 2018; pp 1–48.
- (2). Zemek F; Drtinova L; Nepovimova E; Sepsova V; Korabecny J; Klimes J; Kuca K Outcomes of Alzheimer's disease therapy with acetylcholinesterase inhibitors and memantine. *Expert Opin. Drug Saf* 2014, 13, 759–774. [PubMed: 24845946]
- (3). Glenner GG; Wong CW Alzheimer's disease: initial report of the purification and characterization of a novel cerebrovascular amyloid protein. *Biochem. Biophys. Res. Commun* 1984, 120, 885–890. [PubMed: 6375662]
- (4). Grundke-Iqbal I; Iqbal K; Tung YC; Quinlan M; Wisniewski HM; Binder LI Abnormal phosphorylation of the microtubule-associated protein τ (tau) in Alzheimer cytoskeletal pathology. *Proc. Natl. Acad. Sci. U. S. A* 1986, 83, 4913–4917. [PubMed: 3088567]
- (5). Ferrer I Defining Alzheimer as a common age-related neurodegenerative process not inevitably leading to dementia. *Prog. Neurobiol* 2012, 97, 38–51. [PubMed: 22459297]
- (6). Tsai J; Grutzendler J; Duff K; Gan W-B Fibrillar amyloid deposition leads to local synaptic abnormalities and breakage of neuronal branches. *Nat. Neurosci* 2004, 7, 1181. [PubMed: 15475950]
- (7). Gómez-Isla T; Hollister R; West H; Mui S; Growdon JH; Petersen RC; Parisi JE; Hyman BT Neuronal loss correlates with but exceeds neurofibrillary tangles in Alzheimer's disease. *Ann. Neurol* 1997, 41, 17–24. [PubMed: 9005861]
- (8). Loo DT; Copani A; Pike CJ; Whittlemore ER; Walencewicz AJ; Cotman CW Apoptosis is induced by beta-amyloid in cultured central nervous system neurons. *Proc. Natl. Acad. Sci. U.S.A* 1993, 90, 7951–7955.
- (9). Zhu X; Raina AK; Lee HG; Casadesus G; Smith MA; Perry G Oxidative stress signalling in Alzheimer's disease. *Brain Res.* 2004, 1000, 32–39. [PubMed: 15053949]
- (10). LaFerla FM Calcium dyshomeostasis and intracellular signalling in Alzheimer's disease. *Nat. Rev. Neurosci* 2002, 3, 862–872. [PubMed: 12415294]
- (11). Akiyama H; Barger S; Barnum S; Bradt B; Bauer J; Cole GM; Cooper NR; Eikelenboom P; Emmerling M; Fiebich BL; Finch CE; Frautschy S; Griffin WST; Hampel H; Hull M; Landreth G; Lue L-F; Mrak R; Mackenzie IR; McGeer PL; O'Banion MB; Pachter J; Pasinetti G; Plata-Salaman C; Rogers J; Rydel R; Shen Y; Streit W; Strommeyer R; Tooyoma I; Van Muiswinkel

- FL; Veerhuis R; Walker D; Webster S; Wegrzyniak B; Wenk G; Wyss-Coray T Inflammation and Alzheimer's disease. *Neurobiol. Aging* 2000, 21, 383–421. [PubMed: 10858586]
- (12). Wyss-Coray T; Mucke L Inflammation in neurodegenerative disease—a double-edged sword. *Neuron* 2002, 35, 419–432. [PubMed: 12165466]
- (13). Barger SW; Harmon AD Microglial activation by Alzheimer amyloid precursor protein and modulation by apolipoprotein E. *Nature* 1997, 388, 878–881. [PubMed: 9278049]
- (14). Meda L; Cassatella MA; Szendrei GI; Ottvos L Jr.; Baron P; Villalba M; Ferrari D; Rossi F Activation of microglial cells by β -amyloid protein and interferon- γ . *Nature* 1995, 374, 647–650. [PubMed: 7715705]
- (15). Yang C-N; Shiao Y-J; Shie F-S; Guo B-S; Chen P-H; Cho C-Y; Chen Y-J; Huang F-L; Tsay H-J Mechanism mediating oligomeric A β clearance by naïve primary microglia. *Neurobiol. Dis* 2011, 42, 221–230. [PubMed: 21220023]
- (16). Wang W-Y; Tan M-S; Yu J-T; Tan L Role of proinflammatory cytokines released from microglia in Alzheimer's disease. *Ann. Transl. Med* 2015, 3, 136. [PubMed: 26207229]
- (17). Katona I; Freund TF Multiple functions of endocannabinoid signaling in the brain. *Annu. Rev. Neurosci* 2012, 35, 529–558. [PubMed: 22524785]
- (18). Mechoulam R; Parker LA The endocannabinoid system and the brain. *Annu. Rev. Psychol* 2013, 64, 21–47. [PubMed: 22804774]
- (19). Lutz B; Marsicano G; Maldonado R; Hillard CJ The endocannabinoid system in guarding against fear, anxiety and stress. *Nat. Rev. Neurosci* 2015, 16, 705–718. [PubMed: 26585799]
- (20). Ameri A The effects of cannabinoids on the brain. *Prog. Neurobiol* 1999, 58, 315–348. [PubMed: 10368032]
- (21). Munro S; Thomas KL; Abu-Shaar M Molecular characterization of a peripheral receptor for cannabinoids. *Nature* 1993, 365, 61–65. [PubMed: 7689702]
- (22). Van Sickle MD; Duncan M; Kingsley PJ; Mouihate A; Urbani P; Mackie K; Stella N; Makriyannis A; Piomelli D; Davison JS; Marnett LJ; Di Marzo V; Pittman QJ; Patel KD; Sharkey KA Identification and functional characterization of brainstem cannabinoid CB2 receptors. *Science* 2005, 310, 329–332. [PubMed: 16224028]
- (23). Núñez E; Benito C; Pazos M R; Barbachano, A.; Fajardo, O.; González, S.; Tolón, R M.; Romero, J. Cannabinoid CB2 receptors are expressed by perivascular microglial cells in the human brain: an immunohistochemical study. *Synapse* 2004, 53, 208–213. [PubMed: 15266552]
- (24). Grünblatt E; Zander N; Bartl J; Jie L; Monoranu CM; Arzberger T; Ravid R; Roggendorf W; Gerlach M; Riederer P Comparison analysis of gene expression patterns between sporadic Alzheimer's and Parkinson's disease. *J. Alzheimer's Dis* 2007, 12, 291–311. [PubMed: 18198416]
- (25). Benito C; Núñez E; Tolón R M.; Carrier, E. J.; Rábano, A.; Hillard, C. J.; Romero, J. Cannabinoid CB2 receptors and fatty acid amide hydrolase are selectively overexpressed in neuritic plaque-associated glia in Alzheimer's disease brains. *J. Neurosci* 2003, 23, 11136–11141. [PubMed: 14657172]
- (26). Bisogno T; Oddi S; Piccoli A; Fazio D; Maccarrone M Type-2 cannabinoid receptors in neurodegeneration. *Pharmacol. Res* 2016, 111, 721–730. [PubMed: 27450295]
- (27). Ehrhart J; Obregon D; Mori T; Hou H; Sun N; Bai Y; Klein T; Fernandez F; Tan J; Shytle RD Stimulation of cannabinoid receptor 2 (CB 2) suppresses microglial activation. *J. Neuroinflammation* 2005, 2, 29. [PubMed: 16343349]
- (28). Molina-Holgado F; Molina-Holgado E; Guaza C; Rothwell NJ Role of CB1 and CB2 receptors in the inhibitory effects of cannabinoids on lipopolysaccharide-induced nitric oxide release in astrocyte cultures. *J. Neurosci. Res* 2002, 67, 829–836. [PubMed: 11891798]
- (29). Sheng WS; Hu S; Min X; Cabral GA; Lokensgard JR; Peterson PK Synthetic cannabinoid WIN55, 212-2 inhibits generation of inflammatory mediators by IL-1 β -stimulated human astrocytes. *Glia* 2005, 49, 211–219. [PubMed: 15390091]
- (30). Wu J; Bie B; Yang H; Xu JJ; Brown DL; Naguib M Activation of the CB2 receptor system reverses amyloid-induced memory deficiency. *Neurobiol. Aging* 2013, 34, 791–804. [PubMed: 22795792]

- (31). Martín-Moreno AM; Brera B; Spuch C; Carro E; García-García L; Delgado M; Pozo MA; Innamorato NG; Cuadrado A; de Ceballos ML Prolonged oral cannabinoid administration prevents neuroinflammation, lowers β -amyloid levels and improves cognitive performance in Tg APP 2576 mice. *J. Neuroinflammation* 2012, 9, 1–15. [PubMed: 22212381]
- (32). Koppel J; Vingtdoux V; Marambaud P; d'Abramo C; Jimenez H; Stauber M; Friedman R; Davies P CB2 receptor deficiency increases amyloid pathology and alters tau processing in a transgenic mouse model of Alzheimer's disease. *Mol. Med* 2013, 19, 29–36.
- (33). Davies P; Maloney AJF Selective loss of central cholinergic neurons in Alzheimer's disease. *Lancet* 1976, 308, 1403.
- (34). Arendt T; Brückner MK; Lange M; Bigl V Changes in acetylcholinesterase and butyrylcholinesterase in Alzheimer's disease resemble embryonic development—a study of molecular forms. *Neurochem. Int* 1992, 21, 381–396. [PubMed: 1303164]
- (35). Greig NH; Utsuki T; Yu QS; Zhu X; Holloway HW; Perry T; Lee B; Ingram DK; Lahiri DK A new therapeutic target in Alzheimer's disease treatment: attention to butyrylcholinesterase. *Curr. Med. Res. Opin* 2001, 17, 159–165. [PubMed: 11900310]
- (36). Giacobini E Cholinergic function and Alzheimer's disease. *Int. J. Psychiatry* 2003, 18, S1–S5.
- (37). Grossberg GT Cholinesterase inhibitors for the treatment of Alzheimer's disease: getting on and staying on. *Curr. Ther. Res* 2003, 64, 216–235. [PubMed: 24944370]
- (38). Darvesh S; Hopkins DA; Geula C Neurobiology of butyrylcholinesterase. *Nat. Rev. Neurosci* 2003, 4, 131–138. [PubMed: 12563284]
- (39). Mesulam MM; Guillozet A; Shaw P; Levey A; Duysen E; Lockridge O Acetylcholinesterase knockouts establish central cholinergic pathways and can use butyrylcholinesterase to hydrolyze acetylcholine. *Neuroscience* 2002, 110, 627–639. [PubMed: 11934471]
- (40). Nordberg A; Ballard C; Bullock R; Darreh-Shori T; Somogyi M A review of butyrylcholinesterase as a therapeutic target in the treatment of Alzheimer's disease. *Prim. Care Companion CNS Disord* 2013, 15, 1–30.
- (41). Hartmann J; Kiewert C; Duysen EG; Lockridge O; Greig NH; Klein J Excessive hippocampal acetylcholine levels in acetylcholinesterase-deficient mice are moderated by butyrylcholinesterase activity. *J. Neurochem* 2007, 100, 1421–1429. [PubMed: 17212694]
- (42). Furukawa-Hibi Y; Alkam T; Nitta A; Matsuyama A; Mizoguchi H; Suzuki K; Moussaoui S; Yu QS; Greig NH; Nagai T; Yamada K Butyrylcholinesterase inhibitors ameliorate cognitive dysfunction induced by amyloid- β peptide in mice. *Behav. Brain Res* 2011, 225, 222–229. [PubMed: 21820013]
- (43). Greig NH; Utsuki T; Ingram DK; Wang Y; Pepeu G; Scali C; Yu QS; Mamczarz J; Holloway HW; Giordano T; Chen D; Furukawa K; Sambamurti K; Brossi A; Lahiri DK Selective butyrylcholinesterase inhibition elevates brain acetylcholine, augments learning and lowers Alzheimer β -amyloid peptide in rodent. *Proc. Natl. Acad. Sci* 2005, 102, 17213–17218. [PubMed: 16275899]
- (44). Maurice T; Strehaiano M; Siméon N; Bertrand C; Chatonnet A Learning performances and vulnerability to amyloid toxicity in the butyrylcholinesterase knockout mouse. *Behav. Brain Res* 2016, 296, 351–360. [PubMed: 26306824]
- (45). Morphy R; Rankovic Z Designed multiple ligands. An emerging drug discovery paradigm. *J. Med. Chem* 2005, 48, 6523–6543. [PubMed: 16220969]
- (46). Proschak E; Stark H; Merk D Polypharmacology by design: a medicinal chemist's perspective on multitargeting compounds. *J. Med. Chem* 2019, 62, 420–444. [PubMed: 30035545]
- (47). Dolles D; Decker M Dual-acting compounds acting as receptor ligands and enzyme inhibitors In *Design of hybrid molecules for drug development*, Elsevier: Amsterdam, 2017; pp 137–165.
- (48). Dolles D; Hoffmann M; Gunesch S; Marinelli O; Möller J; Santoni G; Chatonnet A; Lohse MJ; Wittmann H-J; Strasser A; Nabissi M; Maurice T; Decker M Structure-activity relationships and computational investigations into the development of potent and balanced dual-acting butyrylcholinesterase inhibitors and human cannabinoid receptor 2 ligands with pro-cognitive in vivo profiles. *J. Med. Chem* 2018, 61, 1646–1663. [PubMed: 29400965]
- (49). Freeman SE; Dawson RM Tacrine: a pharmacological review. *Prog. Neurobiol* 1991, 36, 257–277. [PubMed: 1714613]

- (50). Summers WK; Majovski LV; Marsh GM; Tachiki K; Kling A Oral tetrahydroaminoacridine in long-term treatment of senile dementia, Alzheimer type. *N. Engl. J. Med* 1986, 315, 1241–1245. [PubMed: 2430180]
- (51). Watkins PB; Zimmerman HJ; Knapp MJ; Gracon SI; Lewis KW Hepatotoxic effects of tacrine administration in patients with Alzheimer's disease. *JAMA* 1994, 271, 992–998. [PubMed: 8139084]
- (52). Milelli A; De Simone A; Ticchi N; H. Chen H; Betari N; Andrisano V; Tumiatti V Tacrine-based multifunctional agents in Alzheimer's disease: an old story in continuous development. *Curr. Med. Chem* 2017, 24, 3522–3546. [PubMed: 28294041]
- (53). Lin H; Li Q; Gu K; Zhu J; Jiang X; Chen Y; Sun H Therapeutic agents in Alzheimer's disease through a multi-target directed ligands strategy: Recent progress based on tacrine core. *Curr. Top. Med. Chem* 2017, 17, 3000–3016. [PubMed: 28714419]
- (54). Chen X; Zenger K; Lupp A; Kling B; Heilmann J; Fleck C; Kraus B; Decker M Tacrine-silibinin codrug shows neuro- and hepatoprotective effects in vitro and pro-cognitive and hepatoprotective effects in vivo. *J. Med. Chem* 2012, 55, 5231–5242. [PubMed: 22624880]
- (55). McEneny-King A; Osman W; Edginton AN; Rao PPN Cytochrome P450 binding studies of novel tacrine derivatives: predicting the risk of hepatotoxicity. *Bioorg. Med. Chem. Lett* 2017, 27, 2443–2449. [PubMed: 28400237]
- (56). Zenger K; Chen X; Decker M; Kraus B In-vitro stability and metabolism of a tacrine-silibinin codrug. *J. Pharm. Pharmacol* 2013, 65, 1765–1772. [PubMed: 24236987]
- (57). Pagé D; Balaux E; Boisvert L; Liu Z; Milburn C; Tremblay M; Wei Z; Woo S; Luo X; Cheng Y-X; Yang H; Srivastava S; Zhou F; Brown W; Tomaszewski M; Walpole C; Hodzic L; St-Onge S; Godbout C; Salois D; Payza K Novel benzimidazole derivatives as selective CB₂ agonists. *Bioorg. Med. Chem. Lett* 2008, 18, 3695–3700. [PubMed: 18522867]
- (58). Dolles D; Nimczick M; Scheiner M; Ramler J; Stadtmüller P; Sawatzky E; Drakopoulos A; Sotriuffer C; Wittmann H-J; Strasser A; Decker M Aminobenzimidazoles and structural isomers as templates for dual-acting butyrylcholinesterase inhibitors and hCB2R ligands to combat neurodegenerative disorders. *ChemMedChem* 2016, 11, 1270–1283. [PubMed: 26548365]
- (59). Dolles D; Strasser A; Wittmann HJ; Marinelli O; Nabissi M; Pertwee RG; Decker M The first photochromic affinity switch for the human cannabinoid receptor 2. *Adv. Ther* 2018, 1, 1700032.
- (60). Nimczick M; Pemp D; Darras FH; Chen X; Heilmann J; Decker M Synthesis and biological evaluation of bivalent cannabinoid receptor ligands based on hCB2R selective benzimidazoles reveal unexpected intrinsic properties. *Bioorg. Med. Chem* 2014, 22, 3938–3946. [PubMed: 24984935]
- (61). Mishra P; Kumar A; Panda G Anti-cholinesterase hybrids as multi-target-directed ligands against Alzheimer's disease (1998–2018). *Bioorg. Med. Chem* 2019, 27, 895–930. [PubMed: 30744931]
- (62). Minarini A; Milelli A; Tumiatti V; Rosini M; Simoni E; Bolognesi ML; Andrisano V; Bartolini M; Motori E; Angeloni C; Hrelia S Cystamine-tacrine dimer: a new multi-target-directed ligand as potential therapeutic agent for Alzheimer's disease treatment. *Neuropharmacology* 2012, 62, 997–1003. [PubMed: 22032870]
- (63). Hu M-K; Wu L-J; Hsiao G; Yen M-H Homodimeric tacrine congeners as acetylcholinesterase inhibitors. *J. Med. Chem* 2002, 45, 2277–2282. [PubMed: 12014965]
- (64). Ellman GL; Courtney KD; Andres V Jr.; Featherstone RM A new and rapid colorimetric determination of acetylcholinesterase activity. *Biochem. Pharmacol* 1961, 7, 88–95. [PubMed: 13726518]
- (65). Bartolini M; Bertucci C; Cavrini V; Andrisano V β -Amyloid aggregation induced by human acetylcholinesterase: inhibition studies. *Biochem. Pharmacol* 2003, 65, 407–416. [PubMed: 12527333]
- (66). Castro A; Martinez A Targeting beta-amyloid pathogenesis through acetylcholinesterase inhibitors. *Curr. Pharm. Des* 2006, 12, 4377–4387. [PubMed: 17105433]
- (67). Zha X; Lamba D; Zhang L; Lou Y; Xu C; Kang D; Chen L; Xu Y; Zhang L; De Simone A; Samez S; Persaresi A; Stojan J; Lopez MG; Egea J; Andrisano V; Bartolini M Novel tacrine-benzofuran hybrids as potent multitarget-directed ligands for the treatment of Alzheimer's

- disease: design, synthesis, biological evaluation, and X-ray crystallography. *J. Med. Chem* 2016, 59, 114–131. [PubMed: 26632651]
- (68). Bartolini M; Bertucci C; Bolognesi ML; Cavalli A; Melchiorre C; Andrisano V Insight into the kinetic of amyloid β (1–42) peptide self-aggregation: elucidation of inhibitors' mechanism of action. *ChemBioChem* 2007, 8, 2152–2161. [PubMed: 17939148]
- (69). Lange JHM; van Stuivenberg HH; Coolen HKAC; Adolfs TJP; McCreary AC; Keizer HG; Wals HC; Veerman W; Borst AJM; de Looft W; Verveer PC; Kruse CG Bioisosteric replacements of the pyrazole moiety of rimonabant: synthesis, biological properties, and molecular modeling investigations of thiazoles, triazoles, and imidazoles as potent and selective CB1 cannabinoid receptor antagonists. *J. Med. Chem* 2005, 48, 1823–1838. [PubMed: 15771428]
- (70). Yao BB; Hsieh GC; Frost JM; Fan Y; Garrison TR; Daza AV; Grayson GK; Zhu CZ; Pai M; Chandran P; Salyers AK; Wensink EJ; Honore P; Sullivan JP; Dart MJ; Meyer MD In vitro and in vivo characterization of A-796260: a selective cannabinoid CB2 receptor agonist exhibiting analgesic activity in rodent pain models. *Br. J. Pharmacol* 2008, 153, 390–401. [PubMed: 17994110]
- (71). Nimczick M; Decker M New approaches in the design and development of cannabinoid receptor ligands: multifunctional and bivalent compounds. *ChemMedChem* 2015, 10, 773–786. [PubMed: 25820617]
- (72). Howlett AC; Barth F; Bonner TI; Cabral G; Casellas P; Devane WA; Felder CC; Herkenham M; Mackie K; Martin BR; Mechoulam R; Pertwee RG International Union of Pharmacology. XXVII. Classification of cannabinoid receptors. *Pharmacol. Rev* 2002, 54, 161–202. [PubMed: 12037135]
- (73). Ross RA; Brockie HC; Stevenson LA; Murphy VL; Templeton F; Makriyannis A; Pertwee RG Agonist-inverse agonist characterization at CB1 and CB2 cannabinoid receptors of L759633, L759656 and AM630. *Br. J. Pharmacol* 1999, 126, 665–672. [PubMed: 10188977]
- (74). Williams C cAMP detection methods in HTS: selecting the best from the rest. *Nat. Rev. Drug Discov* 2004, 3, 125–135. [PubMed: 15040577]
- (75). Waeber G; Thompson N; Chautard T; Steinmann M; Nicod P; Pralong FP; Calandra T; Gaillard RC Transcriptional activation of the macrophage migration-inhibitory factor gene by the corticotropin-releasing factor is mediated by the cyclic adenosine 3', 5'-monophosphate responsive element-binding protein CREB in pituitary cells. *Mol. Endocrinol* 1998, 12, 698–705. [PubMed: 9605932]
- (76). Kato K; Nomoto M; Izumi H; Ise T; Nakano S; Niho Y; Kohno K Structure and functional analysis of the human STAT3 gene promoter: alteration of chromatin structure as a possible mechanism for the upregulation in cisplatin-resistant cells. *Biochim. Biophys. Acta Gene Struct. Expr* 2000, 1493, 91–100.
- (77). Alas S; Bonavida B Inhibition of constitutive STAT3 activity sensitizes resistant non-Hodgkin's lymphoma and multiple myeloma to chemotherapeutic drug-mediated apoptosis. *Clin. Cancer. Res* 2003, 9, 316–326. [PubMed: 12538484]
- (78). Zheng Y; Wang Q; Li T; Qian J; Lu Y; Li Y; Bi E; Reu F; Qin Y; Drazba J; Hsi E; Yang J; Cai Z; Yi Q Role of myeloma-derived MIF in myeloma cell adhesion to bone marrow and chemotherapy response. *J. Natl. Cancer Inst* 2016, 108, djw131.
- (79). Fulp A; Zhang Y; Bortoff K; Seltzman H; Snyder R; Wiethe R; Amato G; Maitra R Pyrazole antagonists of the CB1 receptor with reduced brain penetration. *Bioorg. Med. Chem* 2016, 24, 1063–1070. [PubMed: 26827137]
- (80). Seltzman HH; Shiner C; Hirt EE; Gilliam AF; Thomas BF; Maitra R; Snyder R; Black SL; Patel PR; Mulpuri Y; Spigelman I Peripherally selective cannabinoid 1 receptor (CB1R) agonists for the treatment of neuropathic pain. *J. Med. Chem* 2016, 59, 7525–7543. [PubMed: 27482723]
- (81). Schramm S; Huang G; Gunesch S; Lang F; Roa J; Högger P; Sabaté R; Maher P; Decker M Regioselective synthesis of 7-O-esters of the flavonolignan silibinin and SARs lead to compounds with overadditive neuroprotective effects. *Eur. J. Med. Chem* 2018, 146, 93–107. [PubMed: 29407994]
- (82). Schramm S; Gunesch S; Lang F; Saedtler M; Meinel L; Högger P; Decker M Investigations into neuroprotectivity, stability, and water solubility of 7-O-cinnamoylsilibinin, its hemisuccinate and dehydro derivatives. *Arch. Pharm* 2018, 351, 1800206.

- (83). Davis JB; Maher P Protein kinase C activation inhibits glutamate-induced cytotoxicity in a neuronal cell line. *Brain Res.* 1994, 652, 169–173. [PubMed: 7953717]
- (84). Murphy TH; Miyamoto M; Sastre A; Schnaar RL; Coyle JT Glutamate toxicity in a neuronal cell line involves inhibition of cystine transport leading to oxidative stress. *Neuron* 1989, 2, 1547–1558. [PubMed: 2576375]
- (85). Tan S; Wood M; Maher P Oxidative stress induces a form of programmed cell death with characteristics of both apoptosis and necrosis in neuronal cells. *J. Neurochem* 1998, 71, 95–105. [PubMed: 9648855]
- (86). Tan S; Schubert D; Maher P Oxytosis: a novel form of programmed cell death. *Curr. Top. Med. Chem* 2001, 1, 497–506. [PubMed: 11895126]
- (87). Maurice T; Lockhart BP; Privat A Amnesia induced in mice by centrally administered β -amyloid peptides involves cholinergic dysfunction. *Brain Res.* 1996, 706, 181–193. [PubMed: 8822355]
- (88). Lahmy V; Meunier J; Malmström S; Naert G; Givalois L; Kim SH; Villard V; Vamvakides A; Maurice T Blockade of Tau hyperphosphorylation and $A\beta$ 1–42 generation by the aminotetrahydrofuran derivative ANAVEX2–73, a mixed muscarinic and σ 1 receptor agonist, in a nontransgenic mouse model of Alzheimer’s disease. *Neuropsychopharmacology* 2013, 38, 1706–1723. [PubMed: 23493042]
- (89). McQuiston AR; Saggau P Mu-opioid receptors facilitate the propagation of excitatory activity in rat hippocampal area CA1 by disinhibition of all anatomical layers. *J. Neurophysiol* 2003, 90, 1936–1948. [PubMed: 12750411]
- (90). Batts KP; Ludwig J An update on terminology and reporting. *Am. J. Surg. Pathol* 1995, 19, 1409–1417. [PubMed: 7503362]
- (91). Mathew T; Karunanithy R; Yee M; Natarajan P Hepatotoxicity of dimethylformamide and dimethylsulfoxide at and above the levels used in some aflatoxin studies. *Lab. Invest* 1980, 42, 257–262. [PubMed: 7354621]
- (92). Silverman RB The organic chemistry of enzyme-catalyzed reactions. Academic Press: London, 2002.
- (93). Naiki H; Higuchi K; Nakakuki K; Takeda T Kinetic analysis of amyloid fibril polymerization in vitro. *Lab. Invest* 1991, 65, 104–110. [PubMed: 1906561]
- (94). Mukherjee S; Adams M; Whiteaker K; Daza A; Kage K; Cassar S; Meyer M; Yao BB Species comparison and pharmacological characterization of rat and human CB_2 cannabinoid receptors. *Eur. J. Pharmacol* 2004, 505, 1–9. [PubMed: 15556131]
- (95). Maurice T; Su T-P; Privat A Sigma1 (σ 1) receptor agonists and neurosteroids attenuate β 25–35-amyloid peptide-induced amnesia in mice through a common mechanism. *Neuroscience* 1998, 83, 413–428. [PubMed: 9460750]
- (96). Meunier J; Ieni J; Maurice T The anti-amnesic and neuroprotective effects of donepezil against amyloid beta25–35 peptide-induced toxicity in mice involve an interaction with the sigma1 receptor. *Br. J. Pharmacol* 2006, 149, 998–1012. [PubMed: 17057756]
- (97). Meunier J; Villard V; Givalois L; Maurice T The γ -secretase inhibitor 2-[(1R)-1-[(4-chlorophenyl) sulfonyl](2, 5-difluorophenyl) amino] ethyl-5-fluorobenzenebutanoic acid (BMS-299897) alleviates $A\beta$ 1–42 seeding and short-term memory deficits in the $A\beta$ 25–35 mouse model of Alzheimer’s disease. *Eur. J. Pharmacol* 2013, 698, 193–199. [PubMed: 23123349]
- (98). Villard V; Espallergues J; Keller E; Alkam T; Nitta A; Yamada K; Nabeshima T; Vamvakides A; Maurice T Anti-amnesic and neuroprotective effects of the aminotetrahydrofuran derivative ANAVEX1-41 against amyloid β 25–35-induced toxicity in mice. *Neuropsychopharmacology* 2009, 34, 1552–1566. [PubMed: 19052542]
- (99). Villard V; Espallergues J; Keller E; Vamvakides A; Maurice T Anti-amnesic and neuroprotective potentials of the mixed muscarinic receptor/sigma1 (σ 1) ligand ANAVEX2-73, a novel aminotetrahydrofuran derivative. *J. Psychopharmacol* 2011, 25, 1101–1117. [PubMed: 20829307]
- (100). Zussy C; Brureau A; Delair B; Marchal S; Keller E; Ixart G; Naert G; Meunier J; Chevallier N; Maurice T; Givalois L Time-course and regional analyses of the physiopathological changes

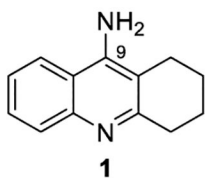
induced after cerebral injection of an amyloid β fragment in rats. *Am. J. Pathol* 2011, 179, 315–334. [PubMed: 21703413]

Author Manuscript

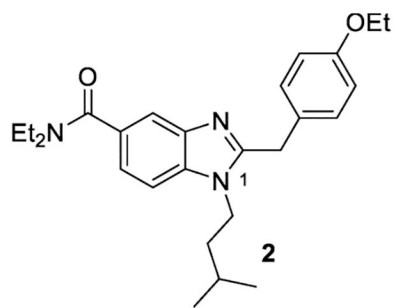
Author Manuscript

Author Manuscript

Author Manuscript



pIC₅₀ (hAChE): 6.8
pIC₅₀ (hBChE): 7.9



K_i (hCB₂R): 36.7 nM⁵⁸
displ. (hCB₁R) at 10 μM: 24%⁵⁸

Figure 1.
Tacrine **1** and selective hCB₂R agonist **2**.⁵⁸

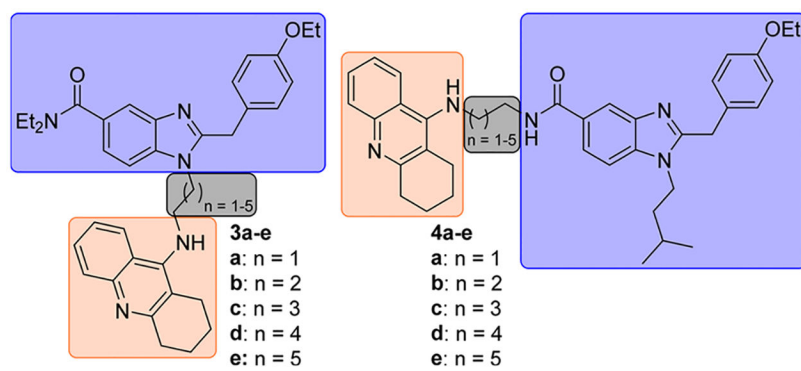


Figure 2. Designed hybrids **3a–e** and **4a–e** used to investigate the optimal spacer length and the attachment point.

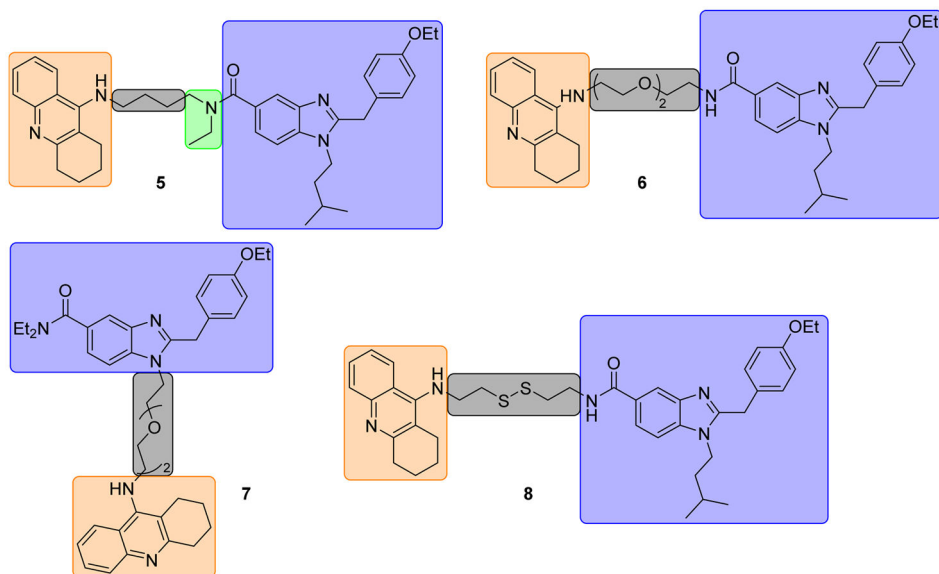


Figure 3.
Designed hybrids 5–8.

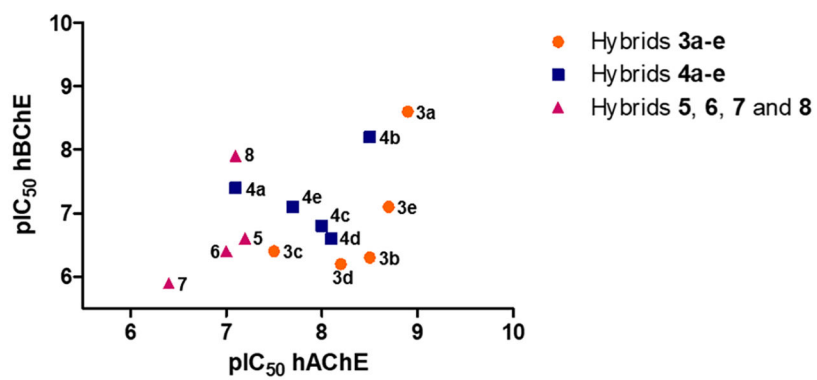


Figure 4. Plot of pIC₅₀ values toward hBChE against pIC₅₀ values toward hAChE of all hybrids.

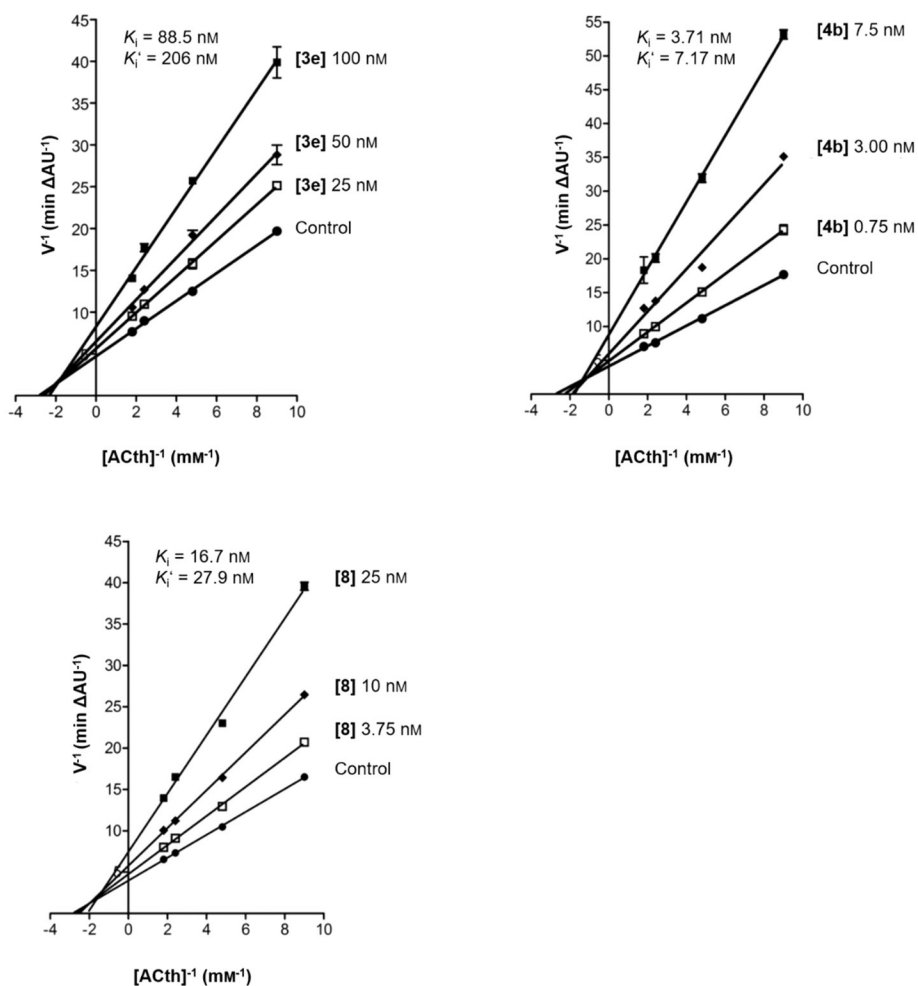


Figure 5. Kinetic study on the mechanism of hAChE inhibition by **3e**, **4b**, and **8**. Lineweaver-Burk reciprocal plots of hAChE initial velocity at increasing substrate (acetylthiocholine, AChth) concentration in the absence of the inhibitor (control) and the presence of increasing concentrations of the inhibitor are shown. Values are the means of at least three independent determinations.

	% inhibition A β aggregation	
	self-induced ^a	AChE-induced ^b
3e	81.5 \pm 0.2	62.9 \pm 5.4
4b	16.4 \pm 4.2	47.8 \pm 9.6
8	83.4 \pm 6.4	5.0 \pm 2.6
1	< 5	< 5

Figure 6.

AChE-mediated and self-induced A β aggregation. Footnote a denotes inhibition of A β ₄₂ self-aggregation investigated by the thioflavin T fluorescence assay. Assays were carried out in the presence of 50 μ M inhibitor and 50 μ M A β ₄₂ ([I] = [A β ₄₂]). Values are expressed as means \pm SEM of two independent experiments, and each was performed in duplicate. Footnote b denotes % inhibition of hAChE-induced A β ₄₀ aggregation at [I] = 100 μ M. The A β ₄₀/hAChE ratio was equal to 100:1. Values are expressed as means \pm SEM of two independent experiments, and each was performed in duplicate.

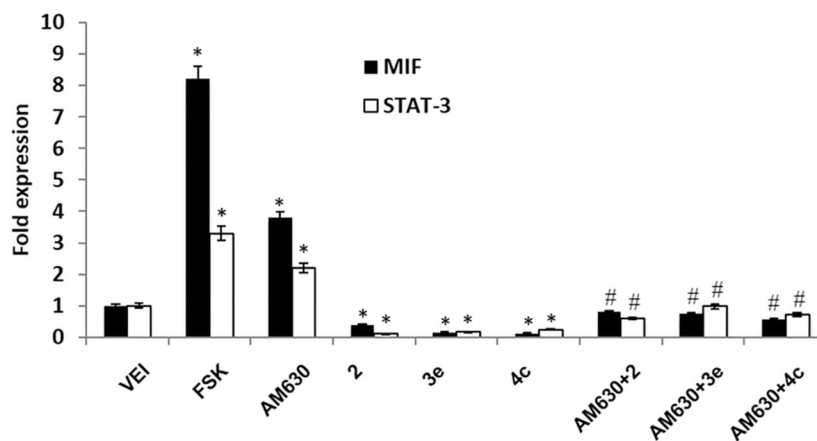


Figure 7.

Test compounds (**2**, **3e**, and **4c**) reduce MIF and STAT-3 gene expression. U266 cells were treated with hybrid compounds ($50 \mu\text{M}$), FSK ($10 \mu\text{M}$), or AM630 ($25 \mu\text{M}$) for 2 h. In a combined experiment (AM630 plus test compounds), U266 cells were preincubated with AM630 for 30 min. Before adding the test compounds, MIF and STAT-3 mRNA levels were determined by qRT-PCR. GAPDH was used for normalization. Data are expressed as relative fold with respect to vehicle-treated cells used as the control. Values are means of at least two independent experiments, and each was performed in duplicate. Data are expressed as means \pm SD * $p < 0.01$ vs untreated; # vs AM630.

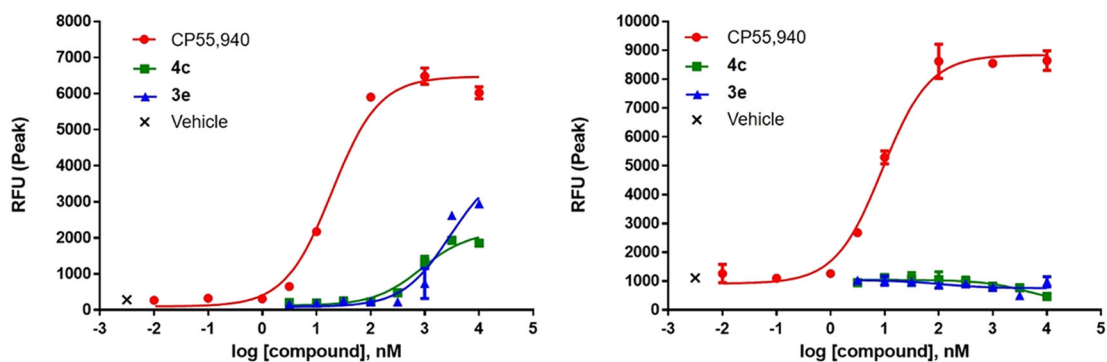


Figure 8.

Calcium mobilization assay in CHO-K1 cells overexpressing hCB₁ or hCB₂ and G_{αq16}. Compounds were tested in each cell type as described under Experimental Section. Agonism was noted in cells expressing hCB₂ (left) but not in cells expressing hCB₁ (right). The synthetic full agonist CP 55,040 served as a comparator and positive control. No significant signal was noted in vehicle control cells.

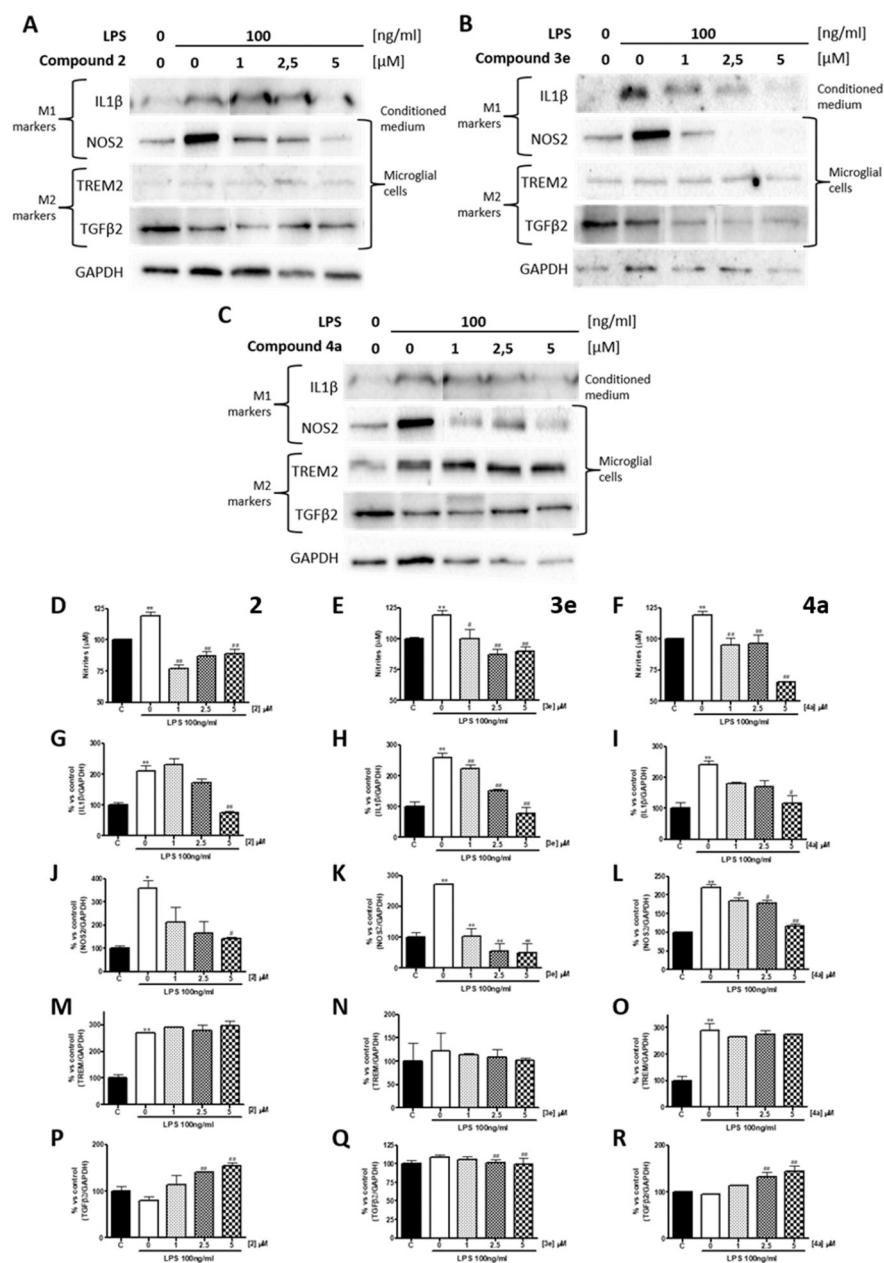


Figure 9. Effect of compounds **2**, **3e**, and **4a** on microglial activation in N9 cells previously activated by LPS (100 ng/mL). IL1 β release and expression of iNOS, TREM2, and TGF β 2 were tested through Western blot analysis after 24 h of treatment with LPS in the presence of increasing concentrations (1, 2.5, and 5 μ M) of compounds (A) **2**, (B) **3e**, and (C) **4a**, respectively, and (G–R) quantified through densitometry. NO release was evaluated through the Griess reaction in media conditioned for 24 h by microglial cells treated by LPS in the presence of compounds (D) **2**, (E) **3e**, and (F) **4a**, showing an increase in NO release in media conditioned by LPS-treated cells that are reduced by the co-treatment with the compounds, with the strongest effect of compound **2**. Both (G–I) IL1 β release and (J–L) iNOS expression, which are markers of M1 neurotoxic microglia, strongly increase in LPS-

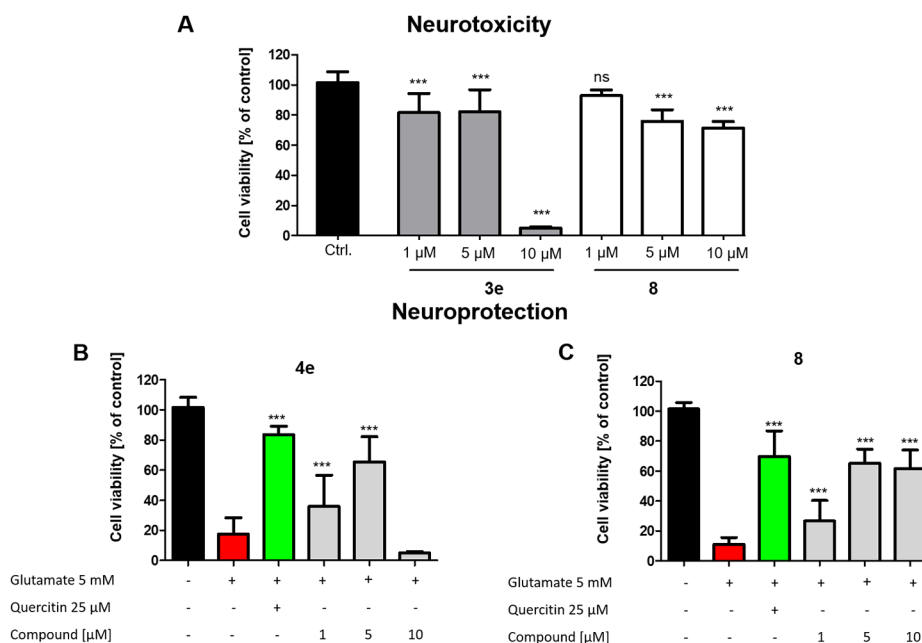
treated cells but significantly decrease in cells co-treated with compounds (G, J) **2**, (H, K) **3e**, and (I, L) **4a** in a dose-dependent way, while the expression of the M2 microglial markers (M–O) TREM2 and (P–R) TGF β 2 is not reduced by co-treatment with the compounds. All quantitative data are presented as means \pm SEM from at least three independent experiments. Statistical significance between different treatments was calculated by using one-way analysis of variance (ANOVA) followed by post hoc comparison through Bonferroni's test. * $p < 0.05$; ** $p < 0.01$ compare to control; # $p < 0.05$; ## $p < 0.01$ compare to LPS.

Author Manuscript

Author Manuscript

Author Manuscript

Author Manuscript

**Figure 10.**

Compounds **4e** and **8** were studied on neuronal HT-22 cells for (A) neurotoxicity effects and (B, C) neuroprotection against glutamate-induced oxidative stress at 1–25 μM . Results of the modified MTT test are presented as means \pm SD of three independent experiments, each performed in sextuplicate, and refer to untreated control cells, which were set as 100% values. Statistical analysis was achieved by applying one-way ANOVA followed by Dunnett's multiple comparison post-test. Levels of significance: * $p < 0.005$; ** $p < 0.01$; *** $p < 0.001$. Treated cells were compared to (A) untreated cells and (B) cells treated with glutamate only.

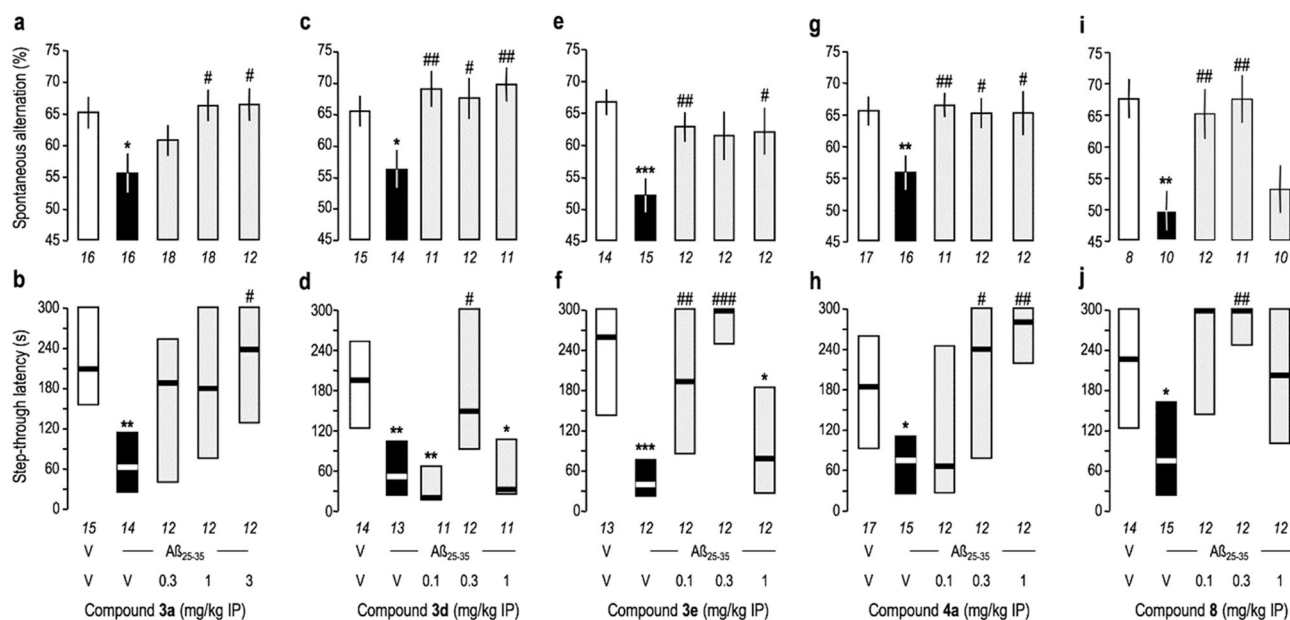
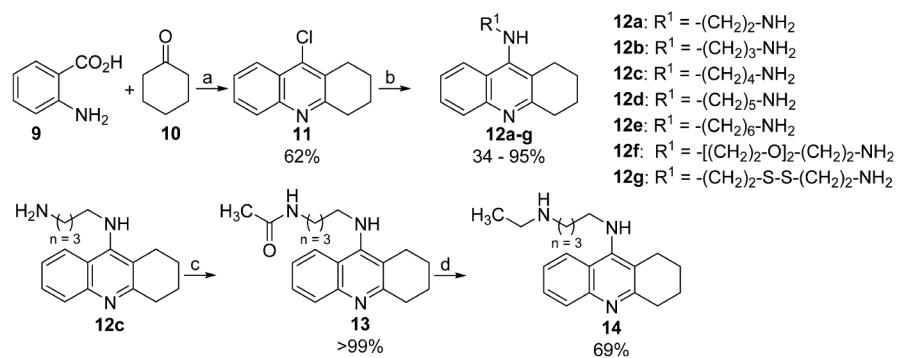


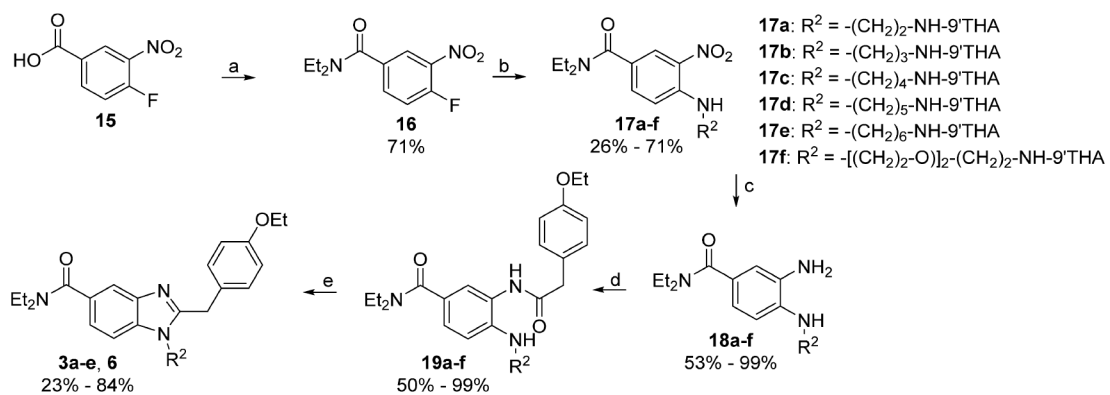
Figure 11.

Effect of the compounds on $A\beta_{25-35}$ -induced learning impairments in mice: spontaneous alternation performance (upper panels) and passive avoidance response (lower panels). Mice received $A\beta_{25-35}$ (9 nmol, i.c.v.) or vehicle solution (3 μ L, i.c.v.) on day 1 and then compound (a, b) **3a**, (c, d) **3d**, (e, f) **3e**, (g, h) **4a**, or (i, j) **8** in the 0.1–3 mg/kg, i.p. dose range, o.d. between day 1 to 7. Mice were then tested for (a, c, e, g, and i) spontaneous alternation on day 8 and (b, d, f, h, and j) passive avoidance on days 9 and 10. Data show means \pm SEM (upper panels) or median and interquartile range (lower panels). ANOVA: $F_{(4,79)} = 3.05$, $p < 0.05$, $n = 12-18$ in (a); $F_{(4,62)} = 3.77$, $p > 0.01$, $n = 11-15$ in (c); $F_{(4,64)} = 3.85$, $p < 0.01$, $n = 10-15$ in (e); $F_{(4,67)} = 3.14$, $p < 0.05$, $n = 11-17$ in (g); $F_{(4,50)} = 5.40$, $p < 0.01$, $n = 8-12$ in (i). Kruskal-Wallis ANOVA: $H = 9.87$, $p < 0.05$, $n = 12-15$ in (b); $H = 17.4$, $p < 0.01$, $n = 11-14$ in (d); $H = 21.9$, $p < 0.001$, $n = 12-13$ in (f); $H = 13.9$, $p < 0.01$, $n = 12-17$ in (h); $H = 11.8$, $p < 0.05$, $n = 12-15$ in (j). Post hoc: * $p < 0.05$, ** $p < 0.01$, and *** $p < 0.001$ vs (V + V)-treated group; # $p < 0.05$, ## $p < 0.01$, and ### $p < 0.001$ vs (V + $A\beta_{25-35}$) treated group; Dunnett's (upper panels) or Dunn's test (lower panels).

**Scheme 1.**

Synthesis of Tacrine-Amine Intermediates 12a–g and 14^a

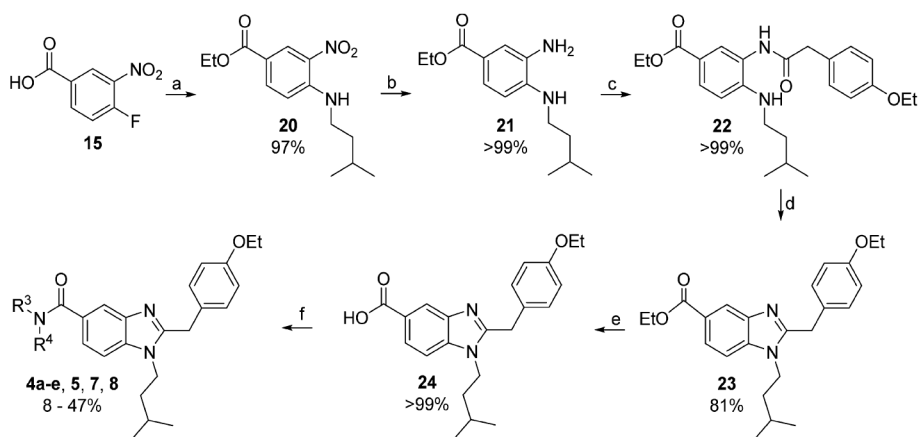
^aReagents and conditions: (a) POCl₃, reflux; (b) respective diamine, hexanol, reflux; (c) Ac₂O, r.t.; (d) LiAlH₄, THF, reflux.



Scheme 2.

Synthesis of Hybrids 3a–e and 6^a

^aReagents and conditions: (a) $HNEt_2$, cat. DMF, $(COCl)_2$, CH_2Cl_2 at 0 °C \rightarrow r.t.; (b) respective amines **12a–f**, THF, NEt_3 , r.t.; (c) $SnCl_2 \cdot 2H_2O$, EtOH, reflux; (d) 2-(4-ethoxyphenyl)acetic acid, HBTU, NEt_3 , DMF, r.t.; (e) AcOH, reflux.

**Scheme 3.**

Synthesis of Hybrids 4a–e, 5, 7, and 8^a

^aReagents and conditions: (a) (I) cat. H₂SO₄ (97%), EtOH, reflux; (II) NEt₃ 3-methylbutan-1-amine, r.t.; (b) cat. Pd/C (10%), MeOH, H₂ atm, 8 bar, r.t.; (c) 2-(4-ethoxyphenyl)acetic acid, HBTU, NEt₃, DMF, r.t.; (d) AcOH, reflux; (e) LiOH, H₂O, reflux; (f) respective amines **12a–g**, **14**, HBTU, NEt₃, DMF, r.t.

Table 1.

Results of the in Vitro Evaluation of the Inhibitory Effect of AChE/BChE and Radioligand Binding Studies at hCB₁R/hCB₂R^a

Cpd.	R ⁵	R ⁶	R ⁷	pIC ₅₀ ± SD or Inhibition [%]	hAChE ^b	SI ^c	hCB ₂ R ^d	hCB ₁ R ^e
Tacrine 1				7.9 ± 0.1	6.8 ± 0.1	1.0	29%	24%
Rimonabant				n.d.	n.d.	n.d.	4%	143 nM ± 15 25.0 nM ⁶⁹
SR-144,528				n.d.	n.d.	n.d.	19.7 ± 4.1 nM 5.7 nM ⁷⁰	687 nM ± 107 264 nM ⁷⁰
2				n.a.	n.a.	n.d.	36.7 ± 4.0 nM 4.5 nM ⁵⁷	24% >5 μM ⁵⁷
3a				8.9 ± 0.1	8.6 ± 0.1	2.3	38.5 ± 16.0 μM	36%
3b				8.5 ± 0.1	6.3 ± 0.1	193	30.7 ± 3.5 μM	15%

Author Manuscript

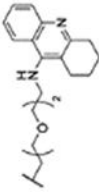
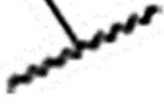
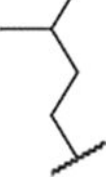

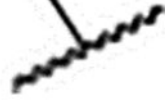

Author Manuscript

Author Manuscript

Author Manuscript

Cpd.	R ⁵	R ⁶	R ⁷	hBChE ^d	hAChE ^b	SI ^c	hCB ₂ R ^d	hCB ₁ R ^e
				pIC ₅₀ ± SD or Inhibition [%]			K _i ± SD or [H]CP 55,940 displ. @10 μM	
3c				7.5 ± 0.1	6.4 ± 0.1	12.0	26.9 ± 3.5 μM	32%
3d				8.2 ± 0.1	6.2 ± 0.1	109	7.3 ± 0.9 μM	21%
3e				8.7 ± 0.1	7.1 ± 0.1	45.3	4.5 ± 0.9 μM	17%
4a				7.1 ± 0.1	7.4 ± 0.1	0.4	2.5 ± 0.8 μM	5%
4b				8.5 ± 0.1	8.2 ± 0.1	1.8	5.0 ± 0.8 μM	20%

Cpd.	R ⁵	R ⁶	R ⁷	hBChE ^d	hAChE ^b	SI ^c	hCB ₂ R ^d	hCB ₁ R ^e
				pIC ₅₀ ± SD or Inhibition [%]			K _i ± SD or [³ H]CP 55,940 displ. @10 μM	
4c				8.0 ± 0.1	6.8 ± 0.1	15.7	2.4 ± 0.3 μM	9%
4d				8.1 ± 0.1	6.6 ± 0.1	3.1	4.0 ± 0.7	15%
4e				7.7 ± 0.1	7.1 ± 0.1	4.6	9.6 ± 1.3 μM	54%
5				7.2 ± 0.1	6.6 ± 0.1	4.3	3.0 ± 0.5 μM	36%
6				7.0 ± 0.1	6.4 ± 0.1	4.3	28.7 ± 8.8 μM	11%

Cpd.	R ⁵	R ⁶	R ⁷	pIC ₅₀ ± SD or Inhibition [%]	hAChE ^b	SI ^c	hCB ₂ R ^d	hCB ₁ R ^e
7				6.4 ± 0.1	5.9 ± 0.1	3.7	17.4 ± 2.7 μM	32%
8				7.1 ± 0.1	7.9 ± 0.1	0.2	6.8 ± 1.3 μM	45%

^d n.a. activity lower than 10% at the highest tested concentration (10 μM); n.d., not determined.

^b Values are the means of at least three independent determinations; hBChE from human serum.

^c Values are the means of at least three independent determinations; recombinant hAChE.

^d Selectivity index (SI) toward hBChE = IC₅₀(hAChE)/IC₅₀(hBChE).

^e Screened on membranes of HEK cells stably expressing hCB₂R using 10 μM of the compound; values are mean values from at least two independent experiments, each performed in triplicate.

^f Screened on membranes of CHO cells stably expressing hCB₁R using 10 μM of the compound; values are mean values from at least two independent experiments, each performed in triplicate.

Table 2.

Results of the Liver Histology Performed with High Dose (3 mg/kg)-Treated Mice

treatment	microvesicular steatosis			necrosis		
	positive/specimen	% of specimen	reported area %	positive/specimen	% of specimen	reported area %
V/V	6/10	60	30-40	5/10	50	2-30
AB/V	7/10	58	10-30	11/12	91	1-30
AB/3a (3 mg/kg)	8/12	66	5-30	8/12	66	2-50
AB/3d (3 mg/kg)	6/6	100	3-45	5/6	83	5-15
AB/4a (3 mg/kg)	2/9	22	10-30	6/9	66	5-10
AB/8 (3 mg/kg)	8/11	72	20-40	8/11	72	5-50